RELIABILITY IMPROVEMENT OF RF MEMS DEVICES BASED ON LIFETIME MEASUREMENTS

A THESIS SUBMITTED TO
THE GRADUATE SCHOOL OF NATURAL AND APPLIED SCIENCES
OF
MIDDLE EAST TECHNICAL UNIVERSITY

BY

OZAN DOĞAN GÜRBÜZ

IN PARTIAL FULFILLMENT OF THE REQUIREMENTS
FOR
THE DEGREE OF MASTER OF SCIENCE
IN
ELECTRICAL AND ELECTRONICS ENGINEERING

SEPTEMBER 2010

Approval of the thesis:

RELIABILITY IMPROVEMENT OF RF MEMS DEVICES BASED ON LIFETIME MEASUREMENTS

submitted by **OZAN DOĞAN GÜRBÜZ** in partial fulfillment of the requirements for the degree of **Master of Science in Electrical and Electronics Engineering Department**, **Middle East Technical University** by,

Prof. Dr. Canan Özgen
Dean, Graduate School of **Natural and Applied Sciences** _____

Prof. Dr. İsmet Erkmen
Head of Department, **Electrical and Electronics Eng.** _____

Assoc. Prof. Dr. Şimşek Demir
Supervisor, **Electrical and Electronics Eng. Dept., METU** _____

Prof. Dr. Tayfun Akın
Co-supervisor, **Electrical and Electronics Eng. Dept., METU** _____

Examining Committee Members:

Prof. Dr. Canan Toker
Electrical and Electronics Eng. Dept., METU _____

Assoc. Prof. Dr. Şimşek Demir
Electrical and Electronics Eng. Dept., METU _____

Assoc. Prof. Dr. Sencer Koç
Electrical and Electronics Eng. Dept., METU _____

Assoc. Prof. Dr. Özlem Aydın Çivi
Electrical and Electronics Eng. Dept., METU _____

Dr. Mustafa Akkul
ASELSAN, REHİS _____

Date: 01.09.2010

I hereby declare that all information in this document has been obtained and presented in accordance with academic rules and ethical conduct. I also declare that, as required by these rules and conduct, I have fully cited and referenced all material and results that are not original to this work.

Name, Last Name: Ozan Doğan Gürbüz

Signature :

ABSTRACT

RELIABILITY IMPROVEMENT OF RF MEMS DEVICES BASED ON LIFETIME MEASUREMENTS

Gürbüz, Ozan Doğan
M.Sc., Department of Electrical and Electronics Engineering
Supervisor : Assoc. Prof. Dr. Şimşek Demir
Co-supervisor : Prof. Dr. Tayfun Akın

September 2010, 119 pages

This thesis presents fabrication of shunt, capacitive contact type RF MEMS switches which are designed according to given mm-wave performance specifications. The designed switches are modified for investigation in terms of reliability and lifetime.

To observe the real-time performance of switches a time domain measurement setup is established and a CV (capacitance vs. voltage) curve measurement system is also included to measure CV curves, pull-in and hold-down voltages and the shifts of these due to actuations.

By using the established setup reliability and lifetime measurements under different bias waveforms in different environments are performed. After investigation for the most suitable condition for improving lifetime long-term tests are performed and the outstanding result of more than 885 hours of operation under cycling bias waveform is obtained.

Keywords: RF MEMS, surface micromachining, switch, reliability, lifetime

ÖZ

RF MEMS AYGITLARIN GÜVENİLİRLİĞİNİN YAŞAM SÜRESİ ÖLÇÜMLERİNE DAYALI OLARAK ARTIRILMASI

Gürbüz, Ozan Doğan
Yüksek Lisans, Elektrik ve Elektronik Mühendisliği Bölümü
Tez Yöneticisi : Doç. Dr. Şimşek Demir
Ortak Tez Yöneticisi : Prof. Dr. Tayfun Akın

Eylül 2010, 119 sayfa

Bu tez çalışmasında belli milimetre dalga başarım ölçütlerine gore tasarlanmış parallel, sığaç değeçli RF MEMS anahtarların üretimi anlatılmıştır. Güvenilirlik ve ömür sınama testleriyle inceleme için tasarlanan anahtarlarda değişiklikler yapılmıştır.

Anahtarların gerçek zamanlı başarımlarını izleyebilmek amacıyla zamana bağlı ölçüm düzeneği kurulmuş ve SG (sığaya karşılık uygulanan gerilim) grafiği ölçümü yapılabilen bir birim de SG grafiklerinin çıkarılabilmesi, aşağı çekme ve geri bırakma gerilimlerinin belirlenebilmesi ve bunlardaki kaymaların gözlenebilmesi için sisteme eklenmiştir.

Kurulan düzenekle değişik hareketlendirme gerilim şekilleri uygulanarak farklı ölçüm ortamlarında güvenilirlik ve ömür sınama testleri gerçekleştirilmiştir. Ömrü uzatmak için en uygun koşulların belirlenmesinden sonra uzun vadeli denemeler yapılmış ve döngülü hareketlendirme gerilim şekli uygulamasında 885 saatlik çalışma başarımı elde edilmiştir.

Anahtar kelimeler: RF MEMS, yüzey mikroişleme, anahtar, güvenilirlik, ömür süresi

Dedicated to my family, my "cat" and

the naughty, immortal child inside me…

ACKNOWLEDGMENTS

Firstly I would like to thank to my advisors Assoc. Prof. Dr. Şimşek Demir for his guidance and support during this thesis and Prof. Dr. Tayfun Akın for his friendly attitude and trust in me. Also I would like to thank both of my advisors for taking me into their teams and providing a comfortable research environment.

Secondly I should express my sincere gratitude to my mentors Dr. Kağan Topallı and Dr. Mehmet Ünlü, both for their supervision and friendship. They have shared their academic background as much as possible, listened and answered me patiently, and always behaved as life coaches, shared their experiences in all fields when we worked together and later when they left. Being in my current position in both academic and social means would be very difficult without them.

I would in addition thank to RF MEMS Group members Ömer Bayraktar, İlker Comart, Korkut Kaan Tokgöz for their friendship and making our 'bridge' office a nice working environment. I should separately thank here a distinctive person, another RF MEMS Group member, Çağrı Çetintepe, both for his friendship and share of his deep knowledge and brilliant ideas on technical issues. Moreover I must express my special thanks to my friends from undergraduate study and office mates for two years during M.Sc.; Caner Güçlü, from RF MEMS Group, Ramazan Çetin and Özgehan Kılıç, from Microwave Research Group for their friendship and funny and enjoyable times together. I, the most facetious member of the office will always miss the lunches that we have gone with all these people.

I would also thank to METU MEMS Center staff, especially to Orhan Akar for sharing his deep knowledge on fabrication processes and his admirable working discipline, and Evrim Özçakır for helping me during my process times.

I would like to thank to members of METU MEMS Group also. Additionally I would like to acknowledge Gürkan Yılmaz and Ekrem Bayraktar from METU BioMEMS Group for both their friendship and converting the boring environment of clean room in uncomfortable suits to an enjoyable place.

I would also thank to The Scientific and Technological Research Council of Turkey (TÜBİTAK) for the scholarship during this M.Sc. study.

Just before the end, I should express my deepest gratitude to all my family members; my father, Halil Gürbüz, for his support, patience and faith; my mother, Ayşe Gürbüz, for her effort and tenderness during my growth; my brother, Kaan Gürbüz, for his self-sacrificing attitude and my grandmother, Şerife Keyifçi, for her warmhearted attitude.

Finally, I have to express my gratefulness to my 'cat', Çağla Adıgüzel, for her love, her patience and tolerance and for the spent wonderful times in tiring days and nights during this study. This thesis is more meaningful with the existence of her.

My last words would be: 'Always keep the child inside alive. Keep the hopes, keep the dreams.'

TABLE OF CONTENTS

ABSTRACT…….....iv

ÖZ…….....v

ACKNOWLEDGMENTS……...vii

TABLE OF CONTENTS…….....ix

LIST OF TABLES……..xii

LIST OF FIGURES……....xiv

CHAPTERS

1. INTRODUCTION 1

1.1 On RF MEMS Reliability Problem.....2

1.2 Research Objectives and Organization of the Thesis.....6

2. A Ka-BAND, SHUNT, CAPACITIVE RF MEMS SWITCH DESIGN AND FABRICATION 7

2.1 Introduction.....7

2.1.1 RF MEMS Switch Types 8

2.1.2 RF MEMS Switch in This Study 12

2.2 Design of RF MEMS Switch 12

2.2.1 Electromagnetic Design Specifications 13

2.2.2 Physical Structure 13
2.2.3 Circuit Model 14
2.2.4 Mechanical Design Constraints 15
2.3 Measurement Results of the RF MEMS Switches 17
2.4 METU RF MEMS Process 21
2.4.1 METU RF MEMS Process Steps 21
2.4.2 Improvements on the METU RF MEMS Process 30
2.4.3 Future Process Improvements 35
2.5 Conclusion 36
3. RELIABILITY AND LIFETIME MEASUREMENT SETUP 37
3.1 Introduction 37
3.1.1 Time Domain Measurements 38
3.1.2 CV Curve Measurements 39
3.2 METU RF MEMS Research Group Reliability and Lifetime Measurement Setup 40
3.2.1 Time Domain Measurement Setup 41
3.2.2 CV Measurement Setup 54
3.2.3 Future Work 57
3.3 Conclusion 58
4. RELIABILITY AND LIFETIME MEASUREMENT RESULTS 59
4.1 Introduction 59
4.1.1 Different Bias Waveforms 60

4.1.2 Different Measurement Environments 62
4.1.3 Different Materials 63
4.1.4 Physical Layout Modifications 63
4.2 Reliability and Lifetime Measurement Samples 64
4.3 Reliability and Lifetime Measurement Results 66
4.3.1 Partial CV Curve Measurements 67
4.3.2 Open Air Measurements 73
4.3.3 Vacuum Measurements 80
4.3.4 N_2 Environment Measurements 89
4.3.5 Long-term Measurements 99
4.3.6 Future Work 107
4.4 Conclusion 108
5. CONCLUSION AND FUTURE WORK 109
REFERENCES 111

LIST OF TABLES

TABLES

Table 2.1: Parameter explanations of Equation (2.1) 11

Table 2.2: Electromagnetic design specifications for the RF MEMS switch 13

Table 2.3: Measured layer thicknesses for center region of *MS10.1-W1* 35

Table 3.1: Curve fitting equation and fitting parameters 53

Table 4.1: Layer thicknesses for the fabricated wafers 65

Table 4.2: Verification of relation between s_V_{PCV}, s_V_{PI-} and s_V_{PI+} for 15 V, unilevel, unipolar, continuous, positive bias in N_2 environment 71

Table 4.3: Results for 15V, unilevel, unipolar, continuous, negative bias in N_2 environment 72

Table 4.4: Results for unilevel, unipolar, continuous, 40 V, positive and negative bias in open air 74

Table 4.5: Results for unilevel, unipolar, cycling, 25 V, 100 Hz, 50% duty cycle, positive bias in open air 76

Table 4.6: Results for unilevel, unipolar, cycling, 25 V, 100 Hz, 50% duty cycle, negative bias in open air 77

Table 4.7: Results for unilevel, unipolar, continuous, 40 V, positive bias in vacuum 82

Table 4.8: Results for unilevel, unipolar, continuous, 25 V, positive bias in vacuum 82

Table 4.9: Results for unilevel, bipolar, continuous, 25 V, 100 Hz, 50% duty cycle bias in vacuum 85

Table 4.10: Results for unilevel, unipolar, cycling, 25 V, 100 Hz, 50% duty cycle, positive bias in vacuum 86

Table 4.11: Results for unilevel, unipolar, cycling, 25 V, 10 kHz, 50% duty cycle, positive bias in vacuum 88

Table 4.12: Results for unilevel, unipolar, continuous, 25 V, positive and negative bias in N_2 environment 90

Table 4.13: Results for unilevel, unipolar, continuous, 25 V, positive and negative bias in N_2 environment 91

Table 4.14: Results for unilevel, bipolar, continuous, 25 V, 100 Hz, 50% duty cycle bias in N_2 environment 93

Table 4.15: Results for unilevel, bipolar, continuous, 25 V, 100 Hz, 50% duty cycle bias in N_2 environment 96

Table 4.16: Shifting amount of CV curves for Sample28 101

Table 4.17: Sample29 DOV data at different instants 103

LIST OF FIGURES

FIGURES

Figure 1.1: Dielectric charging illustration 4

Figure 1.2: CV curve shift illustration 4

Figure 1.3: Simple thought experiment for showing the effect of non-uniform charge distribution 5

Figure 1.4: CV curve narrowing illustration 5

Figure 1.5: Stuck down bridge CV curve illustration 5

Figure 2.1: Different RF MEMS switch types 9

Figure 2.2: Idealized capacitance vs. applied voltage characteristics of a shunt, capacitive RF MEMS switch 10

Figure 2.3: Simplified equivalent circuits for OFF and ON-states of a shunt capacitive contact RF MEMS switch 11

Figure 2.4: States of a shunt, capacitive RF MEMS switch 12

Figure 2.5: Illustration of ON-state of designed RF MEMS switch 14

Figure 2.6: Simplified circuit model of the switch with ground recesses 15

Figure 2.7: Illustration of the partial contact approach 17

Figure 2.8: A realistic capacitance vs. applied voltage characteristics for a shunt, capacitive RF MEMS switch 17

Figure 2.9: $|S_{11}|$ vs. frequency measurement for OFF-state of five sample switches 19

Figure 2.10: $|S_{21}|$ vs. frequency measurement for OFF-state of five sample switches 20

Figure 2.11: $|S_{21}|$ vs. frequency measurement for ON-state of five sample switches 20

Figure 2.12: Base metal gold deposition and patterning 25

Figure 2.13: Isolation dielectric layer deposition and patterning 26

Figure 2.14: Sacrificial polyimide layer deposition and patterning 26

Figure 2.15: Structural metal layer deposition 27

Figure 2.16: Anchor reinforcement electroplating 27

Figure 2.17: Structural metal layer patterning 28

Figure 2.18: Sacrificial polyimide layer removal 28

Figure 2.19: Comparison of cases with and without the etch holes 29

Figure 2.20: Close-up view of polyimide residue strip when there are no etch holes 29

Figure 2.21: A fabricated RF MEMS switch photograph 30

Figure 2.22: Cross-sectional illustration of switches with and without anchor electroplating 31

Figure 2.23: Cross-sectional illustration of comparison between switches with and without anchor extensions 32

Figure 2.24: Simple mechanical model proposed for RF MEMS switch with anchor extensions 33

Figure 2.25: Optical profiler measurement for a switch with anchor extension 34

Figure 2.26: Optical profiler measurement for a switch without anchor extension 35

Figure 2.27: Illustration of the switch when the isolation dielectrics on the side regions are not etched away 36

Figure 3.1: Signal operations in the time domain measurement setup 39

Figure 3.2: Simple actuation waveform and RF signal illustration for cold switching 39

Figure 3.3: A CV curve measurement hysteresis behavior illustration 40

Figure 3.4: Illustration of the ReLiMS 41

Figure 3.5: DC block (Back-to-back waveguide adapters) 42

Figure 3.6: Transmission characteristics of DC blocks in the ReLiMS 43

Figure 3.7: Simple circuit diagram for a bias tee 43

Figure 3.8: Photograph of the waveform generator card 44

Figure 3.9: Waveform generator card simplified schematic 45

Figure 3.10: The HEMT (FHX13LG) 46

Figure 3.11: Krytar 202A detector 47

Figure 3.12: FHX13LG response, internal modulation of HP8350B 49

Figure 3.13: FHX13LG response, internal modulation of HP8350B 49

Figure 3.14: FHX13LG response, external modulation of 1kHz with Agilent 33220A on HP8350B..... 50

Figure 3.15: FHX13LG response, external modulation of 50 Hz with Agilent 33220A on HP8350B..... 50

Figure 3.16: Omega detector response, external modulation of 50 Hz with Agilent 33220A on HP8350B..... 51

Figure 3.17: HP423A detector response, external modulation of 50 Hz with Agilent 33220A on HP8350B..... 51

Figure 3.18: HP423A detector response, AM by RF MEMS switch with an actuation frequency of 25 Hz on microwave signal 52

Figure 3.19: Krytar 202A detector response, AM by RF MEMS switch with an actuation frequency of 25 Hz on microwave signal 52

Figure 3.20: Krytar 202A input RF power vs. output voltage characteristics 53

Figure 3.21: Tri-axial cable cross-sectional view 54

Figure 3.22: A typical P-CV measurement result 55

Figure 3.23: A typical P-CV curve shift 56

Figure 4.1: Illustrations of different bias waveforms 62

Figure 4.2: Types of isolation dielectric layer perforations 64

Figure 4.3: General layout view of MS10 66

Figure 4.4: Sample oscilloscope display showing detector output and actuation waveforms 67

Figure 4.5: Comparison of partial and full CV curves..... 69

Figure 4.6: Comparison of partial and full CV curves..... 69

Figure 4.7: Comparison of partial and full CV curves..... 70

Figure 4.8: PCV result for Sample2.1..... 72

Figure 4.9: Comparison of positive and negative bias for open air environment 74

Figure 4.10: Detector output voltage data for unilevel, unipolar, cycling, 25 V, 100 Hz, 50% duty cycle positive bias in open air..... 75

Figure 4.11: CV curves for unilevel, unipolar, cycling, 25 V, 100 Hz, 50% duty cycle, positive bias in open air 76

Figure 4.12: DOV data for unilevel, unipolar, cycling, 25 V, 100 Hz, 50% duty cycle negative bias in open air 77

Figure 4.13: DOV data for unilevel, unipolar, cycling, 25 V, 50 kHz, 50% duty cycle positive bias in open air 78

Figure 4.14: CV curves for unilevel, bipolar, continuous, 40 V, 100Hz, 50% duty cycle bias in open air 79

Figure 4.15: CV curves for unilevel, bipolar, continuous, 25 V, 100Hz, 50% duty cycle bias in open air 80

Figure 4.16: CV curves for unilevel, unipolar, continuous, 40 V, positive bias in vacuum .. 81

Figure 4.17: CV curves for unilevel, bipolar, continuous, 40 V, 100Hz, 50% duty cycle bias in vacuum..... 84

Figure 4.18: CV curves for unilevel, bipolar, continuous, 25 V, 100Hz, 50% duty cycle bias in vacuum..... 85

Figure 4.19: CV curves for unilevel, unipolar, cycling, 25 V, 100 Hz, 50% duty cycle, positive bias in vacuum..... 86

Figure 4.20: CV curves for unilevel, unipolar, cycling, 30 V, 1 kHz, 50% duty cycle, negative bias in vacuum..... 87

Figure 4.21: CV curves for unilevel, unipolar, cycling, 25 V, 10 kHz, 50% duty cycle, positive bias in vacuum..... 88

Figure 4.22: CV curves for unilevel, unipolar, continuous, 25 V, positive and negative bias in N_2 environment 90

Figure 4.23: CV curves for unilevel, unipolar, continuous, 25 V, positive and negative bias in N_2 environment 91

Figure 4.24: CV curves for unilevel, bipolar, continuous, 40 V, 100Hz, 50% duty cycle bias in N_2 environment 92

Figure 4.25: CV curves for unilevel, bipolar, continuous, 25 V, 100Hz, 50% duty cycle bias in N_2 environment 93

Figure 4.26: DOV data for unilevel, bipolar, cycling, 25 V, 1 kHz, 50% and 2.5% duty cycle bias in N_2 environment 95

Figure 4.27: CV curve for unilevel, bipolar, cycling, 25 V, 1 kHz, 50% duty cycle bias in N_2 environment 95

Figure 4.28: Optical profiler measurement of a sample switch with square shape dielectric islands 98

Figure 4.29: Sample27 CV curves at different instants 100
Figure 4.30: Sample28 CV curves at different instants 101
Figure 4.31: Sample29 CV curves at different instants 104
Figure 4.32: Sample 30 DOV data and CV curve 105
Figure 4.33: Sample31 DOV data and CV curves 107

CHAPTER 1

INTRODUCTION

The never-ending interest of mankind on the unknown has given a birth to science and never-ending needs of mankind have brought the technology. As the physics discipline of science has passed from Classical Era to the Quantum Era the “micro” world has attracted the scientists and got more popular. This popularity has also been projected onto the technology and led to the development of micro technologies. MEMS (Micro Electro Mechanical Systems) technology has born as a sub-division of this area and stands for the integration of mechanical structures and electronics at the micro scale. Idea of embedding this technology into another field of physics, electromagnetism, has brought RF MEMS into play which employs the micro moving structures in microwave applications.

RF MEMS research has started by the development of first MEMS switch (and varactor) designed for microwave applications at the beginning of 1990’s [1]. After realization of the potential of this new approach to be used over a wide range of applications such as wireless communication systems, satellite systems and radar systems [2] it has quickly gained popularity with its low insertion loss, high isolation, high linearity, virtually zero bias power and reconfigurability against its semiconductor counterparts which were dominating the market.

As a consequence of its popularity many studies on RF MEMS have been done. These studies are focused on switches [3-15], varactors [16-24], reconfigurable phase shifters [25-32] and reconfigurable matching networks [33-36], tunable filters [37-48], reconfigurable power dividers [49] and reconfigurable antennas [50-59] where the switches and varactors are the basic components of RF MEMS structures.

As the RF MEMS research got deeper Pandora's Box slowly opened and problematic sides of RF MEMS technology came out where the focus of this study, reliability problem, leads the way among these.

1.1 On RF MEMS Reliability Problem

On the path to usage over a wide area of applications and commercialization, reliable operation and maintaining this reliable operation over the lifetime constitute the key parameters. So RF MEMS reliability is intensively under investigation for long-term applications [60-67].

Putting complex systems aside even the simplest RF MEMS component, the switch exhibits reliability problems and the goal is determined as fabricating a reliable RF MEMS switch by the community as much of the effort concerning reliability is spent on this subject, either in a direct or an indirect manner. Among many of them only a few switches have been commercially available [68, 69] and few of them have been considered to be highly reliable by the authorities [65-67].

Throughout the many reliability studies two failure mechanisms came forward and the concentration has been on them; contact degradation for DC-contact switches and the dielectric charging for capacitive contact switches [60, 61, 64, 70-84]. Since the switch type of interest in this study is a capacitive contact one the dielectric charging is explained in this chapter.

There are several mechanisms that state the charge movement in the insulators [82, 85] and because of the high electric field applied [1] on RF MEMS switches, significant amount of charges are injected into the isolation dielectric from both the top and the bottom electrodes where charging from bottom is hardly identified with respect to top charging [75] resulting with the change of net amount of charge in the dielectric. This is illustrated by Figure 1.1 for positive bias case. The injected charges into the dielectric behave as if an equivalent voltage is applied to the electrodes and this causes two types of result; screening and stiction.

[1] Typically in the order of $5x10^7$ V/m.

- **Screening:** Considering the dominancy of top charging over bottom charging, it is easy to explain the screening by top charging. The injected charges from the top electrode are of the opposite sign with bottom electrode potential. As these charges are placed in the dielectric they decrease the strength of electric field created by the applied voltage. If the dielectric is sufficiently charged, the applied voltage is not enough anymore to create the required electric field for collapsing the bridge and the bridge stays in upstate which is observed in this study in Section 4.3.2.
- **Stiction:** Stiction is an abbreviation for "static friction" and stands for the sticking phenomenon of RF MEMS bridges to the dielectrics. When the bias is terminated while the switch is in ON-state the charges behave as if a voltage is applied on the bridge and if there are sufficient amount of charges the equivalent voltage of charges exceeds hold-down voltage keeping the switch in ON-state which is called the stiction.

Both screening and stiction cause failure of the switch preventing the proper operation. Failure due to stiction can occur as a result of CV curve shift, CV curve narrowing or both.

- **CV curve shift:** This is the most emphasized observation in the reliability studies [63, 64, 71, 72, 79]. Assuming that in the dielectric there is a uniform distribution of charge with single polarity, the CV curve shift happens as illustrated in Figure 1.2 for positive bias. [2] If one of the encircled values in CV curve passes to the other side of 0 V line then stiction occurs.
- **CV curve narrowing:** Even for a dielectric with zero net charge case, an RF MEMS bridge could bend down. A simple thought experiment is given in Figure 1.3 to show this fact [70].

  Think of that there is a dielectric layer and an electrode as shown in Figure 1.3. Assume that the dielectric is neutral i.e. has no net charge but the opposite charges are concentrated at two far ends of the layer. Certainly the charge distribution of the electrode will be rearranged due to the non-uniform distribution of charges in the dielectric beneath it and electrostatic forces will act on the electrode as shown in Figure 1.3 which causes the CV curve narrowing as illustrated in Figure 1.4. As the encircled values meet at 0 V line the stiction occurs.

[2] The shifting direction is reversed for a negative bias case.

While actuating a switch the dielectric can be charged and also this charging might not be uniformly distributed causing the observation of both CV curve shift and narrowing. As long as the pull-out can be observed during CV measurement, any case could be represented by a combination of net charges and non-uniform charge distribution. If no pull-out occurs even for zero applied voltage (Figure 1.5) this means that the bridge has partially stuck to the dielectric which is considered as a failure.

Since charging takes place between two materials, using different materials and even depositing the same material with different conditions while fabricating an RF MEMS switch could affect the dielectric charging behavior hence the reliability. Also since the bridge is a movable structure it can be affected by the environmental factors. Some of the studies in the literature investigate these effects [64, 77, 83, 86].

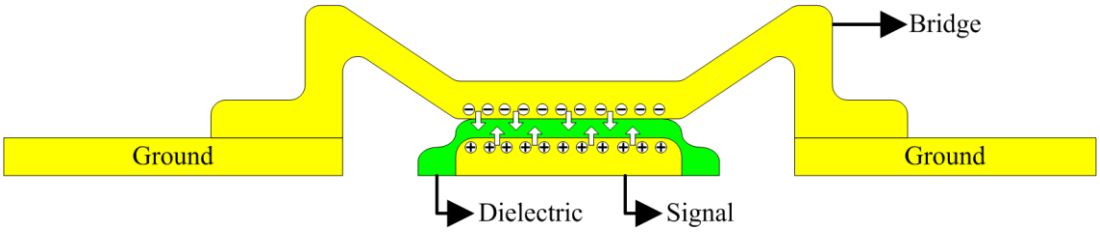

Figure 1.1: Dielectric charging illustration

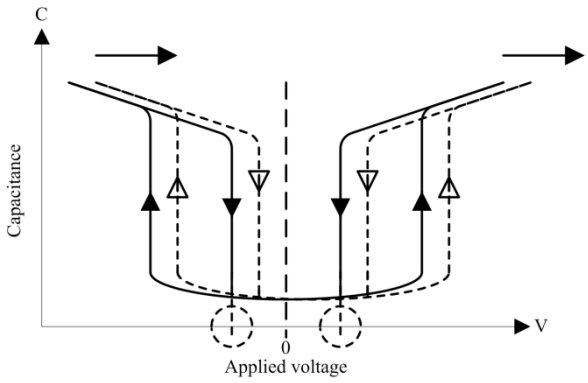

Figure 1.2: CV curve shift illustration

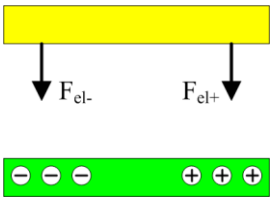

Figure 1.3: Simple thought experiment for showing the effect of non-uniform charge distribution

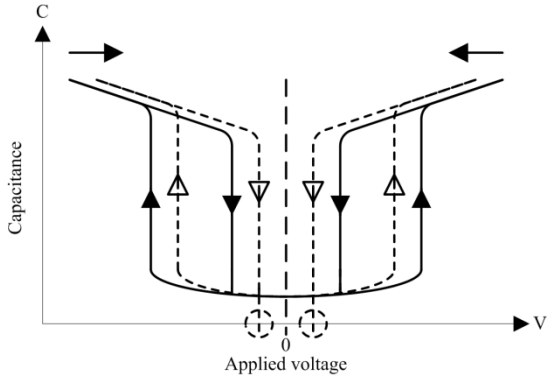

Figure 1.4: CV curve narrowing illustration

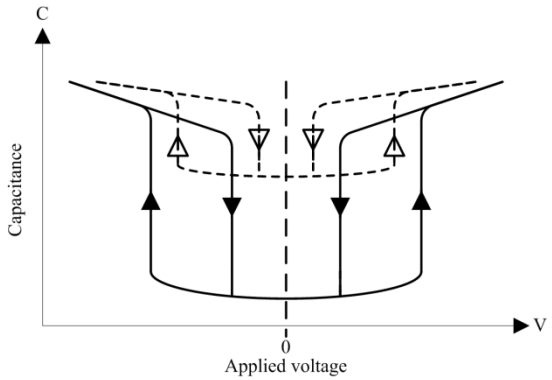

Figure 1.5: Stuck down bridge CV curve illustration

1.2 Research Objectives and Organization of the Thesis

The main aim of this thesis is to fabricate operational RF MEMS switches, investigate the reliability behavior under different conditions and improve their lifetime. Specific objectives of this thesis could be summarized as follows:

- To fabricate many switches on a wafer to be used during reliability and lifetime measurements.
- Establishment of a dedicated reliability and lifetime measurement setup for reliability and lifetime characterization of fabricated RF MEMS switches.
- Measurements on the RF MEMS switches for the investigation of effects of different factors on reliability and lifetime and based on these measurements the improvement of lifetime.

This thesis consists of five chapters which include the accomplishments during this study.

After this introduction chapter, in Chapter 2 general information on RF MEMS switches is provided. The design specifications of an RF MEMS switch which is one of the interests of this thesis, are shortly explained and mm-wave measurement results of fabricated switches for this study are provided. [3] Then the detailed fabrication flow is given together with the process improvements with respect to the previous studies and the chapter is concluded with the proposal of possible future process improvements.

The study continues with Chapter 3 which is about the details of reliability and lifetime measurement setup. The sub-portions of the setup, time domain and CV curve measurement setups are explained in detail.

Next, Chapter 4 comes in which the effects of variation of different parameters are presented. Then the results of measurements are given under five parts; partial-CV curve measurements, open air (uncontrolled environment) measurements, vacuum measurements, N_2 environment measurements and long-term measurements.

Finally in Chapter 5 the work done in this thesis is summarized and all proposed future acts have been compiled for convenience.

[3] The detailed explanation of design progress on this switch is given in another study, [90].

CHAPTER 2

A KA-BAND, SHUNT, CAPACITIVE RF MEMS SWITCH DESIGN AND FABRICATION

This chapter explains the development of a basic RF MEMS component, RF MEMS switch, in terms of design and fabrication. The chapter firstly introduces the RF MEMS switch briefly and mentions the type focused throughout this study in Section 2.1. Section 2.2 is an overview on design of Ka-band shunt, capacitive RF MEMS switch and Section 2.3 gives the scattering parameters measurement results of this switch configuration. Section 2.4 presents an overview of RF MEMS switch fabrication where Section 2.4.1 gives detailed fabrication flow while Section 2.4.2 giving the improvements in fabrication.

2.1 Introduction

RF MEMS is an easily implementable technology allowing us to construct reconfigurable structures for microwave systems [2]. The basic component for the technology is an RF MEMS switch where it can be a variable capacitance or an electrical contact according to its type [2]. The switch considered in this study is a modifiable capacitance type which is connected in parallel to the circuit.

2.1.1 RF MEMS Switch Types

There are basically two types of RF MEMS switches according to their contacts described in the literature: capacitive contact and the ohmic contact. The RF MEMS switch can be connected to the circuit in one of two ways: shunt or series. Then four different switch types can be constructed: shunt connected capacitive contact, series connected capacitive contact, shunt connected ohmic contact and series connected ohmic contact. We are interested in a shunt connected capacitive contact type switch during this study. The illustrations for different types of RF MEMS switches can be seen in Figure 2.1.

A series switch is simply a control element on the signal line where the signal is transmitted in its downstate, theoretically providing zero insertion loss and prevents the transmission of signal during its upstate, virtually having infinite isolation. A shunt switch is the reverse of a series switch operationally and is simply a path from the signal line to the ground line where it allows the transmission of signal in upstate, ideally introducing zero insertion loss and blocks the transmission of RF power in the downstate, as if having infinite isolation.

Series switch types with their physically open configuration in the OFF-state (upstate) are more suitable for relatively low frequency applications (0.1-40 GHz) and the shunt switches are more appropriate for high frequencies (5-100 GHz) since the isolation of a series switch gets worse in the OFF-state as the frequency is increased [2]. The type of our interest, shunt switches practically could not have zero insertion loss due to their OFF-state (upstate) capacitance which is shown in Figure 2.3-a and limited in terms of providing high isolation because of their ON-state (downstate) resistances which can be seen from Figure 2.3-b.

RF MEMS switches are classified also according to the method how the mechanical movement, so called actuation is achieved. The actuation can either be electrostatic [3-15], thermal [87], magneto-static [88] and piezoelectric [89]. The electrostatic actuation mechanism is the most commonly used way owing to the virtually zero power consumption, small device size, relatively short switching times and easier biasing [2]. The type of interest in this study is an electrostatic actuation type RF MEMS switch.

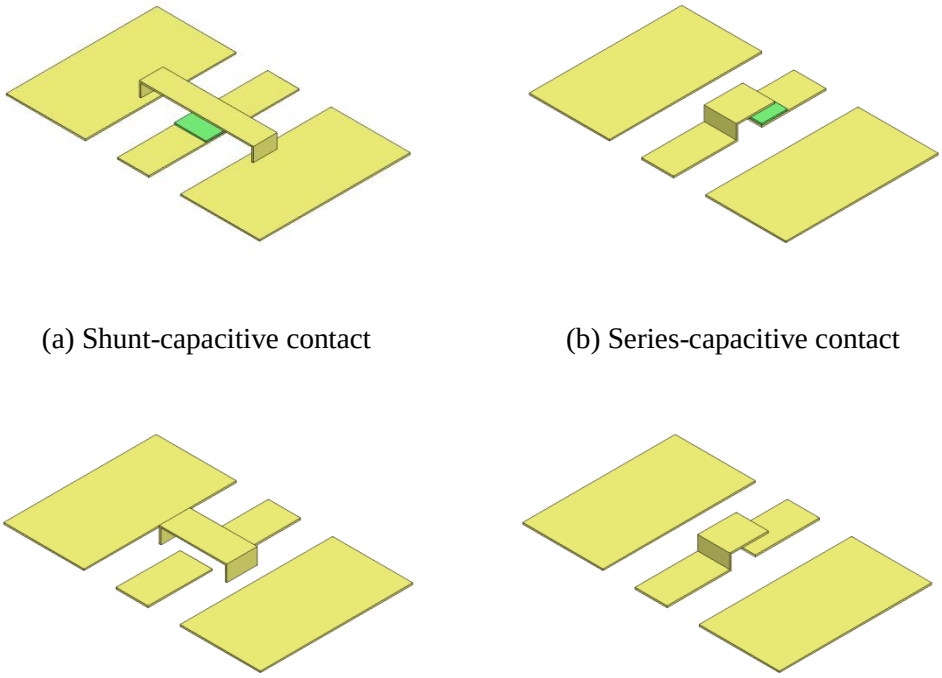

(a) Shunt-capacitive contact (b) Series-capacitive contact

(c) Shunt-ohmic contact (d) Series-ohmic contact

Figure 2.1: Different RF MEMS switch types

A shunt, capacitive contact RF MEMS switch can be simply regarded as a parallel plate capacitor. Applying a potential difference between the two plates creates an electrostatic force attracting them towards each other. This fact forms the basics of electrostatic actuation. Electrostatic actuation for an RF MEMS switch is achieved by applying a potential difference between the signal and ground so the switch comes from OFF-state (Figure 2.4-a) to the ON-state (Figure 2.4-b) at a certain voltage value which is called the pull-in or the actuation voltage. The dielectric layer seen in Figure 2.4 prevents the DC connection hence a high current flow from signal to ground which can cause blowing up of the switch.

Because of the nature of electrostatic actuation as the applied voltage is swept over a sufficient range a hysteresis curve forms between the capacitance of RF MEMS switch and applied voltage as seen from Figure 2.2. This phenomenon comes from the fact that the required voltage to bring down the bridge from OFF to ON-state is higher than the required voltage to hold the bridge in ON-state. The pull-in voltage expression for a shunt,

capacitive RF MEMS switch is given by Equation (2.1) [2] where the parameters of equations are explained in Table 2.1. The dimension parameters are also shown in Figure 2.4-a. Note that *k* parameter is included in Equation (2.1) which refers to the spring constant value associated with the RF MEMS bridges since the vertically moving fixed-fixed beams can be modeled as springs.

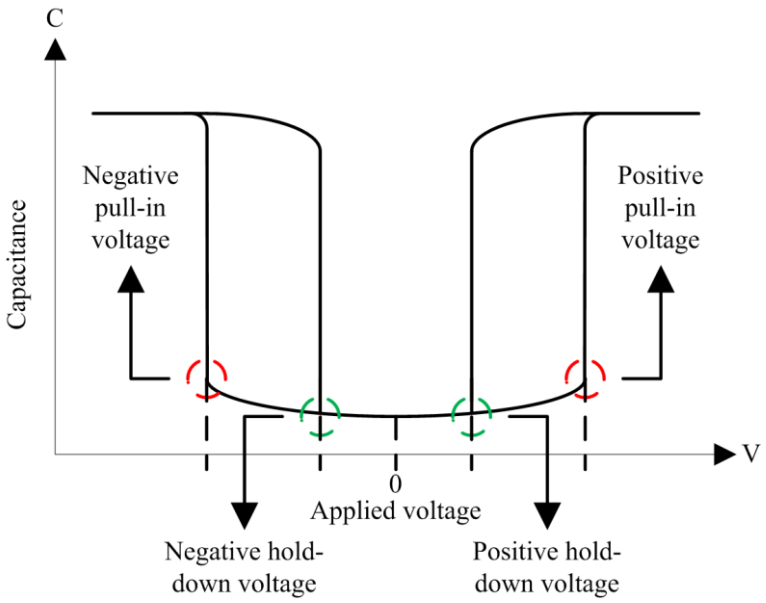

Figure 2.2: Idealized capacitance vs. applied voltage characteristics of a shunt, capacitive RF MEMS switch

$$V_{pi} = \sqrt{\frac{8k}{27\varepsilon_0 W \mathrm{w}} g_0^3} \qquad \textbf{(2.1)}$$

Table 2.1: Parameter explanations of Equation (2.1)

Parameter	Explanation
V_{pi}	Pull-in voltage
k	Spring constant of the RF MEMS bridge
ε_0	Air permittivity
W	Width of the signal line
w	Bridge width
g_0	RF MEMS bridge height in OFF-state

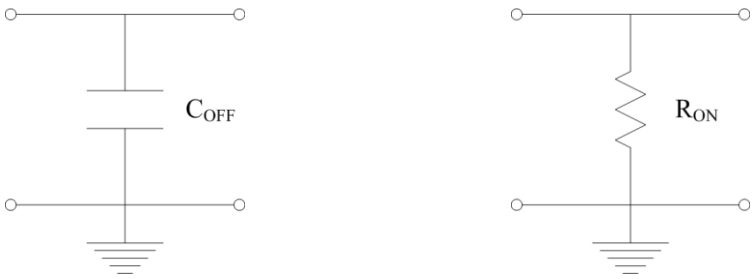

(a) OFF-state (b) ON-state

Figure 2.3: Simplified equivalent circuits for OFF and ON-states of a shunt capacitive contact RF MEMS switch

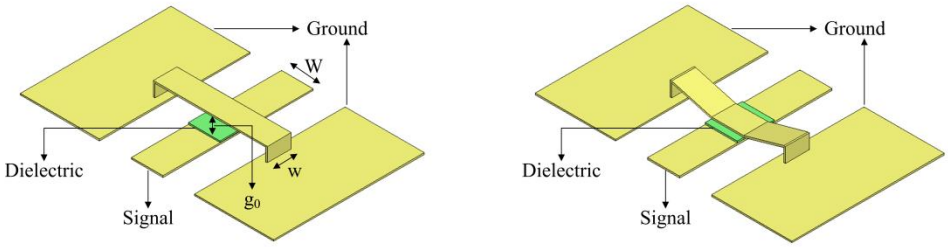

(a) OFF-state (b) ON-state

Figure 2.4: States of a shunt, capacitive RF MEMS switch

2.1.2 RF MEMS Switch in This Study

According to the classifications in Section 2.1.1 the RF MEMS switch considered throughout this thesis has the following properties:

- Circuit configuration : Shunt connected
- Contact type : Capacitive contact
- Actuation mechanism : Electrostatic actuation

This shunt connected, capacitive contact, electrostatically actuated RF MEMS switch is implemented with the coplanar waveguide (CPW) topology by micromachining technology. Electromagnetic and mechanical design specifications, the model parameters and RF measurement results are presented in Section 2.2.

2.2 Design of RF MEMS Switch

This section is an overview on design of RF MEMS switch from two aspects: electromagnetic and mechanical. Electromagnetic design is completed according to the given electromagnetic performance specifications and so the mechanical design according to the structural limitations [90].

2.2.1 Electromagnetic Design Specifications

The RF MEMS switch is desired to operate in mm-wave frequency range, specifically at 35 GHz. The design specifications for OFF and ON-states of the switch are given in Table 2.2 [90].

Table 2.2: Electromagnetic design specifications for the RF MEMS switch

SWITCH STATE	DESIGN SPECIFICATION
OFF-state	RETURN LOSS ≤ -20 dB in Ka-band INSERTION LOSS ≤ 0.5 dB in Ka-band
ON-state	MAXIMUM ISOLATION AT 35 GHZ ISOLATION AT 35 GHZ≥ 20 dB

2.2.2 Physical Structure

Physical illustration for the ON-state of the designed RF MEMS switch can be seen from Figure 2.5. In Figure 2.5 the recessed regions in the ground planes are indicated. These recesses introduce inductances to the structure allowing the designers to form a structure resonating at the desired frequency for good isolation as explained in Section 2.2.3.

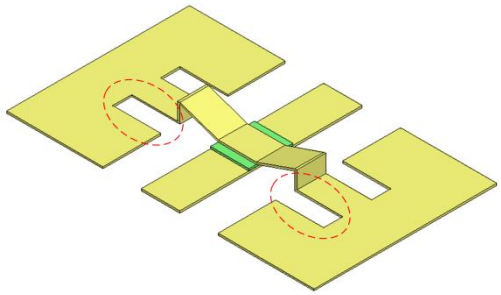

Figure 2.5: Illustration of ON-state of designed RF MEMS switch

2.2.3 Circuit Model

The RF MEMS switch with the recesses on the ground could be very simply modeled with the lumped components disregarding the transmission line segments at the input and the output. Schematic of the simplified model can be seen from Figure 2.6.

The ground recesses pulls up the characteristic impedance of the transmission lines to a higher value forming short length high characteristic impedance transmission lines at the two sides of the bridge. Since short length approximation for high characteristic impedance transmission lines results with series inductance in microwave theory these are modeled with L_{RECESS}. The parallel plate capacitance between the signal and ground with the dielectric isolation layer is modeled by the C_{BRIDGE} parameter. As the signal propagates through the recess it encounters a short circuited transmission line which behaves as an inductance. Hence sum of this inductive effect and the bridge inductance itself is represented by L_{BRIDGE}. Losses of the bridge are modeled by the R_{ON} parameter.

As seen from the circuit model in Figure 2.6, L_{BRIDGE} and C_{BRIDGE} form a series resonant structure dropping the total shunt arm impedance to R_{ON} at the frequency given in Equation (2.2). Considering that R_{ON} has a very low value the RF MEMS switch provides the best isolation around the resonance frequency almost shorting the signal to ground. By adjusting the physical dimensions L_{BRIDGE} and C_{BRIDGE} parameters are adjusted such to bring the resonance frequency close to the given frequency specification. Further improvement of isolation at the desired frequency could be done by optimization on model

parameters. An additional advantage of inductive tuning with recesses is related to the mechanical constraints which will be mentioned in Section 2.2.4.

$$f_{res} = \frac{1}{2\pi\sqrt{L_{BRIDGE}C_{BRIDGE}}} \quad \textbf{(2.2)}$$

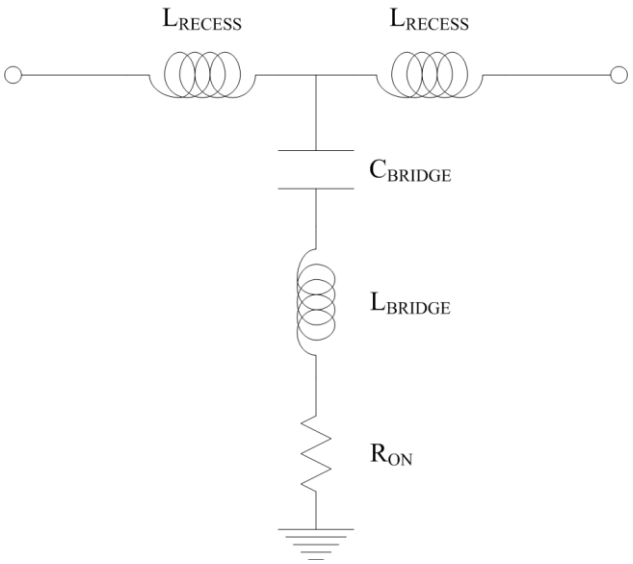

Figure 2.6: Simplified circuit model of the switch with ground recesses

2.2.4 Mechanical Design Constraints

One of the desired properties besides the electromagnetic performance for an RF MEMS switch is small pull-in voltage. High pull-in voltage is not preferable due to two reasons:

- Applying high voltages on the shunt, capacitive contact RF MEMS switch shortens the lifetime of the switch.
- Handling the high voltages result with the need for more complex systems used to bias the RF MEMS switch.

Two factors provide the opportunity of keeping the pull-in voltage at the desired low levels:

- Inductive tuning by recesses
- Determination of ON-state capacitance according to partial contact assumption

Inductive tuning allows the designer to shift the resonance frequency more freely without changing the ON-state capacitance hence the pull-in voltage. This can be deduced from Equation (2.1) with the knowledge that pull-in voltage will change as the dimensional parameters are modified to change the ON-state capacitance.

Designing the RF MEMS switch with partial contact approach enables the switch to operate at the desired frequency with less applied voltage. An illustration of partial contact is presented in Figure 2.7.

Ideally an RF MEMS bridge is expected to cover all the overlapping area on the signal line but in practice that is not the case. According to the applied voltage the bridge can come into contact in a smaller area than the overlapping area as shown in Figure 2.7. This phenomenon which is also called *zipping* can either be noticed by optical investigation or from the CV-curve of the RF MEMS switch as shown in the Figure 2.8. In contrast to the idealized CV-curve in Figure 2.2, RF MEMS switches exhibit CV-curves more similar to the one given in Figure 2.8. It is obvious from Figure 2.8 that after the pull-in voltage the capacitance still continues to increase indicating an enhancement of the physical contact. Considering this phenomenon the design could be done assuming an appropriate partial contact ratio then the capacitance degradation because of the partial contact can be compensated by inductive tuning. Another advantage of the partial contact assumption is the reduced contact area which can reduce the dielectric charging also. The last benefit is related to the electromagnetic performance such that if the resonance frequency stays above the desired frequency then a slight increase of the applied voltage could carry the resonance frequency to the desired frequency.

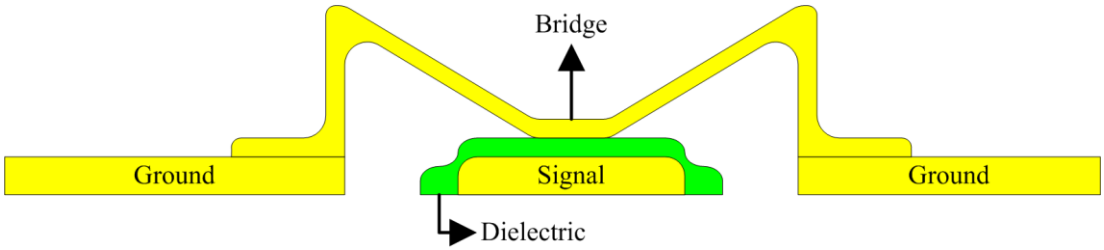

Figure 2.7: Illustration of the partial contact approach

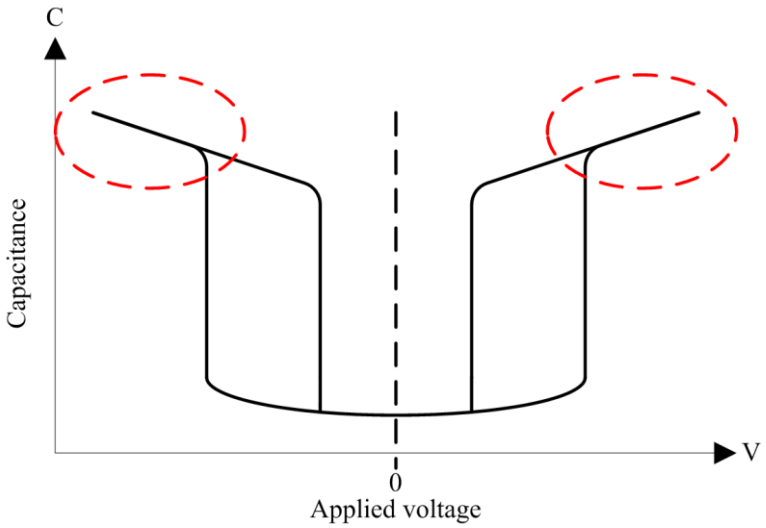

Figure 2.8: A realistic capacitance vs. applied voltage characteristics for a shunt, capacitive RF MEMS switch

2.3 Measurement Results of the RF MEMS Switches

For the electromagnetic characterization of RF MEMS switches, measurements are performed in facilities of Middle East Technical University (METU). The designed RF MEMS switches are fabricated in the METU MEMS Center clean room facilities[4] by using

[4] Fabrication is completed mainly by the author with the help of METU MEMS Center staff.

the RF MEMS process developed in METU MEMS Center[5]. One of the fabricated wafers is picked up which is labeled as the *Mask Set 10.1-Wafer 1* (*MS10.1-W1)* and on some of the selected sample RF MEMS switches from *MS10.1-W1* measurements are performed in the METU Electrical Electronics Engineering Department Millimeter Wave Laboratory by using Cascade Microtech Summit 9000 Analytical Probe Station together with Agilent E8361A Vector Network Analyzer. [6] During the mm-wave measurements Farnell PDD3502A power supply is used to apply DC bias on the RF MEMS switches. For applying the RF signal to the RF MEMS switch Cascade ACP40-GSG-150 coplanar probes are used in the Cascade Microtech Summit 9000 Analytical Probe Station and to eliminate the measurement errors, built-in SOLT calibration feature of Agilent E8361A VNA is used through the 1-40 GHz frequency range.

The measured switch samples are selected from three different regions of *MS10.1-W1,* region between top and center, center region and bottom region. Totally mm-wave measurements of five switches are performed from *MS10.1-W1*.

The reflection in OFF-state namely the return loss measurements of switch samples are presented in Figure 2.9. Note that all switches have similar frequency responses for their OFF-states and the electromagnetic design specification for reflection in OFF-state, (RL<-20 dB, Table 2.2) is satisfied.

The transmission characteristics in OFF-state namely the insertion loss of the same five switches are given in Figure 2.10. The design specification in Table 2.2 for insertion loss in OFF-state was given to be less than 0.5 dB in Ka-band and as seen from Figure 2.10 the OFF-state insertion loss performances of switches are far better than the desired values. Another point to note here is the consistency in the measurement results of the switches. OFF-state insertion losses are very close for different switches.

The transmission characteristics in ON-state namely the isolation measurements of the same five samples are given in Figure 2.11. $|S_{21}|$ responses of the switches slightly differ from each other. These deviations can be linked to the ON-state contact differences between the switches. Since resonant structures have very sharp responses around

[5] Dr. Kağan Topallı and Dr. Mehmet Ünlü are the main contributors in the development of the METU RF MEMS process.

[6] Measurements are performed together with Çağrı Çetintepe.

resonance frequency, the small differences between the ON-state capacitances might cause noticeable differences between resonance frequencies. Despite the discrepancies all five switches could satisfy the design specification for the isolation in ON-state. (Table 2.2) Even the worst switch is able to provide -28.72 dB of isolation at 35 GHz.

Figure 2.9, Figure 2.10 and Figure 2.11 indicate that the fabricated RF MEMS switches with METU RF MEMS process in METU MEMS Center clean room facilities can meet the electromagnetic design requirements. Section 2.4 is a detailed part on METU RF MEMS process.

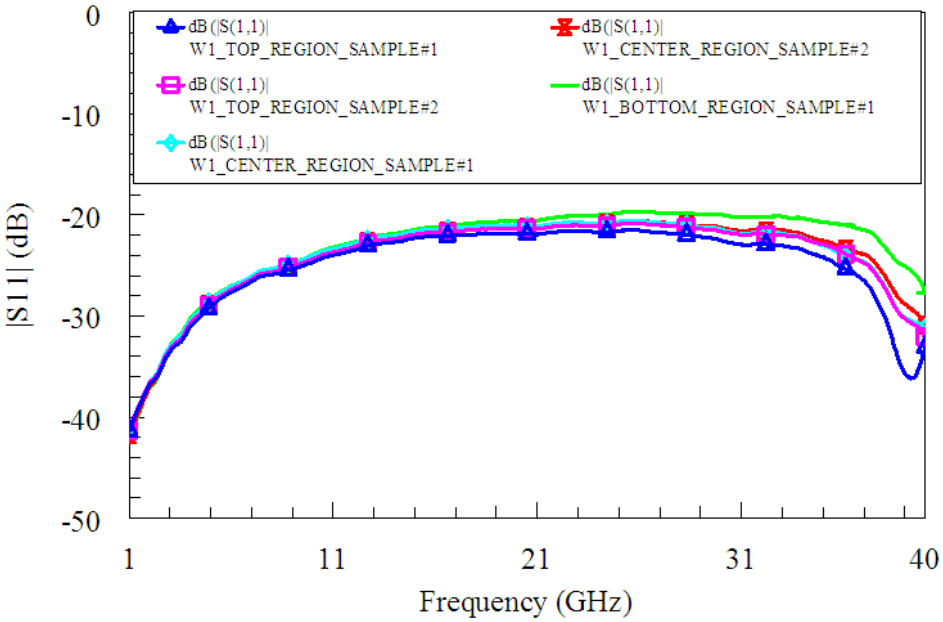

Figure 2.9: $|S_{11}|$ vs. frequency measurement for OFF-state of five sample switches

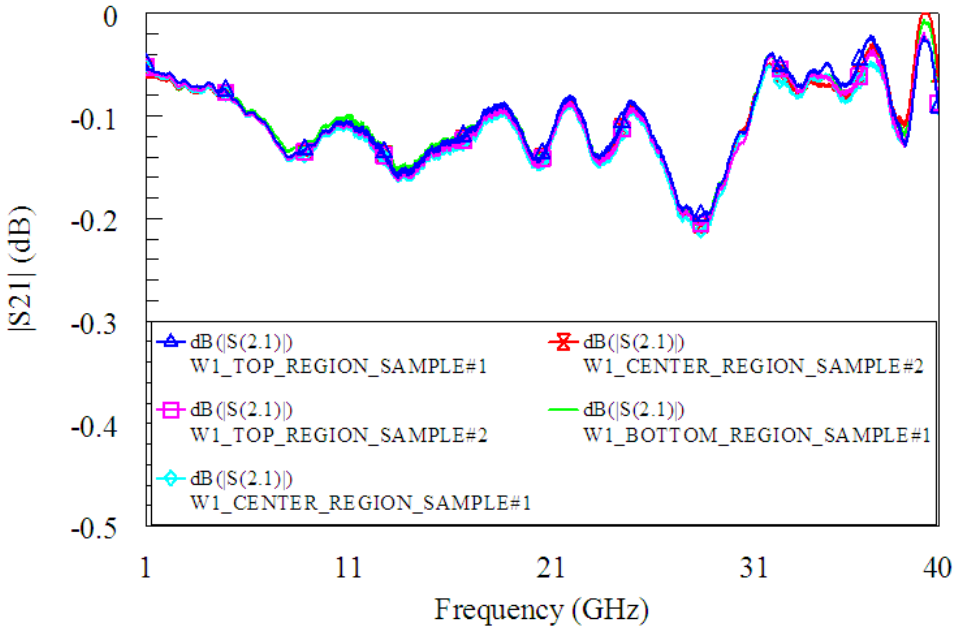

Figure 2.10: $|S_{21}|$ vs. frequency measurement for OFF-state of five sample switches

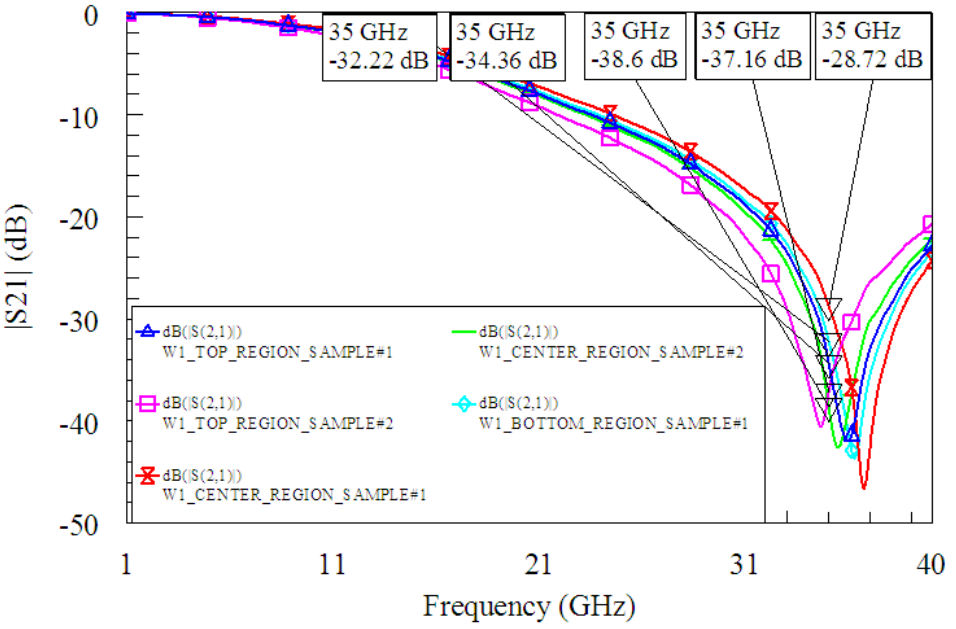

Figure 2.11: $|S_{21}|$ vs. frequency measurement for ON-state of five sample switches

2.4 METU RF MEMS Process

This chapter focuses on the fabrication details, the process steps and process improvements on the METU RF MEMS process.

Micromachining processes can be divided into two main groups according to their types: bulk micromachining and surface micromachining.

- Bulk micromachining uses a substrate to form the devices and substrate is etched.
- Surface micromachining is based on coating thin films on a substrate and patterning them to form the device structures.

METU RF MEMS process is a surface micromachining process developed in METU MEMS Center clean room facilities.

2.4.1 METU RF MEMS Process Steps

Illustrative process flow explanation is given below.

METU RF MEMS process consists of five layers which are base metal layer, isolation dielectric layer, sacrificial layer, structural metal layer, anchor reinforcement electroplating layer.

- First step is the base metal deposition step. The material used for base metal is *gold*. The deposition may either be done by evaporation or by sputtering according to the amount of wafers to be processed and the availability of deposition tools. If evaporation is used then *chromium* is deposited before *gold*. If sputtering is used then *titanium* is deposited before *gold*. Both *chromium* and *titanium* are deposited in tens of nanometers range for adhesion purpose since *gold* has very weak adhesion to the surfaces. Thickness of *gold* may change according to the measured resistivity. Typically it is ranging from 0.5 um to 1 um.
- The base metal is then patterned by photolithography to form the coplanar waveguide lines. (Figure 2.12)
- The second step is the deposition of isolation dielectric layer. Different material types can be used as the isolation dielectric according to their charging, breakdown characteristics and deposition conditions. In this study two different dielectric

materials have been used and investigated in terms of reliability. These are the *silicon nitride (Si_xN_y)* and *aluminum nitride (AlN)* materials. Thickness of these materials can be modified depending on the ON-state capacitance requirement. Typically Si_xN_y is deposited 0.3 um thick.

- Deposition of Si_xN_y could be done with the capabilities of METU MEMS Center facilities by using the plasma-enhanced chemical vapor deposition (PECVD) tool inside. For patterning the Si_xN_y again photolithography is used and etching is done by using the reactive ion etching (RIE) instrument inside the METU MEMS Center clean room. (Figure 2.13)
- Deposition of *AlN* could not be done in METU MEMS Center clean room so collaboration with Fraunhofer-Institut für Siliziumtechnologie (ISIT)-Germany has been established for *AlN* coating on the process wafers.[7] *AlN* has been coated at two different thicknesses: 0.3 um and 0.5 um.
- Etching of *AlN* could be done by TMAH based solutions. For this purpose TMAH based photoresist developer in the METU MEMS Center clean room specifically the MF24A solution is used with any dilution step. Using MF24A caused one more step to be added into the process flow. Since MF24A is basically a photoresist developer it can etch the photoresist. While applying photolithography on the *AlN* layer the photoresist to be spun on the *AlN* layer should be patterned first to make a mask for *AlN* layer and then the *AlN* should be patterned. While patterning the photoresist MF24A can etch both the photoresist and the *AlN* resulting with an inappropriate patterning of *AlN* layer. To prevent this undesired result a *titanium* hard mask is used for patterning the *AlN*. *Titanium* is sputtered on the *AlN* layer. This *titanium* layer is patterned by photolithography. *AlN* layer is patterned by MF24A where the *titanium* mask has protected the *AlN* at certain regions. *Titanium* layer has been stripped off. So patterning of the *AlN* layer has been completed. (Figure 2.13)
- The patterned isolation dielectric layer is used to prevent the DC shortage between signal and ground in capacitive contact switches when the actuation voltage is applied between signal and ground terminals.
- Next step is the sacrificial layer formation. In surface micromachining technology sacrificial layers should be used to create suspended structures. As the name

[7] Coatings have been done by Hans-Joachim Quenzer and his research group.

indicates sacrificial layers are removed at the very end of process. Different materials such as photoresist and copper are tried as sacrificial layers but none of them gave satisfactory results due to outgas, cracking, easy solubility in several solvents and non-uniform growth problems. Finally the polyimide material is determined to be used as the sacrificial layer [91]. Polyimide is an organic material which is resistant to many solvents and etchants used in the following process steps and can be easily coated uniformly by spin.

- Two types of polyimides are used in METU RF MEMS process; *PI2737* and *PI2610*. *PI2737* is a photodefinable one so that it can be exposed with UV light and patterned in its specialized developer solution. *PI2737* is used to obtain sacrificial layer thickness of 1.5 um or higher in METU RF MEMS process and *PI2610* is used to be able to take the sacrificial layer thickness down to 1 um with high spin speed. *PI2610* is a non-photodefinable material so that UV expose has no effect on it. Like in the *AlN* patterning case a *titanium* hard mask together with photoresist is used to add one more protective layer while etching the *PI2610* in the RIE equipment. Patterning of sacrificial polyimide layer is needed to form the anchor regions of the RF MEMS bridge. These regions are the openings of sacrificial polyimide layer seen from the cross-sectional view in Figure 2.14.
- The following step is the deposition of structural layer metal which forms the RF MEMS switch membrane. In METU RF MEMS process *gold* is used as the structural layer metal and it is coated by sputtering. No adhesion layer such as *chromium* or *titanium* is used since the structural *gold* layer can attach to the base metal *gold* layer through the openings of sacrificial polyimide layer. (Figure 2.15) Since structural layer is the moving part of an RF MEMS switch its stress level and thickness is important. The stress level and thickness are directly effective on the value of spring constant, *k*, and so are on the pull-in voltage as seen from Equation (2.1). Not to introduce a stress on the bridge layer a stress-free recipe in the sputtering tool is developed.
- After structural layer formation to reinforce the RF MEMS bridges at their legs, the anchor points are filled with *gold* by using electroplating tool. Although electroplating is a strongly non-uniform process *gold* thicknesses more than 3-4 um can be achieved in short times and in a selective way which means that no etching is required after electroplating; only the desired regions are electroplated. (Figure 2.16)

- After electroplating structural metal layer patterning step comes. The bridge regions and the electroplated regions are protected by the photoresists mask and remaining parts are etched away in the *gold* etchant. The important point here is the openings on the bridge which are called etch holes. (Figure 2.17) The etch holes are critical because of squeeze film damping effect and the sacrificial polyimide layer removal step. The existence of etch holes reduces the squeeze film damping during the actuation and release of the switch hence resulting with a shorter switching time. Other advantage of etch holes occurs in the sacrificial polyimide layer removal step which will be mentioned in that part. Etch holes definitely reduce the bridge area which in turn comes with a reduction in OFF-state capacitance so the designer should take this fact into account. ON-state capacitance is not affected much by the etch holes since the fringing fields can compensate the decrease in bridge area [2].
- Following the structural metal layer patterning, the sacrificial polyimide layer should be removed to form the suspended bridges. (Figure 2.18) A wet etching method is developed for METU RF MEMS process[8] and it is used as the conventional method in METU MEMS Center clean room for sacrificial polyimide layer removal in RF MEMS processes. For this purpose the EKC265 chemical is used. The etch holes come into play at this point. In the absence of etch holes the EKC265 can reach the polyimide layer under the bridge only from the directions shown by *red* arrows in Figure 2.19-a. When there are etch holes the EKC265 can reach the polyimide under the bridge from the directions shown by *red* arrows and additionally through the etch holes shown by *black* arrows in Figure 2.19-b. Obviously EKC265 can reach the polyimide under the bridge from only two sides in Figure 2.19-a and this causes a strip of polyimide residue to remain under the center region of the bridge as photographed in Figure 2.20. This residue is the failure of process since while staying under the bridge it prevents actuation of the RF MEMS switch.
- The last step of the METU RF MEMS process is cleaning of EKC265 and drying of the samples. De-ionized water (DI water) and ultra pure isopropyl alcohol (IPA) cleaning is done respectively on the samples. After IPA cleaning the wafer is taken into the critical point drying (CPD) tool for drying operation. IPA cleaning is a

[8] The method is developed by Dr. Kağan Topallı and Dr. Mehmet Ünlü.

required intermediate step since the CPD tool accepts the samples into the chamber only with ultra pure alcohols. CPD changes the IPA with liquid CO_2 inside the chamber and carries the CO_2 to its supercritical point where the separation line between liquid and gas phases seen in phase diagram disappears. CO_2 is exhausted then in the form of gas leaving a dry environment behind. The samples could also be left directly after cleaning but as the ordinary liquid to gas transition occurs the bridges would definitely stick down due to surface tension forces. CPD prevents this by avoiding the ordinary liquid to gas transition.

- After CPD the samples are ready for measurement. (Figure 2.18)

Figure 2.21 presents the photograph of a successfully fabricated RF MEMS switch.[9] The RF MEMS bridge, anchor electroplating regions and etch holes are clearly seen in Figure 2.21.

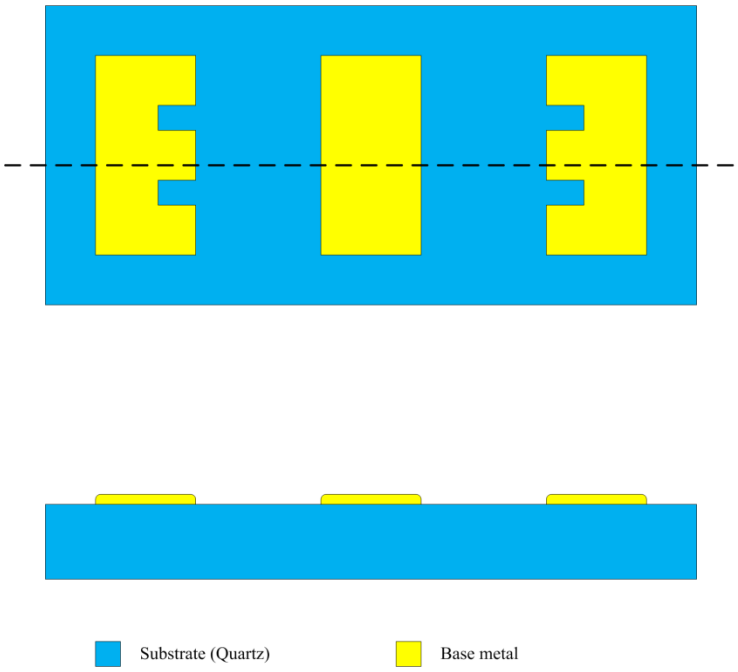

Figure 2.12: Base metal gold deposition and patterning

[9] The photographed switch is chosen from *MS10.1-W1*.

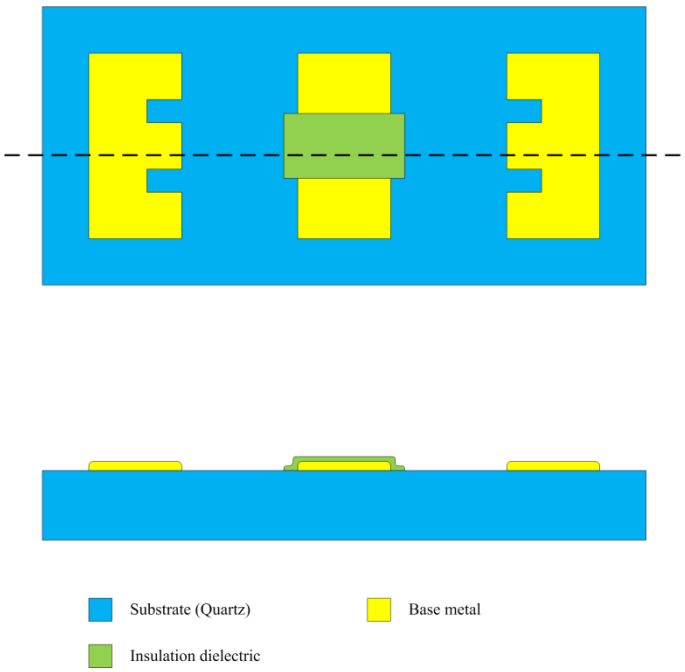

Figure 2.13: Isolation dielectric layer deposition and patterning

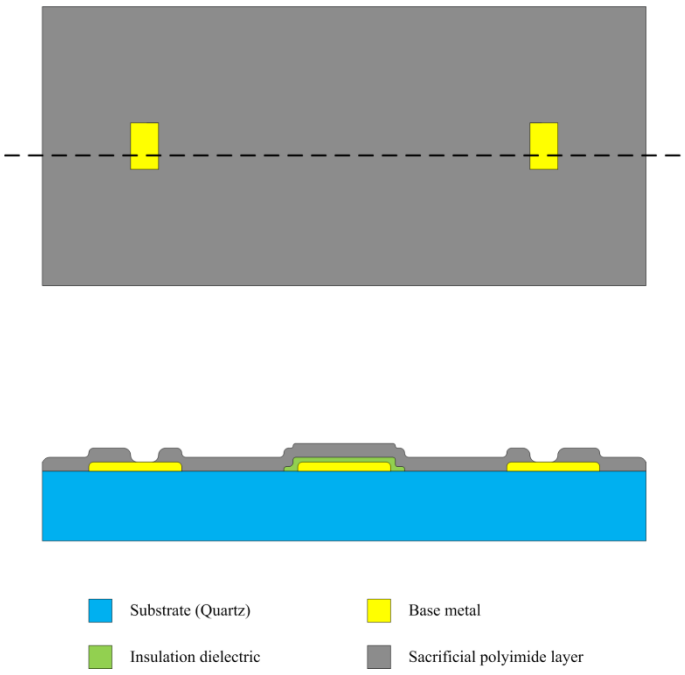

Figure 2.14: Sacrificial polyimide layer deposition and patterning

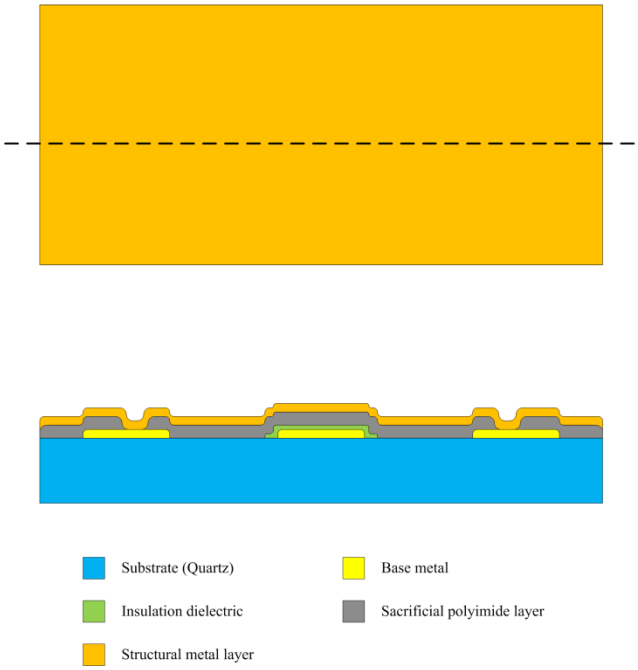

Figure 2.15: Structural metal layer deposition

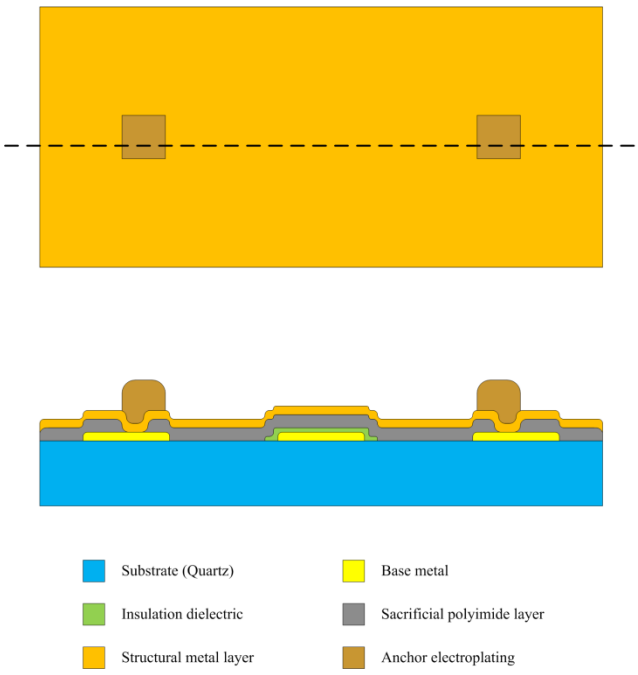

Figure 2.16: Anchor reinforcement electroplating

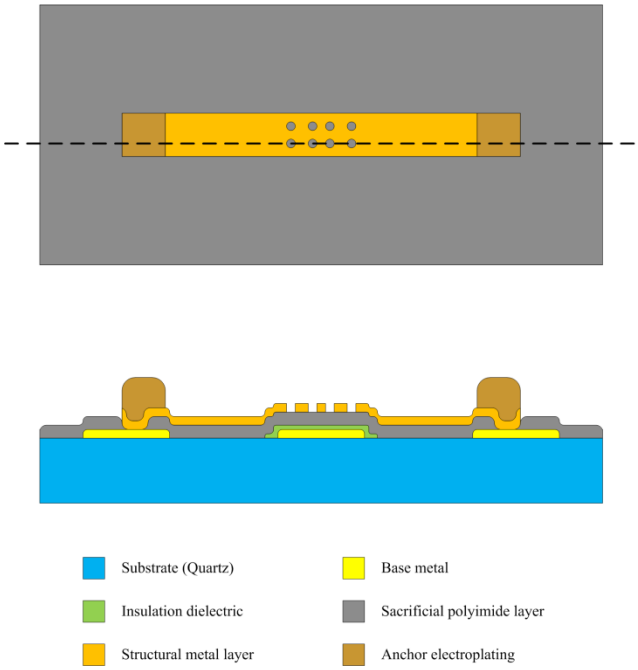

Figure 2.17: Structural metal layer patterning

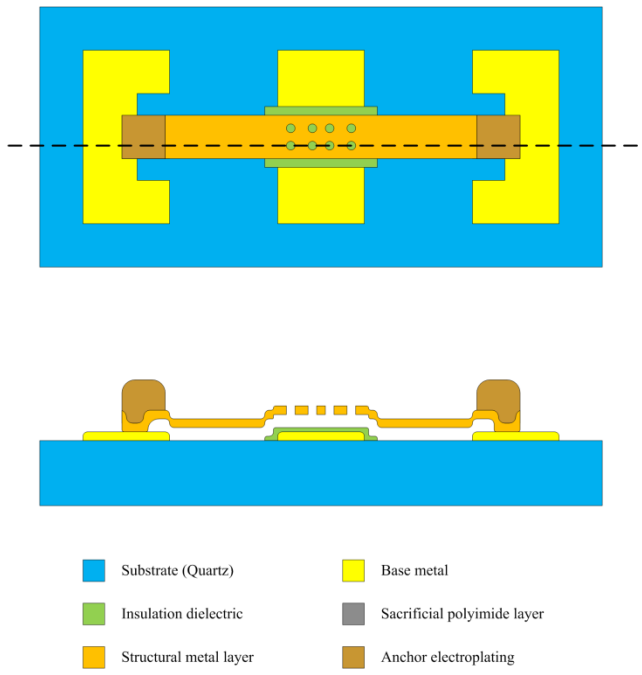

Figure 2.18: Sacrificial polyimide layer removal

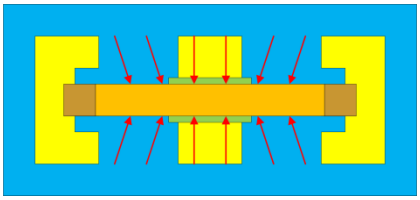

(a)

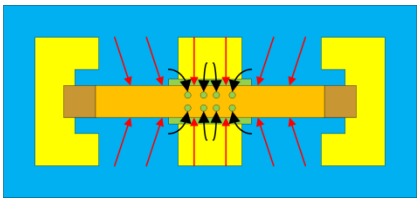

(b)

Figure 2.19: Comparison of cases with and without the etch holes

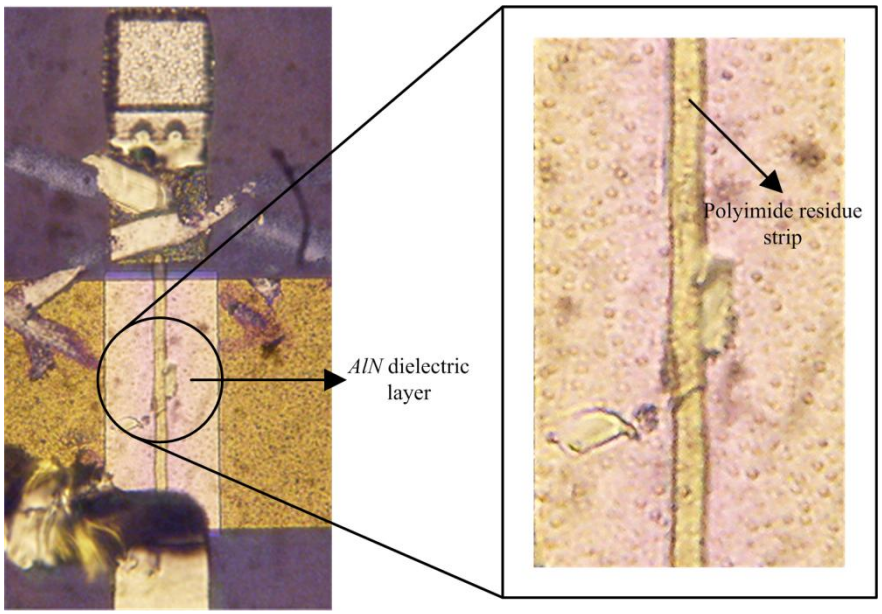

Figure 2.20: Close-up view of polyimide residue strip when there are no etch holes

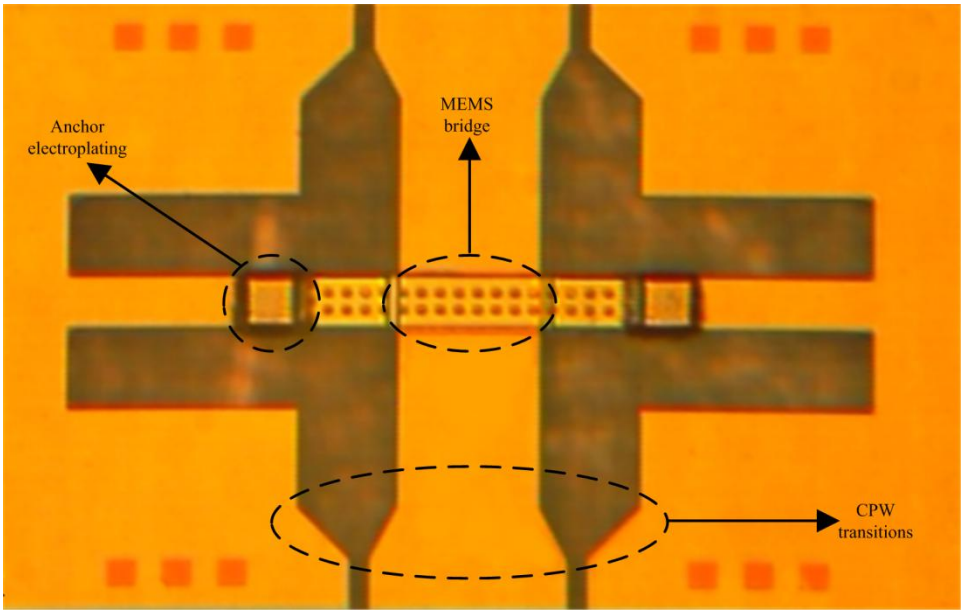

Figure 2.21: A fabricated RF MEMS switch photograph

2.4.2 Improvements on the METU RF MEMS Process

Throughout the RF MEMS studies in METU there have been many modifications on the RF MEMS process but two of these have great contributions in terms of reliability since the last reliability study completed in the METU RF MEMS Research Group [92]. This chapter is dedicated to these two improvements:

- Adding the anchor electroplating step to the process flow
- Extending the ground layer under the bridge towards the signal line

Anchor electroplating step adds thick structures to the bridge legs which definitely increases mechanical stiffness of the bridge. Anchor electroplating provides almost immobile pinch points for the fixed-fixed beam which is advantageous with respect to other case. (Figure 2.22)

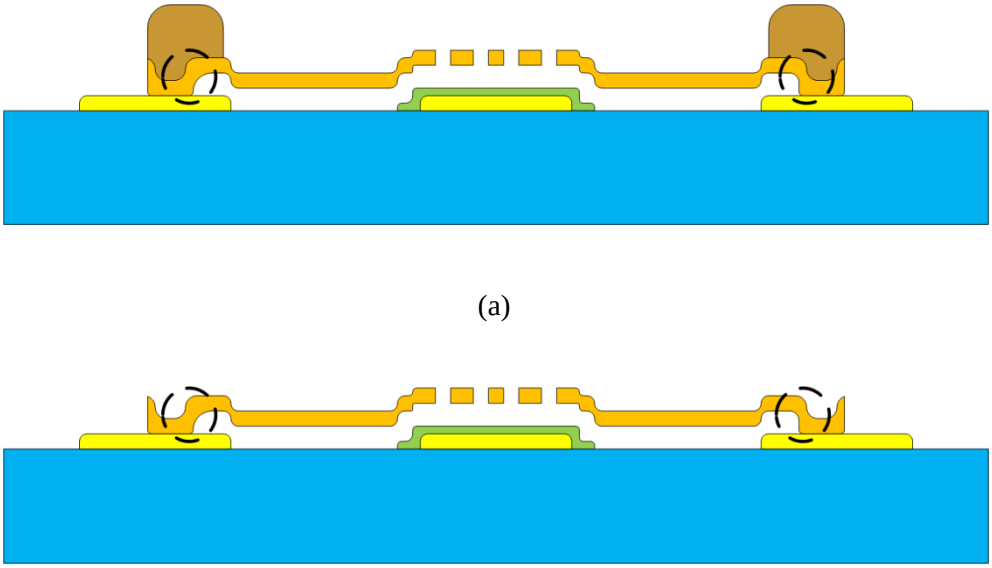

(a)

(b)

Figure 2.22: Cross-sectional illustration of switches with and without anchor electroplating

Another improvement is the anchor extension idea.[10] Due to the conformal coating property of polyimides, either *PI2737* or *PI2610,* the structural metal layer has step-up points at the signal line edges. (Figure 2.23-a) This decreases strength of the bridge causing the center region of bridge to buckle down to a level lower than the desired. The anchor extension idea proposes to extend the ground part under the bridge to a closer point to the signal line (Figure 2.23-b) so that the polyimide layer would not be able to make a conformal cover over the very small area between the signal and ground resulting with a smaller step-up, stiffer bridge and no downward buckling of center region of the bridge.

[10] This idea is developed by Dr. Kağan Topallı, Dr. Mehmet Ünlü and Çağrı Çetintepe.

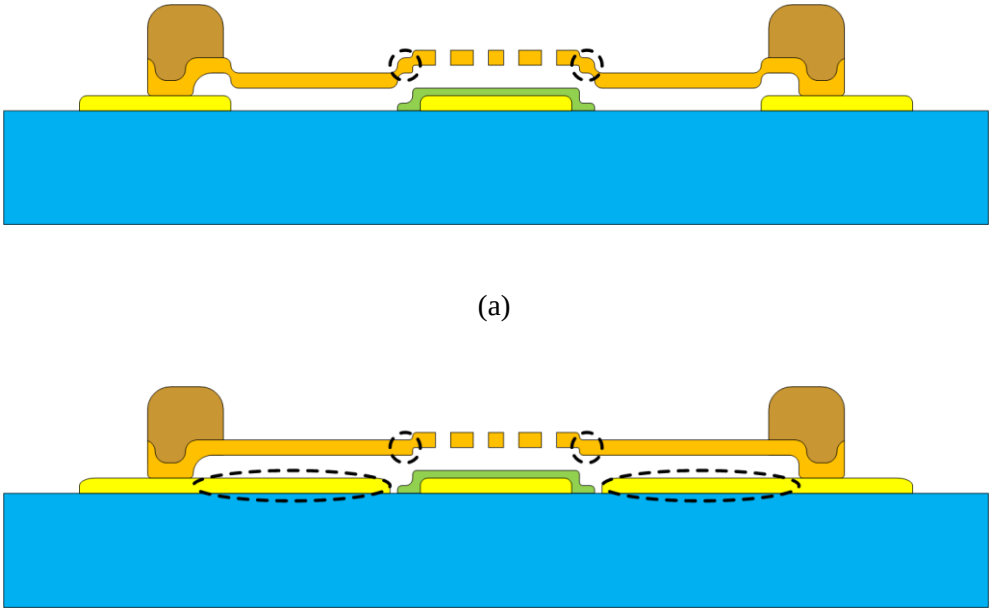

(a)

(b)

Figure 2.23: Cross-sectional illustration of comparison between switches with and without anchor extensions

Anchor extensions have provided enhancement of mechanical properties in a different way, the proposed idea has not worked. According to the idea the polyimide layer would not be able to cover the narrow low level region conformally between the signal and the ground so that it would pass over in a flat manner resulting with a small step-up height which is equal to only isolation dielectric layer thickness and the stiffer bridge would not buckle down. It is verified by optical profiler measurements on many switch samples with anchor extensions from several different wafers that the bridges still buckle down so that the targeted bridge heights could not be achieved precisely but the same optical profiler measurements have shown that height of the bridge in center region is the same with the bridge height in side regions both for the switches with and without anchor extensions. (Figure 2.24) A simple mechanical model is proposed to explain this fact. The bridge at the center and side regions are modeled by beams and the step-up parts of bridge between center and side region are represented by springs. The tensile stress applied laterally to the bridge depicted by *horizontal* arrows in Figure 2.24, most probably by the high stress level of anchor electroplating regions, might cause the beams to align horizontally. The spring

structures decrease the stiffness of the bridge probably causing the center and side regions to come to the same height.

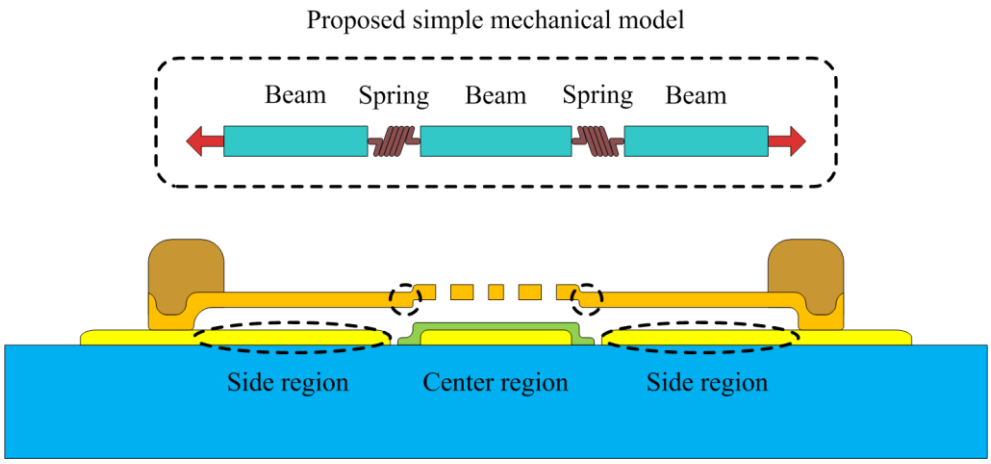

Figure 2.24: Simple mechanical model proposed for RF MEMS switch with anchor extensions

Figure 2.25 gives the optical profiler measurement results of a switch with anchor extensions and Figure 2.26 shows the results for a switch without anchor extensions.[11] The thickness values of layers measured from dedicated thickness monitoring structures on the wafer are given in Table 2.3.

X profile measurements in Figure 2.25 and Figure 2.26 give the height difference between structural metal layer surface and base metal surface so a thickness equal to sum of base metal thickness, isolation dielectric layer thickness, sacrificial polyimide layer thickness and structural metal layer thickness is expected. In Figure 2.25 this height difference for the switch with anchor extension (SWAE) is measured to be 3.198 um and in Figure 2.26 for the switch without anchor extension (SWoAE) it is measured as 2.812 um. In both cases this value is expected to be 3.4 um. Amount of deflection downward for SWAE is nearly 0.2 um and for SWoAE it is almost 0.6 um.

[11] Both switches are selected from the center region of *MS10.1-W1*.

Y profile measurements in Figure 2.25 and Figure 2.26 give the height difference between the center and side regions of the RF MEMS bridge. This measurement value should be equal to the thickness of isolation dielectric since the only height difference between center and side regions is caused by the isolation dielectric. (Figure 2.24) For both SWAE and SWoAE this height difference is measured as 0. It is obvious from this result that independent of the existence of anchor extension, the structural metal layer level in center region and side region are the same. Since side region height of SWAE is expected to be higher than side region height of SWoAE with an amount of base metal thickness the bridge height for SWAEs will definitely be closer to the expected height than the SWoAE.[12] This is the obvious advantage of anchor extensions.

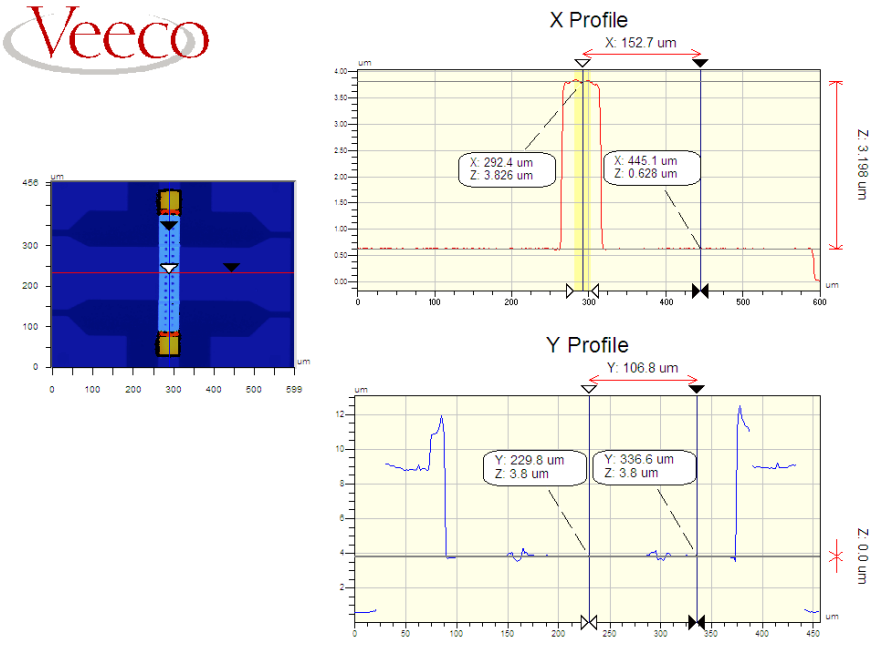

Figure 2.25: Optical profiler measurement for a switch with anchor extension

[12] Amount of deflections for both SWAE and SwoAE is lower than the expected deflection values since the side region heights for SWAE and SWoAE are measured to be higher than the expected values. Most probably due to the lateral force created by tensile stress of anchor electroplatings caused the side regions to buckle up resulting with greater heights than expected.

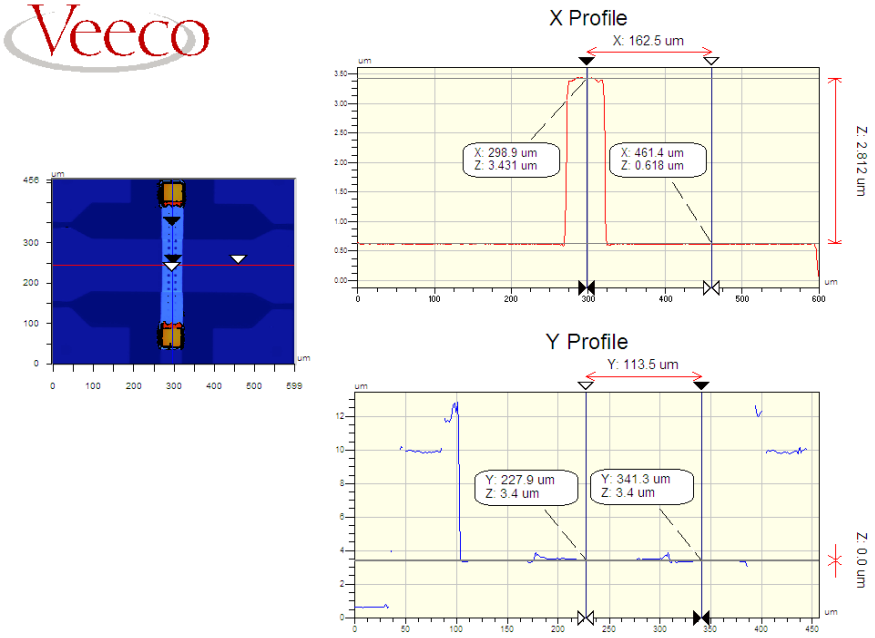

Figure 2.26: Optical profiler measurement for a switch without anchor extension

Table 2.3: Measured layer thicknesses for center region of *MS10.1-W1*

Layer name	Thickness (um)
Base metal	0.6
Isolation dielectric	0.3
Sacrificial polyimide	1.6
Structural metal	1.5

2.4.3 Future Process Improvements

A method to avoid the bridge buckle down can be proposed as a future work. As the center regions of bridges will come to the same level with the side regions, the isolation dielectric on the side regions might also be protected by a change in photolithography mask of isolation dielectric patterning step and so the structural metal layer on the side region will

be higher (Figure 2.27) By this way the RF MEMS bridge might be fabricated at the desired height.

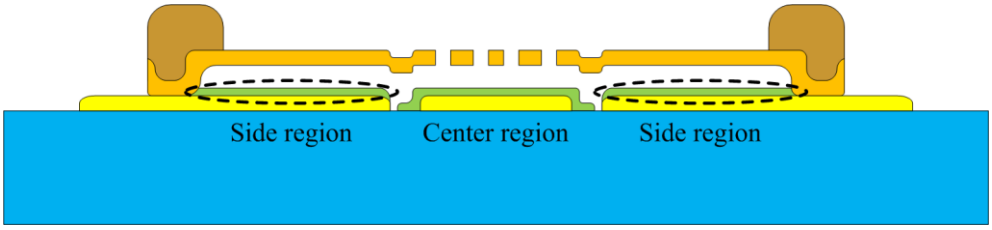

Figure 2.27: Illustration of the switch when the isolation dielectrics on the side regions are not etched away

As an alternative to the proposed way of protecting the isolation dielectric layer on side regions the step-up points on the bridge can be eliminated by planarizing the surface of the sacrificial polyimide layer just after spin. By this way the dips of sacrificial polyimide layer between center and side regions will be flattened and deposited structural metal layer will have a smooth profile. For this purpose precisely controlled chemical mechanical polishing (CMP) operation can be used.

2.5 Conclusion

This chapter has given a brief introduction on RF MEMS switches, their types and their basic properties. The switch type of interest in METU RF MEMS Research Group is explained and an overview on design of a Ka-band, shunt, capacitive contact RF MEMS switch is provided. The mm-wave measurement results are presented to show that the electromagnetic design specifications have been met at the end of a successful fabrication. The details of METU RF MEMS process are given and the steps are listed. Improvements on the METU RF MEMS process are explained and further improvements are proposed.

CHAPTER 3

RELIABILITY AND LIFETIME MEASUREMENT SETUP

High reliability and long lifetime are key components of a developing technology while passing from research to commercial availability as is the case for RF MEMS. As the RF MEMS technology gained popularity in the microwave world the reliability problems soon appeared. To identify and overcome these problems many studies have been done [60, 61, 63-67, 70-72, 74-77, 79, 81, 83, 84]. As a result of these studies it is found that many factors exist affecting the lifetime of an RF MEMS device such as the environmental effects, material impacts. This gives rise to the requirements for dedicated reliability and lifetime measurement setups providing control over some parameters directly related to reliability. Since a common standard for testing the RF MEMS devices has not been defined, all mentioned setups in the literature are custom designs [61, 65, 67, 72, 79, 92]. This chapter is dedicated to the designed and implemented reliability and lifetime measurement setup developed for the reliability research in METU RF MEMS Research Group.

3.1 Introduction

For the reliability studies in METU RF MEMS Research Group a setup is established mostly consisting of commercial products. Idea of the form of the setup has originated from the publications in the literature.

Most commonly two types of measurements are done to evaluate the performance of RF MEMS devices as seen from the publications in the literature:

- Time domain measurements
- CV measurements

3.1.1 Time Domain Measurements

Time domain measurement setups in the literature are used for lifetime monitoring of the tested RF MEMS devices [65-67]. The idea is to measure a parameter of the switch with time and record it. The parameter should give information about performance of the switch so that the degradation during operation could be monitored. The parameters used in the studies can be listed as follows:

- A high frequency signal can be applied to the input of the switch and the output signal power can be monitored.
- At certain times with a slow sweep of applied voltage the pull-in and hold-down voltages can be extracted.
- Hybridization might be done and both the output signal power and pull-in and hold-down voltages can be monitored.

If the output signal power detection method is used, generally a cycling actuation waveform is applied to open and close the RF MEMS switch with the actuation waveform frequency. The main aim is to extract the modulation effect of mechanical movement of the RF MEMS switch on the high frequency signal to give a demodulated final output. (Figure 3.1) There are two alternative ways for this measurement that should be mentioned in the test results. These are the switching types:

- **Cold switching:** Just before the instant of switching (OFF to ON or ON to OFF-state transition) the high frequency signal is interrupted and just after switching the high frequency signal is applied so that the switch does not sense any applied signal during the transitions. This can be easily seen from the simple illustration in Figure 3.2.
- **Hot switching:** During hot switching the high frequency signal is never terminated so the switch senses the signal even during the state transitions.

Cold switching is generally used for ohmic contact switches since the signal power might cause undesired arcs during the transitions. Hot switching is generally used for capacitive

contact switches since there is no difference for a capacitive switch due to the absence of a direct physical contact.

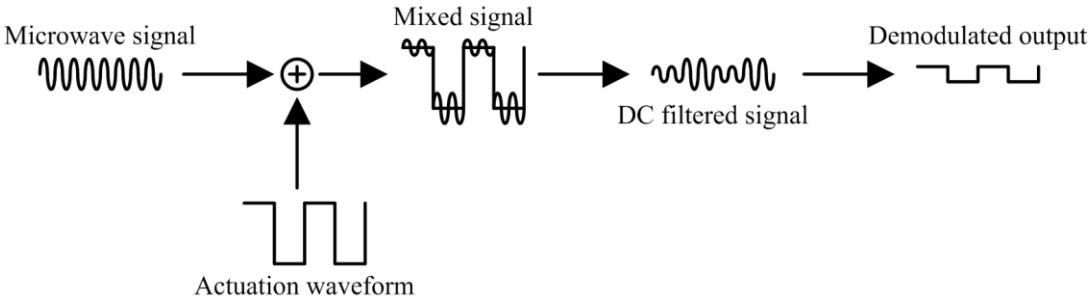

Figure 3.1: Signal operations in the time domain measurement setup

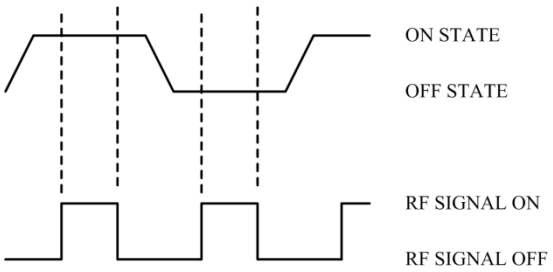

Figure 3.2: Simple actuation waveform and RF signal illustration for cold switching

3.1.2 CV Curve Measurements

CV curve measurement is a method to evaluate the performance of an RF MEMS switch at only certain times. The differences between the CV curves before and after the actuation are investigated in the studies [63, 64, 71, 79, 84].

The capacitance of the RF MEMS switch is measured by a capacitance measurement unit while sweeping the applied voltage. The capacitance value follows a path like shown in Figure 3.3. While increasing the voltage OFF to ON-state transition occurs at pull-in

voltage (Figure 2.2) and while decreasing it ON to OFF-state transition occurs at hold-down voltage (Figure 2.2). By CV curve measurements both the performance degradation can be figured out and the pull-in and hold-down voltage shifts can be found.

For the reliability and lifetime measurement setup both time domain and CV curve measurement setups are established for more comprehensive measurements.

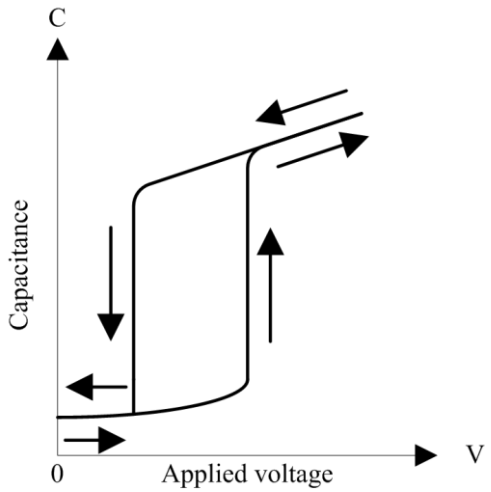

Figure 3.3: A CV curve measurement hysteresis behavior illustration

3.2 METU RF MEMS Research Group Reliability and Lifetime Measurement Setup

This section is a detailed part on the METU RF MEMS Research Group Reliability and Lifetime Measurement Setup (ReLiMS).

ReLiMS consists of two main parts as mentioned in Section 3.1.2; time domain measurement and CV curve measurement. Time domain measurement setup employs a high frequency signal generator together with a bias waveform generator structure. The high frequency signal and the actuation waveform is mixed with a bias tee and applied to the RF MEMS switch on a probe station. The output is measured by a detector and detector

output is recorded. An overall illustration of the ReLiMS showing both the time domain and CV measurement setups can be seen from Figure 3.4.

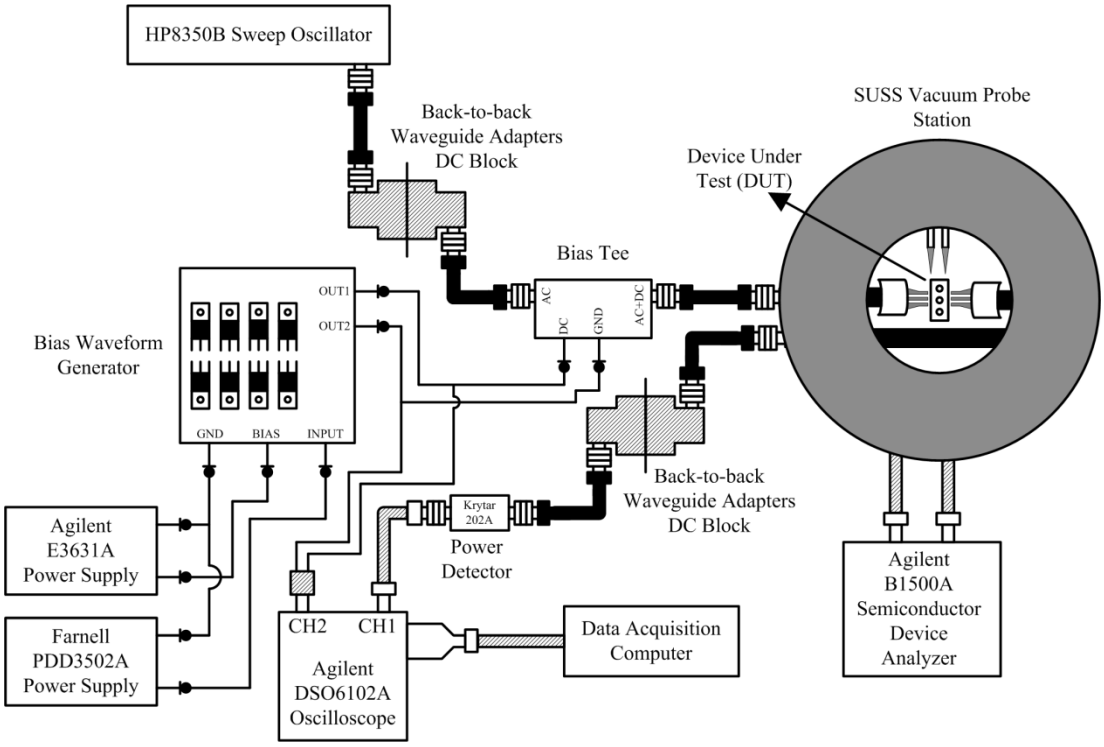

Figure 3.4: Illustration of the ReLiMS

3.2.1 Time Domain Measurement Setup

The time domain measurement setup is established mostly of commercial products and instruments for real-time performance evaluation. With this setup both RF performance degradation and switching times can be determined.

The RF signal power level at the output is recorded and hence the transmitted power difference between OFF and ON-state can be measured. Also from the transition times between OFF and ON-states the switching times can be determined.

3.2.1.1 Signal generation

For the microwave signal generation a sweep oscillator, HP8350B, is operated at a single frequency (Figure 3.1). After establishment of the whole setup according to the overall response 19.95 GHz is determined as the testing frequency and output of the sweep oscillator is set to 15 dBm since the most easily measured output data from the ReLiMS are obtained for this frequency.

3.2.1.2 DC blocking structure (Input)

To protect the signal generator against the high voltage actuation waveform that might leak from the next bias tee stage a DC blocking structure is used just after the signal generator. One of the DC blocks used in the setup can be seen from Figure 3.5. Two WR90 waveguide adapters are back-to-back connected to each other which allows the microwave signal transmission but blocks the actuation waveform. A dielectric layer has been placed between the adapters to enhance the isolation level. The frequency responses of DC blocks are also measured. The transmission characteristics ($|S_{21}|$) are given in Figure 3.6 for both blocks. Note that the response degrades as going to high frequencies most probably due to higher-mode generations in the WR90 waveguide adapters outside the X-band.

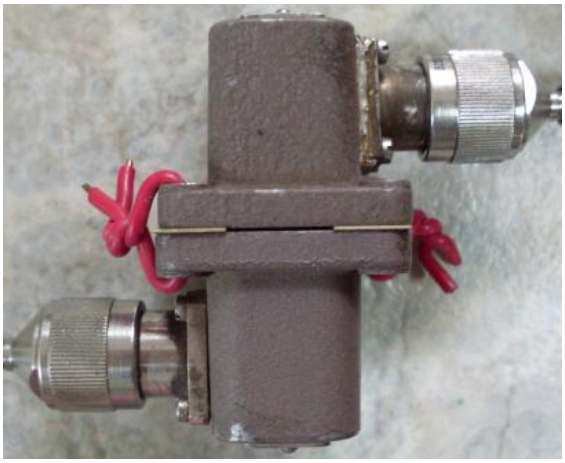

Figure 3.5: DC block (Back-to-back waveguide adapters)

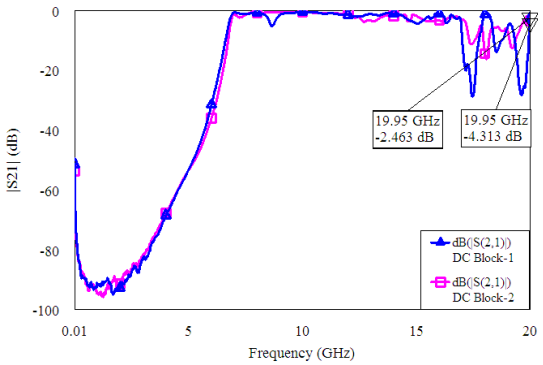

Figure 3.6: Transmission characteristics of DC blocks in the ReLiMS

3.2.1.3 Bias Tee

A Picosecond Labs bias tee is used to mix the microwave signal and the actuation waveform to apply together on the RF MEMS device when the bias waveform is applied between RF signal line and the RF ground plane. A bias tee is simple a combination of an inductor and a capacitor (Figure 3.7). Bias tee is responsible for forming the mixed signal seen in Figure 3.1.

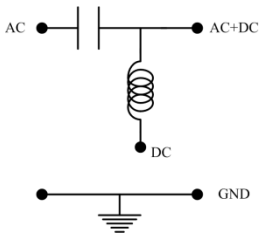

Figure 3.7: Simple circuit diagram for a bias tee

3.2.1.4 Bias waveform generation

To generate the actuation waveform two devices are used for different actuation waveforms. One is a commercial product, Agilent 8114A High Power Pulse Generator.

The other is a specially designed[13] high voltage waveform generator card [92]. The photograph of the waveform generator card (WGC) is given in Figure 3.8 and the simplified schematic is given in Figure 3.9.

The operation principle of WGC is simply controlling the transistors by digital signals to generate the actuation waveform. Required digital signals are produced by the microcontroller, PIC16F877, and applied to the gate driver integrated circuit chips. Gate driver circuits are the interfaces between digital signal generation part and the high power part. Gate drivers might be considered as the amplification stage of the digital controlling signals because of the fact that digital controller may not be able to drive the power transistors of the output stage. Gate drivers as the name indicates are connected to the gates of power transistors and digital signals are applied to the gates of transistors through gate drivers. The simplified schematic in Figure 3.9 indeed shows the output stage of WGC. Gates of the transistors are biased with the control circuitry and the path from power supply to the output is opened or closed. With WGC arbitrary period, arbitrary duty cycle rectangular actuation waveforms can be obtained. (Figure 3.1)

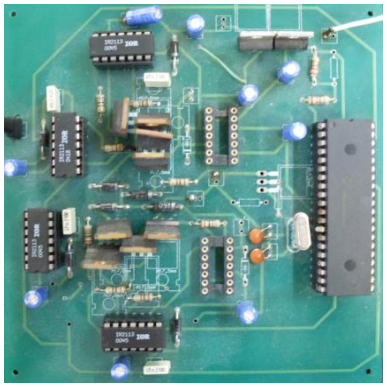

Figure 3.8: Photograph of the waveform generator card

[13] The design and implementation is done by a former METU RF MEMS Research Group member, Halil İbrahim Atasoy. Later one more implementation of the card is done by the author.

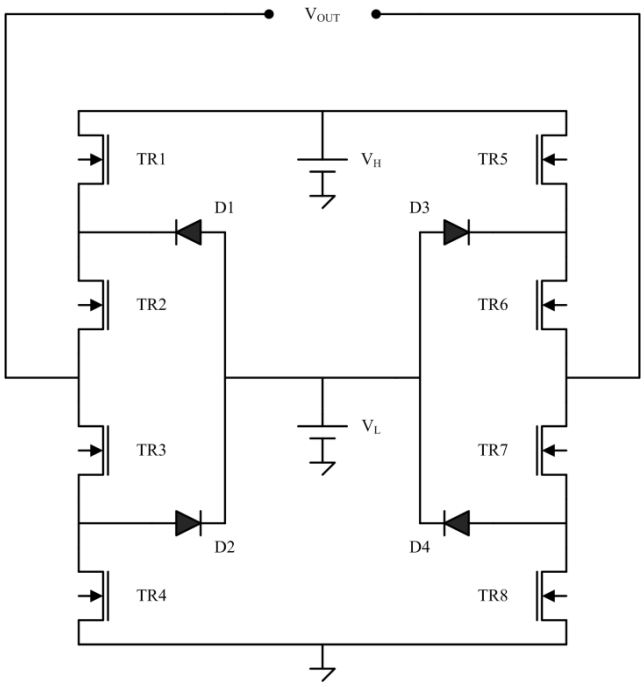

Figure 3.9: Waveform generator card simplified schematic

3.2.1.5 Vacuum Probe Station

The measurement environment for micromechanical devices is important so a controlled chamber is needed. To obtain the controlled environment a SUSS PMV200 probe station is used which is a huge chamber that allows the environmental gas, pressure and temperature control. Both high frequency and DC measurements can be done with the SUSS probe station since it can take both RF and DC probes inside. The RF probes are part of the time domain measurement setup and the DC probes are part of the CV measurement setup.

3.2.1.6 DC block (Output)

Output of the vacuum of the probe station is directly connected to the DC block to protect the power detector from high voltage bias waveform. This DC block provides the DC filtered signal seen in Figure 3.1.

3.2.1.7 Power detector

The DC filtered signal at the output of DC block should be demodulated by a structure to give the demodulated output. (Figure 3.1) For this purpose a Krytar 202A Zero Bias Schottky Detector is used. Krytar 202A detector is chosen among four candidates. The three alternatives are a HEMT (FHX13LG), a crystal power detector (HP423A) and another crystal power detector (Omega). Different methods are applied on the detectors to investigate the switching performances.

Figure 3.10 shows the HEMT connected to a fixture with SMA connectors [92] and Figure 3.11 shows the photo of a Krytar 202A detector [93]. Input of Krytar 202A is the 3.5 mm male connector and output is the SMA female connector.

For speed characterizations of the detectors three different amplitude modulation ways are used; internal modulator of sweep oscillator, HP8350B, external modulation of HP8350B with an Agilent 33220A Arbitrary Waveform Generator (AWGC) and the ReLiMS itself since the switch mechanical movement causes amplitude modulation on the microwave signal generated by HP8350B. The internal modulator of HP8350B applies a 27.8 kHz amplitude modulation signal on the high frequency signal. The modulations on the high frequency signal are detected by the Agilent DSO6102A Digital Storage Oscilloscope (DSO) at the characterization step. The term fall-time in this section indicates the required time for coming from OFF-state to ON-state and the term rise-time accounts for vice versa.

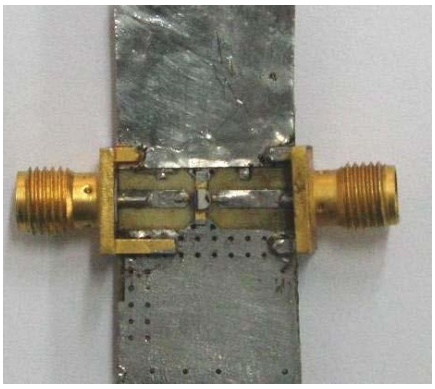

Figure 3.10: The HEMT (FHX13LG)

Figure 3.11: Krytar 202A detector

FHX13LG was used as the detector in the former lifetime measurement setup of METU RF MEMS Research Group[14] so firstly FHX13LG is characterized.

Figure 3.12 shows the FHX13LG output when internal modulation is applied on the microwave signal. Obviously the transistor can track the changes properly with an overshoot for the OFF-state case but with stable output response. Fall-time is close to 75 nsec (Figure 3.13-a) and rise-time is close to 50 nsec (Figure 3.13-b) which can be considered to be fast compared to the usec order transition times of RF MEMS switches. The problem with FHX13LG occurs at the modulation frequencies close to the actuation frequencies that we use in lifetime measurements. Figure 3.14 shows the FHX13LG response for external modulation of 1 kHz with Agilent 33220A on HP8350B. Figure 3.15 shows the FHX13LG response for external modulation of 50 Hz with Agilent 33220A on HP8350B. Note the distorted output waveforms of FHX13LG from Figure 3.14 and Figure 3.15. By thinking in the bi-state context the up and down movement of the RF MEMS switch can be realized from the output responses similar to ones in Figure 3.14 and Figure 3.15 but microwave performance of the switch can not be monitored properly. Another disadvantage is about the measurement of switching times. The detector output itself can not settle down properly preventing the measurement of rise and fall-times of the RF MEMS switch so FHX13LG is eliminated from the alternatives list.

Next measurements belong to the comparison between HP423A and Omega. For a fair comparison, measurements for both detectors (Figure 3.16 and Figure 3.17) are performed with completely the same settings such as the identical microwave and amplitude

[14] The former setup was established by Halil İbrahim Atasoy and the details of that setup are given in [92].

modulation (AM) signals. Figure 3.16 shows the rise and fall-times of Omega detector for external AM of 50 Hz with Agilent 33220A on HP8350B. Figure 3.17 shows the rise and fall-times of HP423A detector for external AM of 50 Hz with Agilent 33220A on HP8350B. Fall-time is 4.4 usec and rise-time is 4 usec for Omega detector. Fall-time is 21.2 usec and rise-time is 12 usec for HP423A detector. Superiority of Omega over HP423A in terms of speed is obvious but Omega detector has responses with overshoot for both OFF-to-ON-state transition and ON-to-OFF-state transition. Measurement of rise and fall-time from a response with overshoots might not be so reliable so Omega should not be preferred instead of HP423A since one of the aims of time domain measurement setup is to determine the switching times of RF MEMS switches.

Following measurements are for comparing the HP423A and Krytar 202A detectors in terms of speed. For this comparison external modulation signal is not used but an actuation waveform is applied to a switch resulting with the AM of mechanical movement of RF MEMS switch on the microwave signal. For both detector measurements actuation frequency is kept at 25 Hz. Fall-time is 16.8 usec (Figure 3.18-a) and rise-time is 21.5 usec (Figure 3.18-b) for HP423A detector. Fall-time is 3.6 usec (Figure 3.19-a) and rise-time is 6.3 usec (Figure 3.19-b) for Krytar 202A detector. Definitely Krytar 202A has a better speed performance than the HP423A detector. Additionally since there are no overshoots in the Krytar 202A response it is selected to be used in time domain measurement setup.

After employing Krytar 202A in the setup it should be characterized for the recorded data to make sense. To evaluate Krytar 202A data a conversion table between output voltage of Krytar 202A and power input to the Krytar 202A is needed. For this purpose at the operation frequency power output of HP8350B is swept over a range and power at the input of Krytar 202A is measured by an Agilent E4408B ESA-L Series Spectrum Analyzer. The corresponding detector output voltage is recorded. The measurement result is given in Figure 3.20. To be able to make interpolation a curve which is also shown in Figure 3.20 is fitted on the data points. Parameters of the fitted curve are given in Table 3.1. From the same measurement also the loss of the system from HP8350B output to the Krytar 202A input is found to be approximately 22.7 dB.

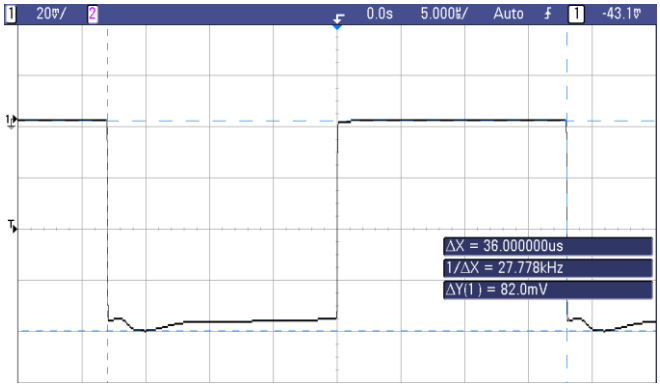

Figure 3.12: FHX13LG response, internal modulation of HP8350B

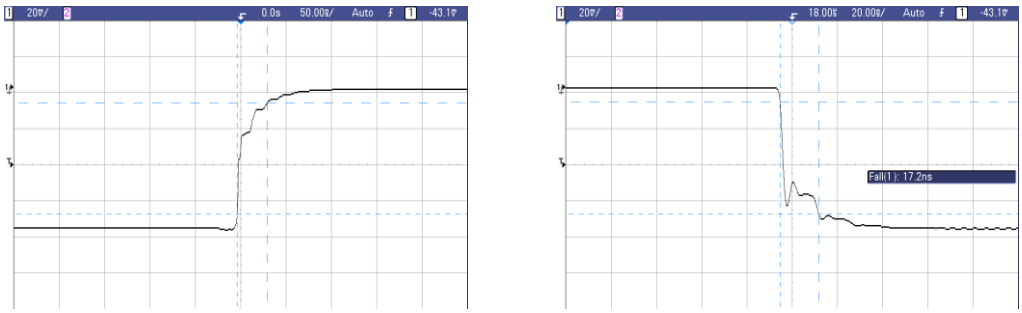

(a) Fall-time (OFF-to-ON-state transition) (b) Rise-time (ON-to-OFF-state transition)

Figure 3.13: FHX13LG response, internal modulation of HP8350B

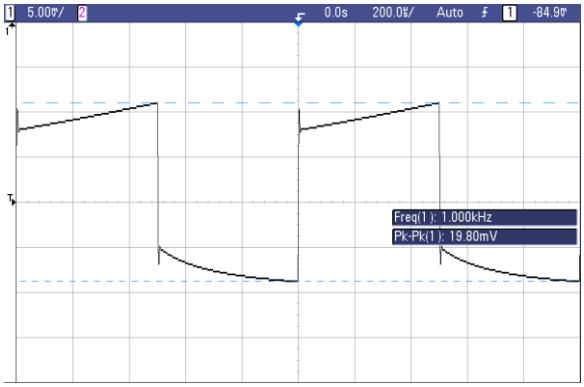

Figure 3.14: FHX13LG response, external modulation of 1kHz with Agilent 33220A on HP8350B

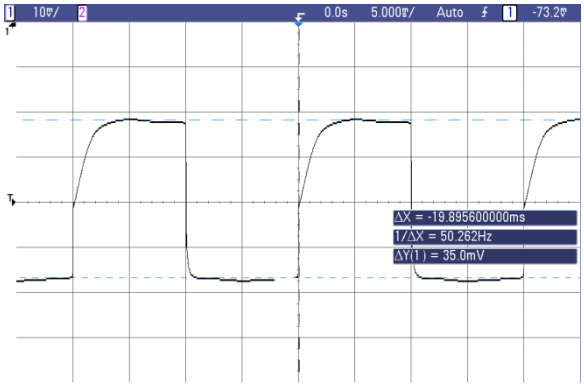

Figure 3.15: FHX13LG response, external modulation of 50 Hz with Agilent 33220A on HP8350B

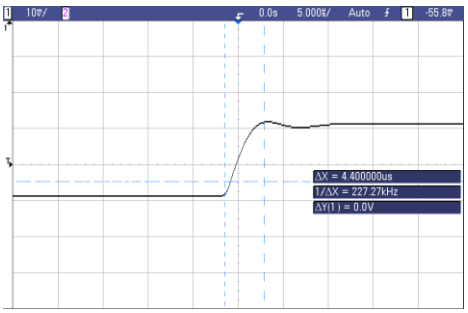

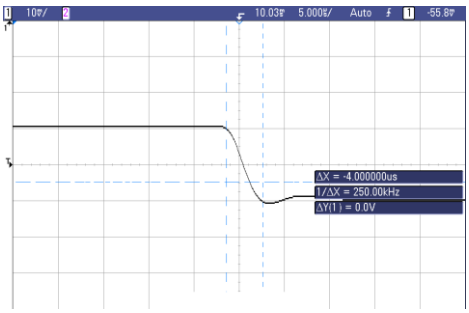

(a) Fall-time (OFF-to-ON-state transition) (b) Rise-time (ON-to-OFF-state transition)

Figure 3.16: Omega detector response, external modulation of 50 Hz with Agilent 33220A on HP8350B

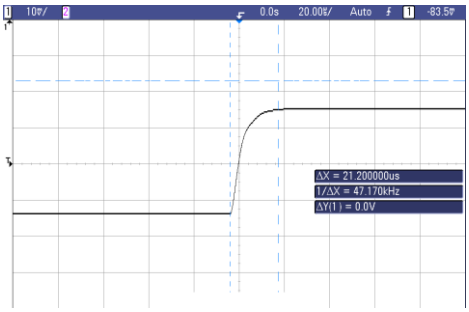

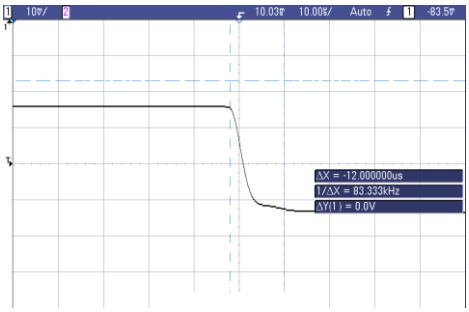

(a) Fall-time (OFF-to-ON-state transition) (b) Rise-time (ON-to-OFF-state transition)

Figure 3.17: HP423A detector response, external modulation of 50 Hz with Agilent 33220A on HP8350B

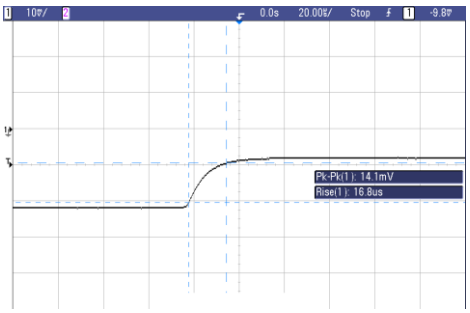

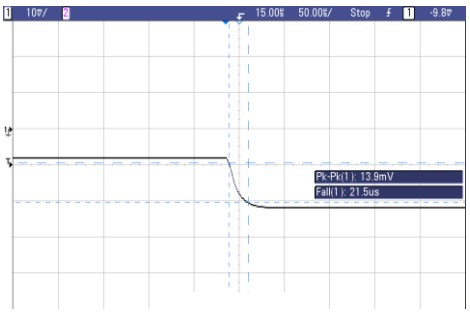

(a) Fall-time (OFF-to-ON-state transition) (b) Rise-time (ON-to-OFF-state transition)

Figure 3.18: HP423A detector response, AM by RF MEMS switch with an actuation frequency of 25 Hz on microwave signal

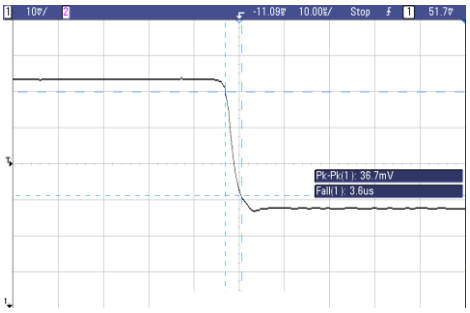

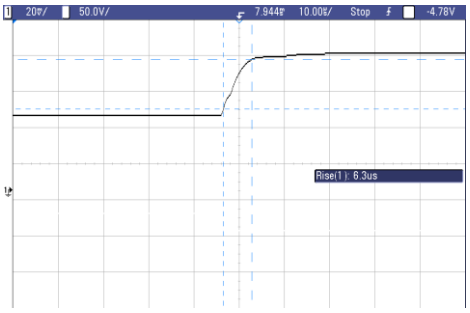

(a) Fall-time (OFF-to-ON-state transition) (b) Rise-time (ON-to-OFF-state transition)

Figure 3.19: Krytar 202A detector response, AM by RF MEMS switch with an actuation frequency of 25 Hz on microwave signal

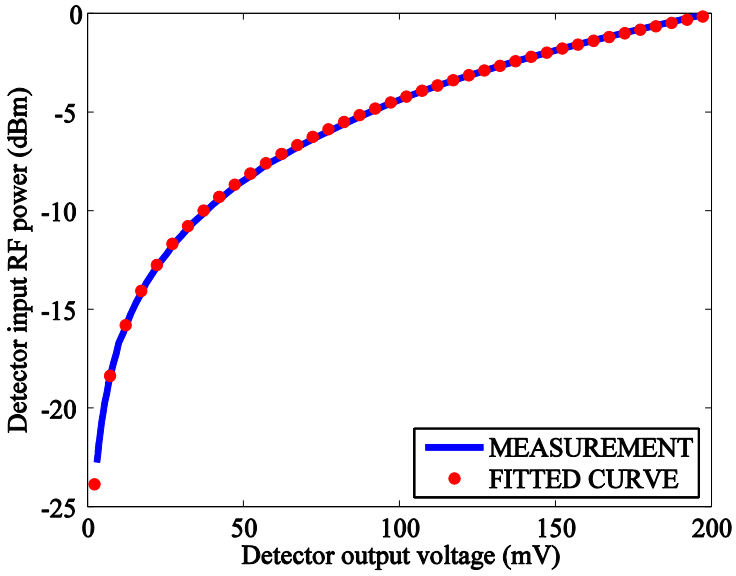

Figure 3.20: Krytar 202A input RF power vs. output voltage characteristics

Table 3.1: Curve fitting equation and fitting parameters

$P = c_1 * V^{c_2} + c_3;\ [P(dBm),\ V(mV)]$	
c_1	41.2
c_2	0.09394
c_3	-67.8

3.2.1.8 Data Acquisition

For examining the RF MEMS switch performance with respect to time the data should be collected and recorded. The Agilent DSO6102A is used for reading the data from Krytar 202A and recording is done by a computer via an HP-VEE program through GPIB connection interface.

HP-VEE is an HP supported visual programming environment to establish communication between computer and the devices. HP-VEE is programmed to be able to read the data from Agilent DSO6102A and write them to a text file. Then the data in the text file could be easily read and processed by using data processing software such as MatLab.

3.2.2 CV Measurement Setup

The CV measurement part of ReLiMS actually consists of only one measurement device, Agilent B1500A Semiconductor Device Analyzer since it has a built-in CV measurement module. The device applies DC voltage between two probe tips and measures the capacitance between two probes by applying a small amplitude AC signal. The CV measurement is performed in SUSS Vacuum Probe Station like the time domain measurements.

Important point in the measurement of capacitance is the type of cables used. Using the tri-axial cables improves the measurement accuracy. Cross-sectional view of a tri-axial cable is shown in Figure 3.21. At the center the signal path goes and guard path encloses the signal path. The device keeps the signal and the guard at the same potential. The shield is at the outermost part of the cable and it is kept at ground potential. The measurement is taken between the signal and ground terminals. In a conventional coaxial cable the AC signal applied for capacitance measurement can leak through the dielectric between signal and shield forming a parasitic capacitance between them. For tri-axial cable the leakage might occur between the guard and shield and no leakage occurs from signal since signal and guard are at the same potential. Hence the measurement is not affected by leakages so that the parasitic capacitances are eliminated.

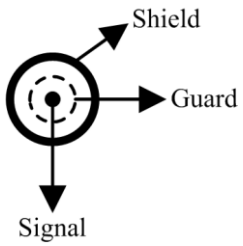

Figure 3.21: Tri-axial cable cross-sectional view

In CV measurements two methods might be used for performance evaluation; *partial* CV (P-CV) curve measurement and *full* CV (F-CV) curve measurement. In P-CV the applied voltage is swept over a small range without collapsing the bridge. A typical P-CV result

should look like as in Figure 3.22. In F-CV the applied voltage is swept to a point beyond the hold-down and pull-in voltages so the collapse of the bridge occurs. A realistic F-CV result is already given in Figure 2.8. The P-CV does not disturb the RF MEMS switch much since the applied stress is small, application time is short and no down contact occurs but does not provide much information. The F-CV disturbs the RF MEMS switch more but the gathered information sufficiently characterizes the change of capacitance with voltage.

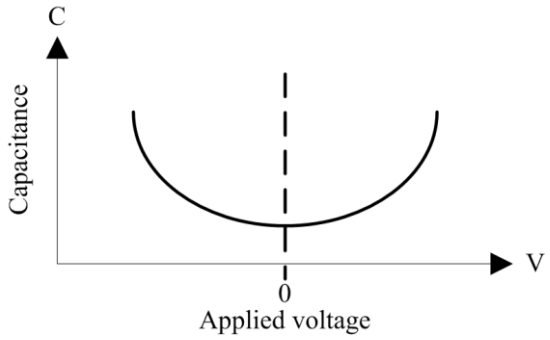

Figure 3.22: A typical P-CV measurement result

Although it does not give much information, usage of P-CV method in measurements depends on the simple force equation relating the applied voltage on an RF MEMS switch to the attracting force between bottom and top electrodes of the bridge and it is proposed in [79].

The force between two electrodes with different potentials, *F*, is given by (3.1) when we neglect the fringing capacitances and the dielectric between the electrodes.

g accounts for the distance between electrodes, *V* accounts for the potential difference between electrodes and other parameter explanations can be seen from Table 2.1 and Figure 2.4.

$$F = -\frac{1}{2}\frac{\varepsilon_0 W \mathrm{w} V^2}{g^2} \tag{3.1}$$

It is obvious from Equation (3.1) that *F* has a parabolic relation to the applied voltage, *V* so that when the applied voltage is swept under the pull-in voltages, the CV curve should have a parabolic shape. (Figure 3.22) After biasing for a certain time the CV curve might shift in a direction as explained in Section 1.1 and if the shift stays in the sweeping range in P-CV measurement then by fitting a quadratic equation to the measured data, value of the shift can be determined from shift of dip of the parabola. This case can be illustrated as in Figure 3.23.

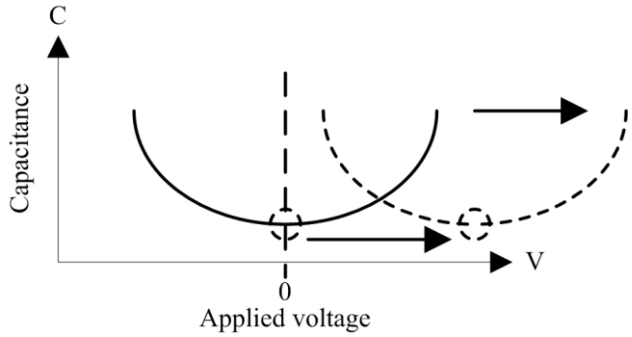

Figure 3.23: A typical P-CV curve shift

After considering the curve shifts the handicaps for P-CV measurement can be listed as follows in total:

- It is useful only if a curve shift is of concern. If there exists narrowing instead of a shift then the dip point of parabola would not shift giving no information on the narrowing amount.
- The amount of shift could be greater than the voltage sweeping range so the voltage sweep window might be shifted according to the amount of curve shift causing several iterations for finding the dip of parabola.
- Certainly the hold-down and pull-in voltages could not be found by this method.

P-CV measurement has also advantages which can be listed as follows:

- If a CV curve shift is the issue then amount of shift could be measured by sweeping the applied voltage around zero in a small range avoiding the bridge from contacting with the dielectric.
- Bridge buckle down for the OFF-state case could be identified in terms of capacitance since the OFF-state capacitance can be measured with a small applied stress.

Just for a comparison, pros and cons of F-CV measurement should also be listed. The disadvantages are as follows:

- Due to the applied voltage higher than pull-in, the bridge comes into contact with the dielectric which is a disturbing effect on the RF MEMS switch.
- For the same voltage sweeping speed the RF MEMS switch is held under stress longer than P-CV method.

The positive aspects of F-CV method can be listed as follows:

- Hold-down and pull-in voltages of the RF MEMS switch can be found.
- After applying bias the changes in the capacitance vs. voltage behavior which can be a measure for dielectric charging of RF MEMS switch, could be identified both qualitatively (shift, narrowing or both) and quantitatively (amount of shift or narrowing).
- The bridge buckle down for OFF-state could be quantified also by this method.

3.2.3 Future Work

Although giving satisfactory results the ReLiMS can be further improved.

- To remove the DC blocks employing back-to-back waveguide adapters, couplers might be designed and implemented at the testing frequency. This will decrease the power loss and occupied physical area. Couplers might also prevent the mode conversions at the coaxial-waveguide transitions.
- After packaging, fixtures might be produced to provide robust test beds.

3.3 Conclusion

This chapter has presented a general overview on reliability and lifetime measurements on RF MEMS devices and two basic setup types; time domain and CV measurements. Then the focusing is turned to the semi-automated time domain and CV measurement setups established for METU RF MEMS Research Group. Details for time domain setup are given and all sub-components are explained individually. Finally the CV measurement is explained in detail and two CV measurement methods, P-CV and F-CV, are compared.

CHAPTER 4

RELIABILITY AND LIFETIME MEASUREMENT RESULTS

As the research effort today in RF MEMS world is focused on integrating this technology to the applications investigation of the reliability of RF MEMS devices may be considered to be the hot topic. As is the case for test setups also there is no common standard defined about the reliability and lifetime of RF MEMS; no commonly accepted methods, no commonly accepted criteria, no strongly verified and developed theory. Because of this reason results of each study are important in the trip towards commercial and reliable applications of RF MEMS. This chapter is dedicated to the introduction of different testing condition and results of reliability measurements on RF MEMS switches fabricated by METU RF MEMS Research Group.

4.1 Introduction

The main aim of whole study has been the examination of RF MEMS switch behavior and performance monitoring under different conditions to bring the devices to a better point in terms of reliability. To come out with a comprehensive study many parameters have been determined and changed to see the effect of them to reach optimized conditions for reliable operation of RF MEMS switches. The parameters are classified in four groups.

4.1.1 Different Bias Waveforms

For electrostatic actuation of an RF MEMS switch many different bias types might be used. These different waveforms can be grouped as follows and the illustrations of them are given in Figure 4.1.

4.1.1.1 Unipolar Unilevel Continuous Bias

This is the way of actuating and holding and RF MEMS switch in the ON-state by directly applying DC voltage from a power supply. The polarity might be either positive or negative since the degradation mechanism progress might be different under different polarities.

4.1.1.2 Unipolar Bilevel Continuous Bias

In terms of holding the switch in ON-state this is similar to the unipolar unilevel continuous bias but to actuate the switch a DC voltage higher than the pull-in is applied first and it is lowered to a value between pull-in and hold-down voltage since pull-in voltage is not needed any more to hold down the bridge once it is actuated. This lowering aims to apply a lower bias stress on the switch to increase lifetime. Again for this case the polarity might be either positive or negative.

4.1.1.3 Unipolar Unilevel Cycling Bias

This waveform is the simplest way of testing an RF MEMS switch in a cycling fashion i.e. actuating the switch, holding down for a short time, releasing back and repeating this continuously. The actuation is done by applying a unilevel voltage always in the same polarity.

4.1.1.4 Unipolar Bilevel Cycling Bias

This is very similar to unipolar unilevel cycling bias but in this case to take down the switch a voltage greater than pull-in is applied and lowered to a value between pull-in and hold-down voltages and then lowered to zero to release the bridge.

4.1.1.5 Bipolar Unilevel Continuous Bias

This waveform is the way holding down the bridge with a continuously changing waveform. Since the bridge could not respond to the positive negative transitions it is always in ON-state.

4.1.1.6 Bipolar Bilevel Continuous Bias

This is very similar to the bipolar unilevel continuous bias but again for this waveform the switch is actuated with a high voltage and as the bridge collapses the applied voltage is pulled down to lower value.

4.1.1.7 Bipolar Unilevel Cycling Bias

This is very similar to the unipolar unilevel cycling bias. The switch is taken down and released continuously but in this bias type the polarity is alternated in consecutive cycles. If the bridge is actuated with a positive voltage in a cycle then it is actuated with a negative voltage in the next cycle.

4.1.1.8 Bipolar Bilevel Cycling Bias

The only difference from bipolar unilevel cycling bias is again the applied voltage to actuate the bridge. In every cycle high voltage is applied, lowered down and dropped to zero to release.

4.1.1.9 Bipolar Unilevel Alternating Cycling Bias

Different from unipolar and bipolar unilevel cycling bias the bridge is held down by an alternating waveform during actuation times. The alternation speed is so high that the switch could not respond.

4.1.1.10 Bipolar Bilevel Alternating Cycling Bias

The bridge is actuated with an alternating waveform but again two levels voltages are applied for actuation and holding down the bridge.

Just for keeping the complexity at a level none of the alternating and bilevel waveforms are used in this study. The unipolar unilevel continuous, unipolar unilevel cycling, bipolar unilevel continuous and bipolar unilevel cycling bias types are applied throughout this study. For unipolar bias types both positive and negative polarities are used in separate tests. Usage of different bias waveforms allows the testing staff to investigate the effects on dielectric charging to form the optimum biasing strategy.

Voltage level can also be regarded as a parameter. Adjustment of applied voltage has a direct effect on the lifetime of an RF MEMS switch.

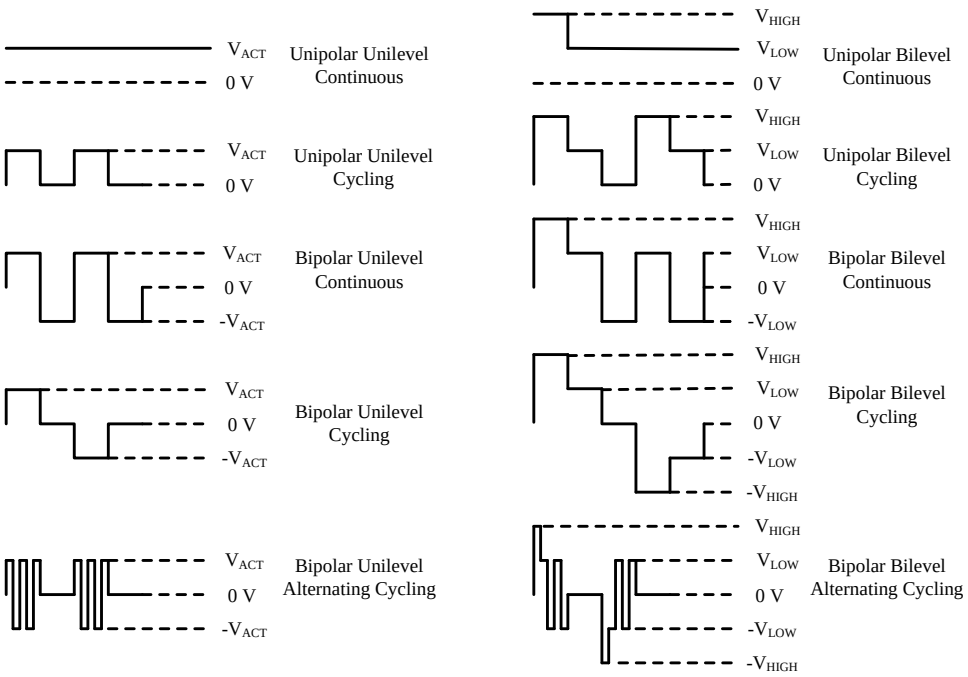

Figure 4.1: Illustrations of different bias waveforms

4.1.2 Different Measurement Environments

Since RF MEMS devices are based on movements at micro level the environmental factors could easily affect the operation. The main threat for an unprotected RF MEMS device is the humidity due to the forces which are highly effective in micro world and for comparison tests should be done in both humid and dry ambient.

All environmental conditions could be obtained by using SUSS Vacuum Probe Station and the different environments used during this study are listed as follows:

- **Open air:** The most challenging environment with its vulnerability to external effects from environment such as the humidity and particle contamination.
- **Vacuum:** This case provides both a dry ambient and removes the damping effect of environmental gas resulting with a change in dynamic response.
- **Nitrogen filled chamber:** This case provides both a dry environment and measurement at different environmental pressures including the atmospheric pressure.

Testing in different environments is an important point at deciding the packaging conditions. The devices should be packaged in best environmental conditions.

4.1.3 Different Materials

To enhance the reliability many different materials can be tried. The base metal layer, the dielectric layer, the sacrificial polyimide layer, the structural layer, all these can affect the mechanical properties and dielectric charging characteristics of an RF MEMS switch. This study has been directed to changing the dielectric materials while keeping the base metal layer, the sacrificial polyimide layer and the structural metal layer the same.

Different materials used as isolation dielectric layer are listed as follows:

- **Silicon nitride (Si_xN_y):** The conventional METU RF MEMS process employs this material as the dielectric due to its relatively high dielectric permittivity. (ε_R=7) In the process Si_xN_y is deposited by PECVD tool using a mixed frequency recipe.
- **Aluminum nitride (AlN):** For the comparison of dielectric charging characteristics, RF MEMS switches with AlN dielectric layer are also fabricated. Similar to Si_xN_y, AlN has also a relatively high dielectric constant which is equal to 9.

4.1.4 Physical Layout Modifications

Structural modifications have been done on two layers of the RF MEMS switch. One is the on the base metal layer and the other is on the isolation dielectric layer.

Modification on base metal layer is the anchor extension and switches with anchor extension and without anchor extensions are fabricated. The details on anchor extension are given in Section 2.4.2.

Modification on the isolation dielectric layer is to pattern the layer for reducing the contact area with the electrodes. The three different patterned geometries are given in Figure 4.2. The simplest way of forming the islands with a CAD tool, square or rectangular shape, is given in Figure 4.2-a. The circular shape islands are shown in Figure 4.2-b. The square and circular shape perforations occupy not the same but close areas and they are put to see if there is an effect of the shape in terms of enhancing the mechanical endurance while being

squeezed under the actuated bridge. Figure 4.2-c shows the square shape islands which are electrically isolated. The blank regions around the base metal and dielectric islands represent the substrate. By this way the dielectric has no electrical contact to the signal line enabling itself to guard against the applied high electric field. Handicap for the case in Figure 4.2-c is the reduction of overlap area between bridge and signal line causing an increase in the pull-in voltages.

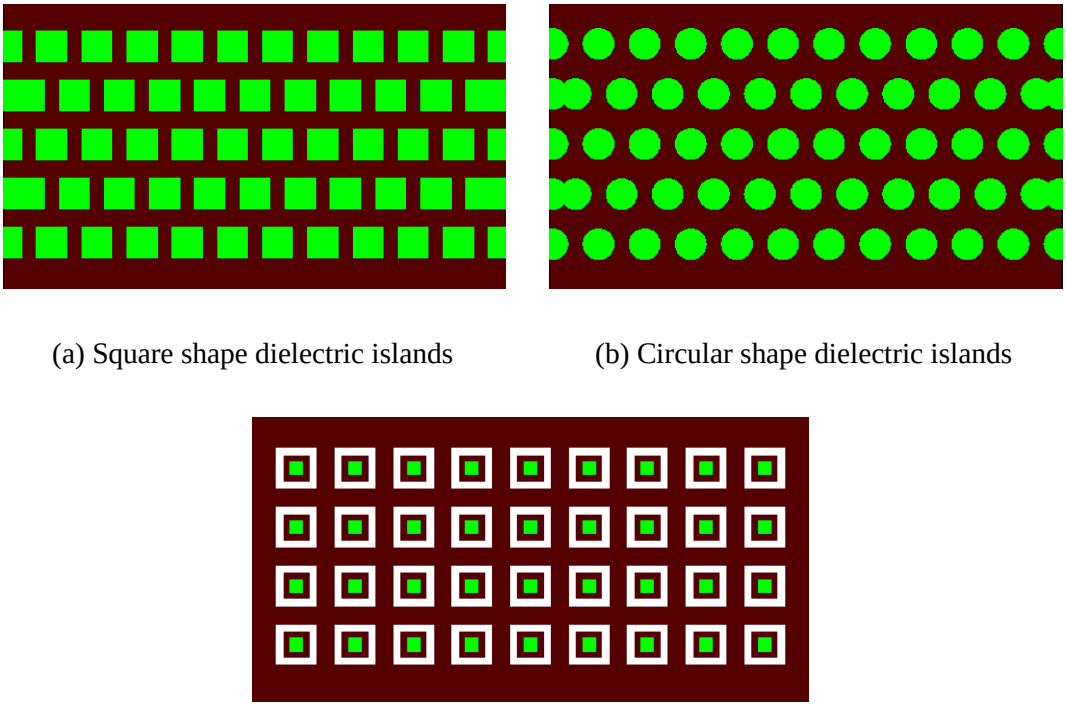

(a) Square shape dielectric islands

(b) Circular shape dielectric islands

(c) Square shape, totally isolated dielectric islands

Figure 4.2: Types of isolation dielectric layer perforations

4.2 Reliability and Lifetime Measurement Samples

To meet the requirement of large number of samples for reliability and lifetime measurements a lithography mask set (RF MEMS-Mask Set 10) is dedicated to this study. The wafers fabricated by using MS10 consist mostly of RF MEMS switches. Different types of switches are arranged in the form of a 7x7 matrix while drawing the layout and

this 7x7 switch block is distributed over the entire layout. The general layout view can be seen from Figure 4.3. A 7x7 switch block from the center region of the layout is enclosed by a *yellow* rectangle for better indication. Also samples from fabricated wafers before MS10 process are used for measurements such as the usage of RF MEMS switches from MS9.2 for partial CV curve measurements.

For measurement, several wafers are fabricated and the thicknesses of layers all measured from switch samples at the center of region of wafer are given in Table 4.1.

- To distinguish the Si_xN_y and AlN an index number is added to the mask set number. MS10.1 represents the wafers with Si_xN_y and MS10.2 represents the wafers with AlN.
- Bridge height accounts for the distance between signal line and the bottom surface of structural metal layer i.e. includes isolation dielectric thickness and air gap thickness under the bridge.

After this introduction for the reliability measurements the next section presents the results and the deductions from them.

Table 4.1: Layer thicknesses for the fabricated wafers

Wafer Label	Base Metal Layer (um)	Dielectric Layer (um)	Sacrificial Polyimide Layer (um)	Structural Metal Layer (um)	SWAE Bridge Height (um)	SWoAE Bridge Height (um)
MS10.1 W1	0.6	0.3	1.6	1.5	1.7	1.3
MS10.1 W3	0.6	0.3	1.5	1.5	1.6	1.2
MS10.1 W4	0.6	0.3	1.6	1.1	1.66	1.3
MS10.1 W5	0.65	0.3	2.27	1.3	2.35	1.76
MS10.2 W9	0.6	0.3	1.43	1.7	1.3	1.0

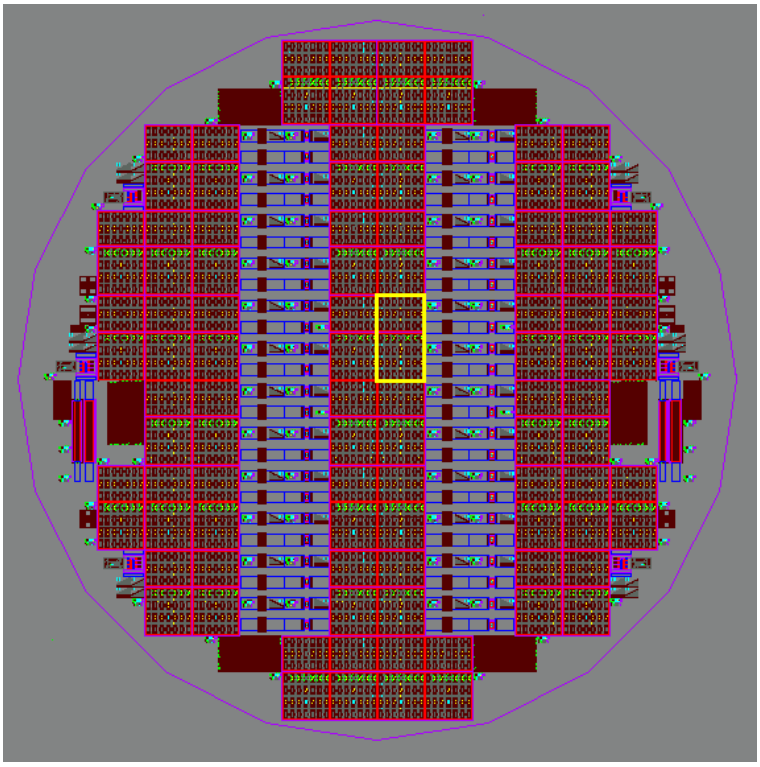

Figure 4.3: General layout view of MS10

4.3 Reliability and Lifetime Measurement Results

In this part first the results of partial CV curve measurements are presented in Section 4.3.1 and all other results are grouped according to the measurement environments and given in Section 4.3.2, 4.3.3, and 4.3.4. The cross comparisons between environments are provided at the end, in Section 4.3.5.

The CV curve measurements are given in the form of capacitance vs. applied voltage graphs as illustratively shown before in Figure 2.8.

In real-time detector voltage measurements the ON-state and OFF-state detector voltages are recorded to a text file through HP-VEE program to see if the bridge is properly moving up and down. A sample image can be seen from Figure 4.4 showing both the detector output waveform and the actuation waveform.

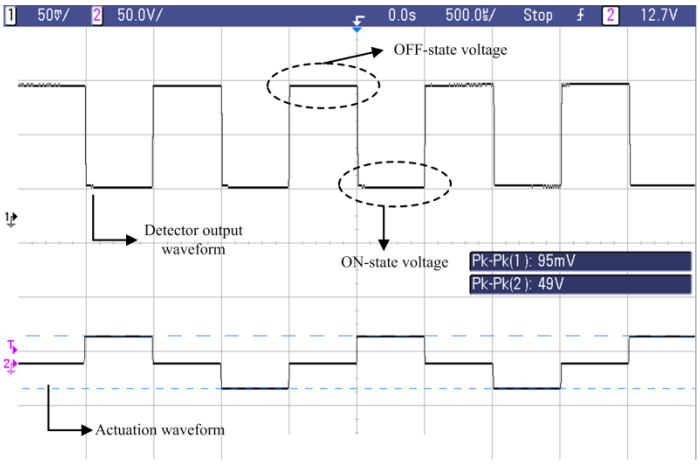

Figure 4.4: Sample oscilloscope display showing detector output and actuation waveforms

To be considered as a reference the voltage polarity convention is as follows:

- **Bias voltages:** If the high voltage pin of bias generator is connected to the signal line then this is considered to be positive voltage application. For the negative polarity the case is vice versa.
- **CV curves:** The case for both the partial and full CV curves is the same as bias voltages consideration. The positive voltage in the CV curve says that the higher voltage is connected to the signal line.

All of the measurements presented in this section are performed at room temperature.

4.3.1 Partial CV Curve Measurements

This section focuses on partial CV curve measurements and validity investigation of the method.

In partial CV curve figures the *blue* plot represents the start. The *green* points account for the fitted curve onto the start case. The *red* plot shows the partial CV characteristics at the end of the particular test. The *black* points show the fitted curve onto the end of test data.

- The results in Figure 4.5 are given for an RF MEMS switch from MS9.2-W9. Measurement parameters are as follows:

  Actuation type: Unipolar, unilevel, continuous, positive bias

  Applied voltage: 15 V

  Bias period: From START to 10 minutes (MIN)

  Environment: Open air (26% humidity)

  The shift of fitted parabola (s_V_{PCV}) is found to be 3.7 V from Figure 4.5-a. The shift of negative pull-in voltage (s_V_{PI-}) is found to be 3.6 V and shift of positive pull-in voltage (s_V_{PI+}) is found to be 3.4 V from Figure 4.5-b. Note that the full CV curve shift can be considered to be symmetrical in terms of pull-in voltage shifts i.e. s_V_{PI-} and s_V_{PI+} have close values. The shift amount found from PCV measurement is also close to s_V_{PI-} and s_V_{PI+}. Note from this measurement that the bridge buckles down a bit since the ON-state capacitance increases at the end of testing period.
- The results in Figure 4.6 give another valuable PCV measurement from MS9.2-W9.

  Actuation type: Unipolar, unilevel, continuous, positive bias

  Applied voltage: 15 V

  Bias period: From START to 20 MIN

  Environment: Open air (26% humidity)

  s_V_{PCV} is found to be 4 V. s_V_{PI-} is found to be 4 V and s_V_{PI+} is also found to be 4 V. The shift of CV curve is symmetric so that the results are very consistent.

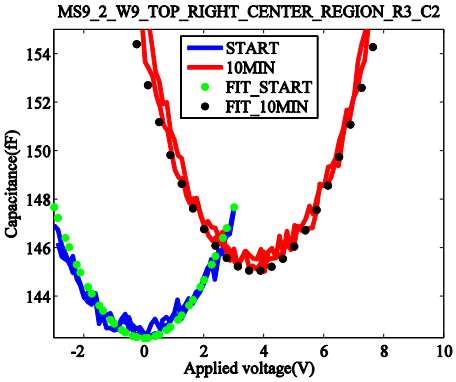

(a) Partial CV curve

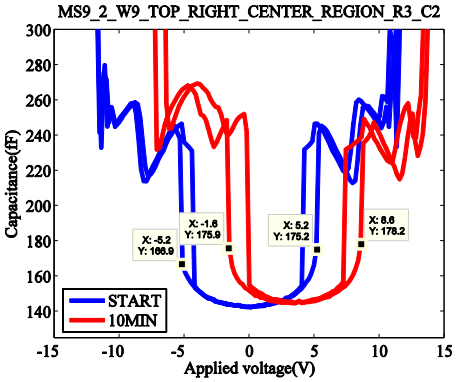

(b) Full CV curve

Figure 4.5: Comparison of partial and full CV curves

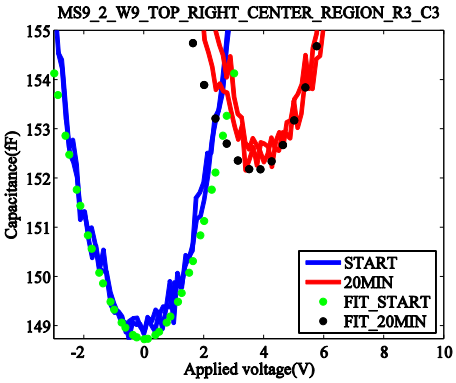

(a) Partial CV curve

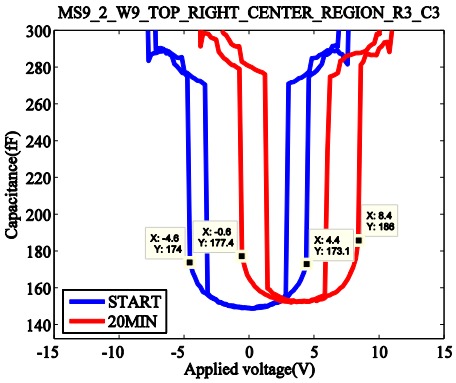

(b) Full CV curve

Figure 4.6: Comparison of partial and full CV curves

Results presented in Figure 4.5 and Figure 4.6 verifies the idea of PCV measurement method but shift in symmetry is not always the case for RF MEMS switches.

- Figure 4.7 clearly indicates the asymmetric CV curve shift case. The measurement is again from MS9.2-W9.

  Actuation type: Unipolar, unilevel, continuous, positive bias

  Applied voltage: 15 V

Bias period: From START to 10 MIN

Environment: N_2 environment

s_V_{PI-} is found to be 3.6 V and s_V_{PI+} is found to be 2.8 V from Figure 4.7-b. s_V_{PCV} is found to be 3.3 V from Figure 4.7-a. The difference between s_V_{PI-} and s_V_{PI+} shows us that the CV curve does not shift as a whole so the s_V_{PCV} value becomes inconsistent with the s_V_{PI-} and s_V_{PI+}. This is most probably caused by the combined effect of uniform dielectric charging resulting with CV curve shift and the non-uniform dielectric charging resulting with CV curve narrowing. Note that even for these cases the shift of CV curves center point i.e. s_V_{PCV} should be nearly equal to the arithmetic mean of s_V_{PI-} and s_V_{PI+} since the CV curve is still expected to have a symmetric characteristics around its center point. Considering the measurement shown in Figure 4.7, the arithmetic mean of s_V_{PI-} and s_V_{PI+} is found to be 3.2 V which is close to s_V_{PCV}. This relation is also verified by another measurement with identical measurement parameters and results are tabulated in Table 4.2 together with the results from Figure 4.7.

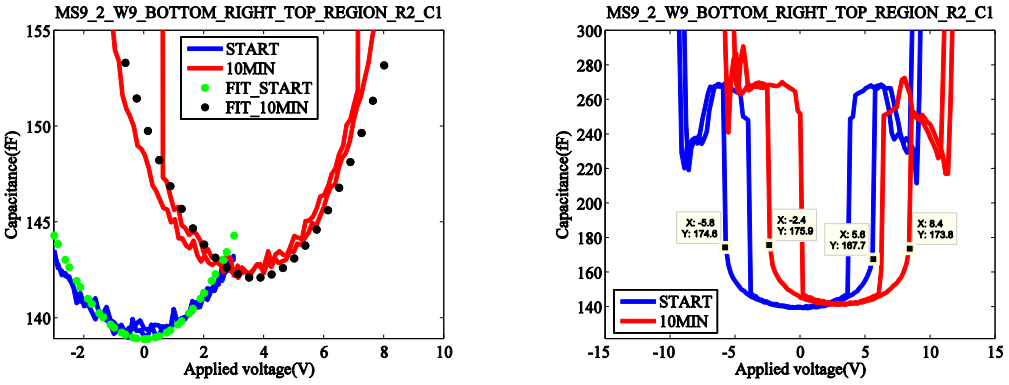

(a) Partial CV curve (b) Full CV curve

Figure 4.7: Comparison of partial and full CV curves

Table 4.2: Verification of relation between s_V_{PCV}, s_V_{PI-} and s_V_{PI+} for 15 V, unilevel, unipolar, continuous, positive bias in N_2 environment

Switch Label	s_V_{PCV} (V)	s_V_{PI-} (V)	s_V_{PI+} (V)	$(s\_V_{PI-} + s\_V_{PI+})/2$ (V)
Sample1.1 (Figure 4.7)	3.3	3.6	2.8	3.2
Sample1.2	2.7	3	2.2	2.6

- Asymmetric CV curve shift is observed also for similar measurement configuration in Figure 4.7 but with negative bias polarity. The measurement parameters are as follows:

  Actuation type: Unipolar, unilevel, continuous, negative bias

  Applied voltage: 15 V

  Bias period: From START to 10 MIN

  Environment: N_2 environment

  As expected for negative bias the CV curve shifts towards left as seen from PCV curve of Sample2.1 in Figure 4.8. Since the CV curve measurement voltage sweep has become large at 10MIN case, sharp transitions in 10MIN curve are seen which indicate pull-in. This shows the importance of careful adjustment of voltage sweep since in partial CV curve measurements pull-in not desired. The results for three different switches are tabulated in Table 4.3. Because of shifting direction all of the shifting amounts have negative values in Table 4.3.

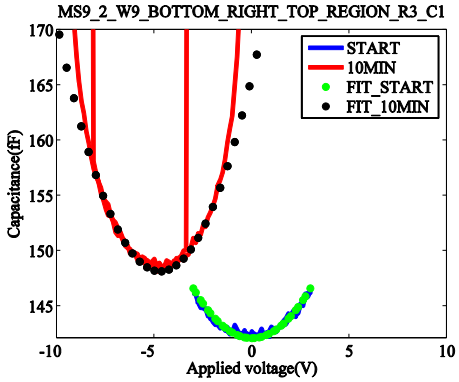

Figure 4.8: PCV result for Sample2.1

Table 4.3: Results for 15V, unilevel, unipolar, continuous, negative bias in N_2 environment

Switch Label	s_V_{PCV} (V)	s_V_{PI-} (V)	s_V_{PI+} (V)	$(s\_V_{PI-} + s\_V_{PI+})/2$ (V)
Sample2.1	-4.7	-3.8	-6	-4.9
Sample2.2	-4	-3.2	-5.2	-4.2
Sample2.3	-3.1	-2.2	-4.2	-3.2

In conclusion for the PCV measurements the following items can be written:

- Considering the close values of s_V_{PCV}, s_V_{PI-} and s_V_{PI+} for open air measurements it can be said that non-uniform charging stays weak with respect to the uniform charging. For N_2 environment measurements the difference between the values of s_V_{PI-} and s_V_{PI+} easily stand out minding the additional effect of non-uniform charging although the bias polarity is not changed throughout each test.
- Both open air and N_2 environment measurements confirm the symmetry of CV curves around the center points verifying the Equation (4.1).

$$s\_V_{PCV} = \frac{s\_V_{PI-} + s\_V_{PI+}}{2} \quad \textbf{(4.1)}$$

- Notice that shift of the pull-in voltage with the opposite polarity of bias voltage, is larger than the shift of other pull-in voltage i.e. for positive bias $s\_V_{PI-} > s\_V_{PI+}$ and for negative bias $s\_V_{PI+} > s\_V_{PI-}$.

Due to the limited information obtained, no PCV measurements are done for the presented measurements in the following sections.

4.3.2 Open Air Measurements

This section presents the results obtained from the open air measurements. The measurements are performed on the SWAE's.

- To verify the asymmetric CV curve shift for MS10.1 samples positive and negative bias is applied on the switches. The switches are chosen from MS10.1-W4. The result for positive bias on Sample3.1 is shown in Figure 4.9-a and Figure 4.9-b shows the result for negative bias on Sample4.1.
  Actuation type: Unipolar, unilevel, continuous, positive and negative bias
  Applied voltage: 40 V
  Bias period: From START to 10 MIN
  Environment: Open air

For the samples of this test the asymmetric CV curve shift is obvious from Figure 4.9 for both positive and negative bias. The results obtained for this test from different samples are given in

Table 4.4. Note also from Figure 4.9 that the contact enhancement could be easily seen from the difference of ON-state capacitances between START and 10MIN cases. The ON-state capacitance obviously increases after stopping the actuation period.

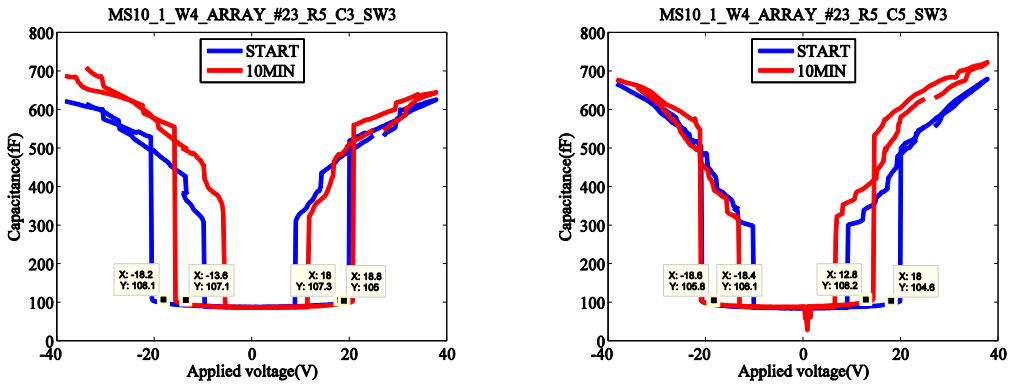

(a) Sample3.1 CV curve (b) Sample4.1 CV curve

Figure 4.9: Comparison of positive and negative bias for open air environment

Table 4.4: Results for unilevel, unipolar, continuous, 40 V, positive and negative bias in open air

Switch Label	s_V_{PI-} (V)	s_V_{PI+} (V)	Switch Label	s_V_{PI-} (V)	s_V_{PI+} (V)
Sample3.1	4.6	0.8	**Sample3.2**	4.8	1.6
Sample3.3	3.6	1.2	**Sample3.4**	3.6	0.2
Sample3.5	4.2	2.4	**Sample3.6**	4.2	-0.6
Switch Label	s_V_{PI-} (V)	s_V_{PI+} (V)	**Switch Label**	s_V_{PI-} (V)	s_V_{PI+} (V)
Sample4.1	0	-5.2	**Sample4.1**	-0.4	-4

- This part presents the results of measurements performed to investigate the behavior of RF MEMS switches under unilevel, unipolar cycling bias waveform in open air. Samples are from MS10.1-W4. Measurement parameters are as follows:
  Actuation type: Unipolar, unilevel, cycling, positive bias
  Actuation frequency: 100 Hz (50% duty cycle)
  Applied voltage: 25 V
  Bias period: From START to 10 MIN
  Environment: Open air

The behavior of switch during the actuation period can be deduced from the real-time monitored detector output voltage data so that they are presented in this part in addition to the CV curves. Figure 4.10-a and Figure 4.10-b show the real-time monitoring results for Sample5.1 and Sample5.2. Note that Sample5.1 operates properly approximately for 1 minute and so is Sample5.2 for approximately 4 minutes. After a certain time for both switches the ON-state voltage rises to the value of OFF-state voltage. OFF-state voltage remains almost constant showing no degradation occurs for the OFF-state position. This phenomenon minds the occurrence of dielectric charging resulting with screening. The charges are injected into the dielectric and the voltage is applied is no more enough to overcome the opposition of injected charges so the bridge could not come to ON-state. High detector output voltage for ON-state definitely shows that the microwave power is transmitted although actuation waveform is still applied on the RF MEMS switch. For the verification of charging in dielectric also CV curves of Sample5.1 and Sample5.2 are measured and given in Figure 4.11. CV curve shifts for five samples are given in Table 4.5 where all five samples exhibited screening effect as shown in Figure 4.10. Note that asymmetric CV curve shift is again observed for this case.

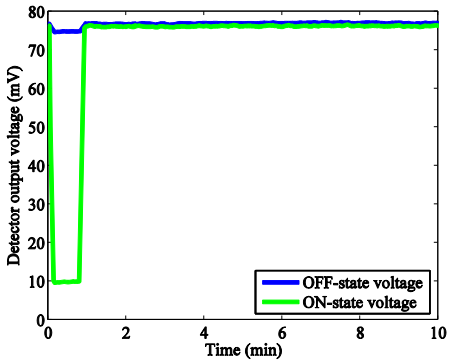

(a) Sample5.1 detector output voltage (DOV) vs. time

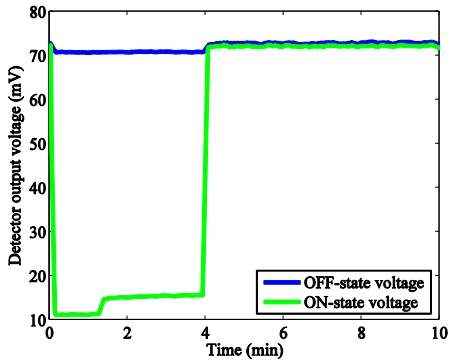

(b) Sample5.2 detector output voltage vs. time

Figure 4.10: Detector output voltage data for unilevel, unipolar, cycling, 25 V, 100 Hz, 50% duty cycle positive bias in open air

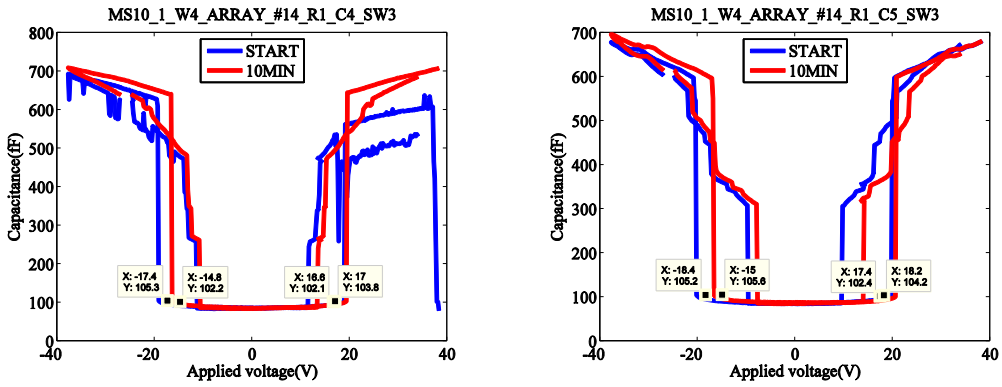

(a) Sample5.1 CV curve (b) Sample5.2 CV curve

Figure 4.11: CV curves for unilevel, unipolar, cycling, 25 V, 100 Hz, 50% duty cycle, positive bias in open air

Table 4.5: Results for unilevel, unipolar, cycling, 25 V, 100 Hz, 50% duty cycle, positive bias in open air

Switch Label	s_V_{PI-} (V)	s_V_{PI+} (V)	Switch Label	s_V_{PI-} (V)	s_V_{PI+} (V)
Sample5.1	2.6	0	**Sample5.2**	3.4	0.8
Sample5.3	3.4	0.4	**Sample5.4**	2.2	0
Sample5.5	2	0			

- To investigate the unilevel, unipolar, cycling bias waveform effect more comprehensively the negative polarity is also applied with the same configuration applied on the Sample5 group. Samples are from MS10.1-W4.

  Actuation type: Unipolar, unilevel, cycling, negative bias

  Actuation frequency: 100 Hz (50% duty cycle)

  Applied voltage: 25 V

  Bias period: From START to 10 MIN

  Environment: Open air

  As expected from the measurements on Sample4 group the screening effect has also been observed for this case as shown in Figure 4.12. As well as the screening phenomenon no failure effect during 10 minutes is seen on two other samples,

Sample6.2 and Sample6.3. The common point between these samples is the expected asymmetric CV curve shift. The results are given in Table 4.6. These results indicate that in the open air if the actuation is obtained by unilevel, unipolar waveforms for fast switching purposes this environment is not a suitable candidate. The dielectric charging most probably prevents the actuation after a certain time causing failure.

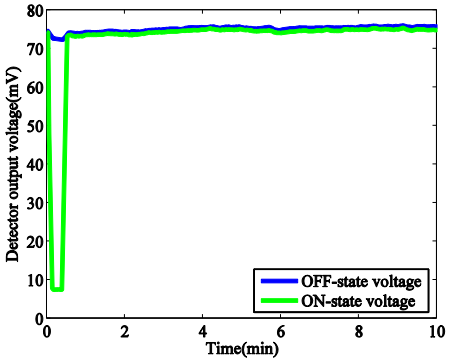

Sample5.1 DOV vs. time

Figure 4.12: DOV data for unilevel, unipolar, cycling, 25 V, 100 Hz, 50% duty cycle negative bias in open air

Table 4.6: Results for unilevel, unipolar, cycling, 25 V, 100 Hz, 50% duty cycle, negative bias in open air

Switch Label	s_V_{PI-} (V)	s_V_{PI+} (V)
Sample6.1	-2	0
Sample6.2	-3	-0.4
Sample6.3	-2.2	0

- With the knowledge of importance of ON-state time on dielectric charging, the actuation frequency is increased to 50 kHz so that the switch could not respond properly, could not settle in ON-state causing a decrease of the ON-state time.
  Actuation type: Unipolar, unilevel, cycling, positive bias
  Actuation frequency: 50 kHz (50% duty cycle)
  Applied voltage: 25 V
  Bias period: From START to 10 MIN
  Environment: Open air
  This most probably allows the switch to get rid of the screening effect. Results for Sample7.1 and Sample 7.2 can be seen from Figure 4.13. Note that ON-state voltage value stays almost constant during whole bias period and no decrease in OFF-state voltage occurs indicating no failure of the switch in 10 minutes.

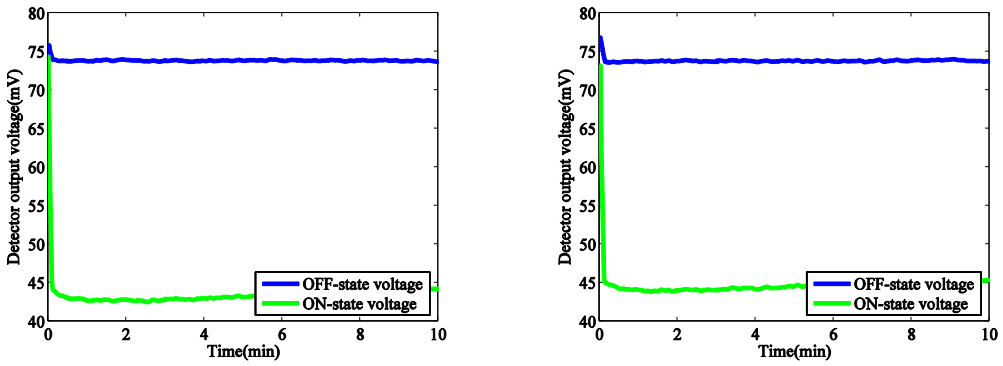

(a) Sample7.1 DOV vs. time (b) Sample7.2 DOV vs. time

Figure 4.13: DOV data for unilevel, unipolar, cycling, 25 V, 50 kHz, 50% duty cycle positive bias in open air

- To prevent the degrading effect of unipolar, continuous bias applying a bipolar, continuous bias might be tried. To make a fair comparison the same configuration applied on the Sample3 and Sample4 group is used by only changing bias type to bipolar. Samples are from MS10.1-W4. Parameters are as follows:
  Actuation type: Bipolar, unilevel, continuous bias
  Alternation frequency: 100 Hz (50% duty cycle)

Applied voltage: 40 V

Bias period: From START to 10 MIN

Environment: Open air

Although having the same voltage amplitude this case comes with a total failure on three samples. More than CV curve narrowing, stiction occurs as indicated by the CV curve of Sample8.1 and Sample8.2 in Figure 4.14. The CV curve for another sample is very similar to Figure 4.14; a stuck down bridge, increased OFF-state capacitance due to stiction. Also note that the ON-state capacitance also increased at the bias values of 35 V in CV curve pointing to a contact enhancement.

The obvious difference between unipolar and bipolar bias cases might be explained by the high voltage transitions included in the bipolar bias waveforms. Although the transitions are quite short, staying in the order of nanoseconds the observation minds this idea. A similar observation is made also for vacuum case and mentioned in Section 4.3.3.

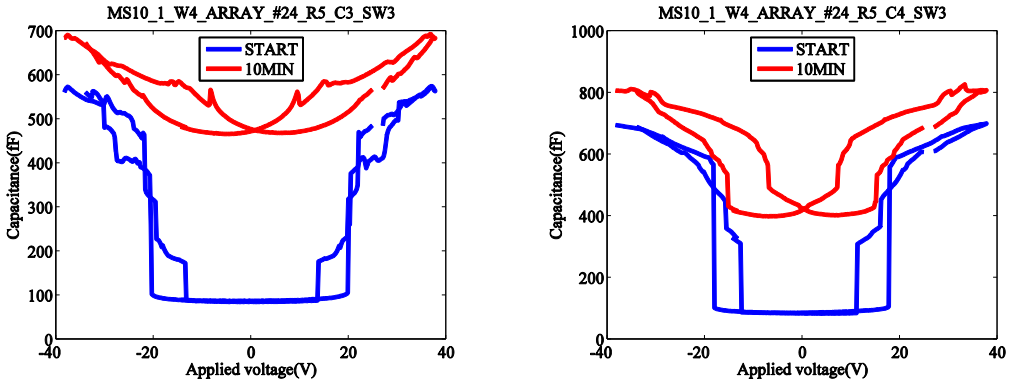

(a) Sample8.1 CV curve (b) Sample8.2 CV curve

Figure 4.14: CV curves for unilevel, bipolar, continuous, 40 V, 100Hz, 50% duty cycle bias in open air

- To protect the switch from the effects of high transitions during bipolar bias application a reduction in voltage amplitude is tried. Samples are chosen from MS10.1-W4 and measurement parameters are as follows:

  Actuation type: Bipolar, unilevel, continuous bias

Alternation frequency: 100 Hz (50% duty cycle)

Applied voltage: 25 V

Bias period: From START to 10 MIN

Environment: Open air

Two different results for Sample9.1 and Sample9.2 are given in Figure 4.15. The effect of voltage amplitude is quickly noticed as the less contact enhancement with respect to the 40 V case of this measurement configuration, the ON-state capacitance value at START and 10MIN are closer to each other for 25 V case. Moreover notice that Sample9.1 exhibits no failure at the end of 10 minutes and CV curve narrowing is observed as expected but Sample9.2 sticks down and a high OFF-state capacitance is measured after 10 minutes. This fact tells that even applying bipolar waveform with low voltage may not be enough to keep the RF MEMS switch operational.

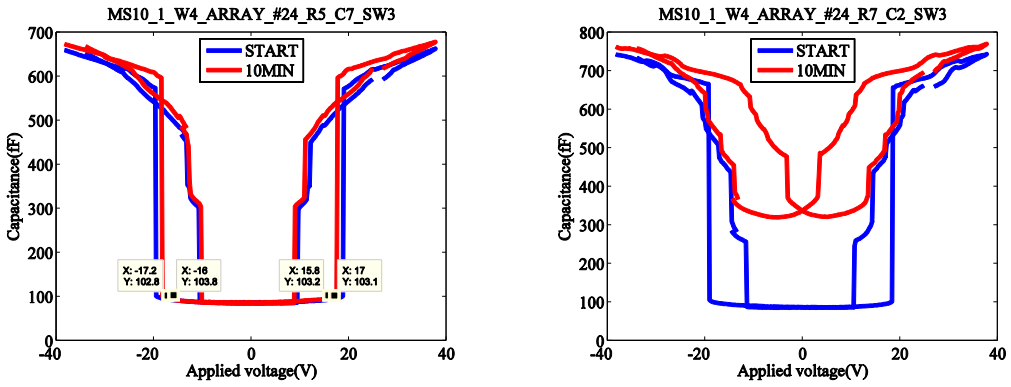

(a) Sample9.1 CV curve

(b) Sample9.2 CV curve

Figure 4.15: CV curves for unilevel, bipolar, continuous, 25 V, 100Hz, 50% duty cycle bias in open air

4.3.3 Vacuum Measurements

It is widely known that humidity is a serious threat for the MEMS devices. One method for removing the water vapor might also be to pump out the environment gas, taking into vacuum. Both for removing humidity and to see the effect on dynamic response,

measurements in vacuum environment are performed. All vacuum measurement samples are SWAE's.

- This part investigates the effect of unilevel, unipolar, continuous positive bias in vacuum. It is stated in [64] that failure depends on the number of cycles instead of ON-state time for vacuum measurements. The validity of this proposed idea has also been tested by this measurement. Samples are from MS10.1-W4. Measurement parameters are as follows:

  Actuation type: Unipolar, unilevel, continuous bias

  Applied voltage: 40 V

  Bias period: From START to 10 MIN

  Environment: Vacuum

  In opposition to the statement in [64] the CV curve shift hence dielectric charging is obviously seen from the measurements on Sample10.1 and Sample10.2 as given in Figure 4.16. Results for this test including other samples are given in Table 4.7. This test shows that removal of humidity by vacuum does not protect the dielectric from charge injection. Again the asymmetric CV curve shift and ON-state contact enhancement is observed.

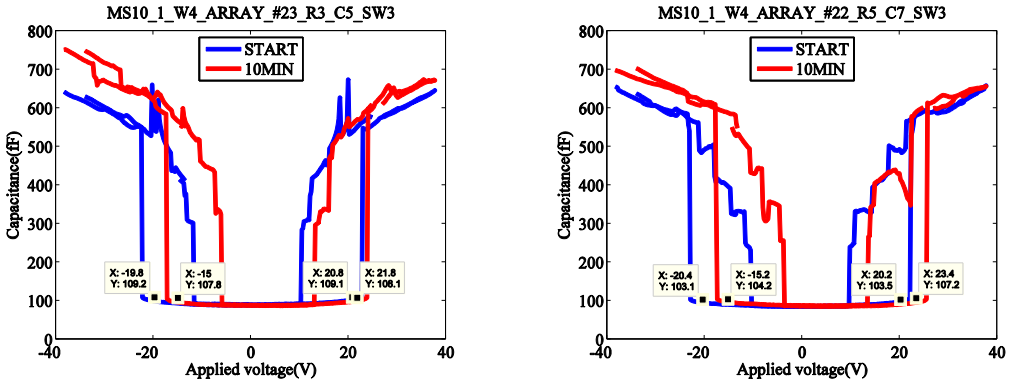

(a) Sample10.1 CV curve (b) Sample10.2 CV curve

Figure 4.16: CV curves for unilevel, unipolar, continuous, 40 V, positive bias in vacuum

Table 4.7: Results for unilevel, unipolar, continuous, 40 V, positive bias in vacuum

Switch Label	s_V_{PI-} (V)	s_V_{PI+} (V)	Switch Label	s_V_{PI-} (V)	s_V_{PI+} (V)
Sample10.1	4.8	1	**Sample10.2**	5.2	3.2
Sample10.3	5.6	3.4	**Sample10.4**	14.2	4.8
Sample10.5	14.4	5.2	**Sample10.6**	12	3.4

- Considering that applied voltage amplitude is directly effective on dielectric charging, the voltage amplitude is lowered to 25 V, closer to pull-in voltage to roughly get an idea if there is a threshold voltage value that the dielectric could not be charged by unipolar, continuous bias in vacuum. Samples are from MS10.1-W4.

  Actuation type: Unipolar, unilevel, continuous bias

  Applied voltage: 25 V

  Bias period: From START to 10 MIN

  Environment: Vacuum

  The results are given in Table 4.8 and as expected from Sample10 measurements CV curve shifting is observed but shift is smaller with respect to Sample10 measurement since the applied voltage is smaller. This minds that there is no threshold voltage to be exceeded for dielectric charging in vacuum, charge is injected as far as the contact between bridge dielectric layer forms. The contradiction between this test and [64] might be caused by the length of testing time where 98 seconds is reported in [64] and 10 minutes is the length of test on Sample11 group.

Table 4.8: Results for unilevel, unipolar, continuous, 25 V, positive bias in vacuum

Switch Label	s_V_{PI-} (V)	s_V_{PI+} (V)	Switch Label	s_V_{PI-} (V)	s_V_{PI+} (V)
Sample11.1	2.2	0	**Sample11.2**	1.2	0.4
Sample11.3	1.4	0.6	**Sample11.4**	1.8	0.4

- Taking the CV curve shift under unipolar, continuous bias in vacuum into account bipolar, continuous bias waveform is applied on samples from MS10.1-W4.

  Actuation type: Bipolar, unilevel, continuous bias

  Alternation frequency: 100 Hz (50% duty cycle)

  Applied voltage: 40 V

  Bias period: From START to 10 MIN

  Environment: Vacuum

  The results for Sample12.1 and Sample12.2 are given in Figure 4.17. Quite surprisingly none of the tested seven samples could withstand without failure after 10 minutes of bias, all of them have similar responses given in Figure 4.17. The results clearly indicate that under this bias the RF MEMS switch strongly sticks to the dielectric layer with no attempt for restoring back even at zero applied voltage. As an expected result of this strong stiction the contact enhancement is also observed for this test. Since only CV curve shift is observed for unipolar bias of the same amplitude, 40 V, this strong stiction minds the catastrophic impact of high voltage transitions which is equal to 80 V while going from -40 V to 40 V for this case, on the switch in vacuum environment. This makes vacuum unsuitable for high voltage bipolar biasing.

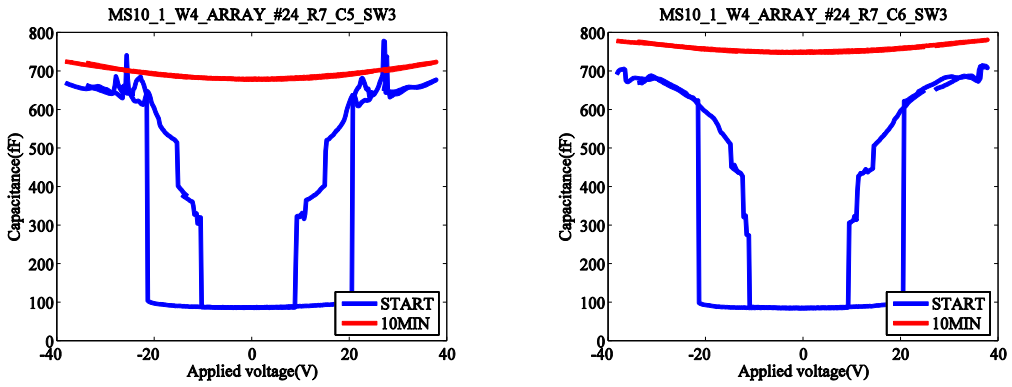

(a) Sample12.1 CV curve (b) Sample12.2 CV curve

Figure 4.17: CV curves for unilevel, bipolar, continuous, 40 V, 100Hz, 50% duty cycle bias in vacuum

- To see if 40 V of voltage amplitude is very effective on dielectric charging or not the voltage amplitude is lowered to 25 V with the same configuration. Samples are from MS10.1-W4.

  Actuation type: Bipolar, unilevel, continuous bias

  Alternation frequency: 100 Hz (50% duty cycle)

  Applied voltage: 25 V

  Bias period: From START to 10 MIN

  Environment: Vacuum

  CV curves of Sample13.1 and Sample13.2 are given in Figure 4.18. None of the five measured switches in Sample13 group exhibit any failure, CV curve narrowing and ON-state capacitance increases are observed. This test proves that the voltage amplitude hence the level of voltage transition for bipolar bias is very effective on dielectric charging for vacuum environment. High voltage transitions cause welding like effects in vacuum environment. CV curve shift results for all Sample13 group switches are given in Table 4.9. It can be deduced from the results that CV curve narrowing characteristics for vacuum environment is not substantially asymmetric, s_V_{PI-} and s_V_{PI+} values are close to each other with respect to the unipolar bias cases.

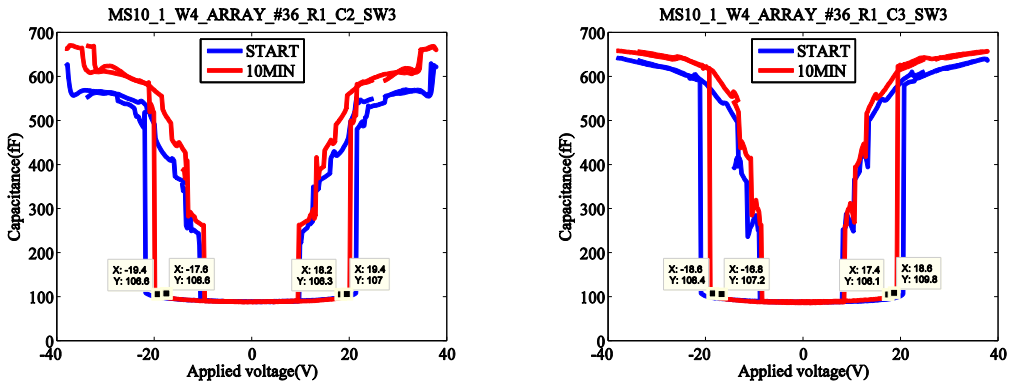

(a) Sample13.1 CV curve

(b) Sample13.2 CV curve

Figure 4.18: CV curves for unilevel, bipolar, continuous, 25 V, 100Hz, 50% duty cycle bias in vacuum

Table 4.9: Results for unilevel, bipolar, continuous, 25 V, 100 Hz, 50% duty cycle bias in vacuum

Switch Label	s_V_{PI-} (V)	s_V_{PI+} (V)	Switch Label	s_V_{PI-} (V)	s_V_{PI+} (V)
Sample13.1	1.8	-1.2	**Sample13.2**	1.8	-1.2
Sample13.3	1.4	-1.2	**Sample13.4**	1.6	-0.8
Sample13.5	1.2	-0.8			

- Facing with the screening fact in open air measurements due to very fast dielectric charging the unilevel, unipolar, cycling bias is also used for vacuum environment. Samples are from MS10.1-W4.

  Actuation type: Unipolar, unilevel, cycling, positive bias

  Actuation frequency: 100 Hz (50% duty cycle)

  Applied voltage: 25 V

  Bias period: From START to 10 MIN

  Environment: Vacuum

  None of the measured four samples in Sample14 group exhibited screening effect and CV curves for Sample14.1 and Sample14.2 are given in Figure 4.19. As a result of unipolar bias stress a zero or positive s_V_{PI+} value is the expected

consequence of a unipolar, cycling bias as verified in open air case. A negative s_V_{PI-} was not observed in open air but it is observed for vacuum environment under identical bias configuration which is surprising since negative s_V_{PI+} values are only seen in bipolar bias cases. Results for Sample14 group are provided in Table 4.10. This fact minds that charging non-uniformity is dominant for unipolar, cycling bias in vacuum environment.

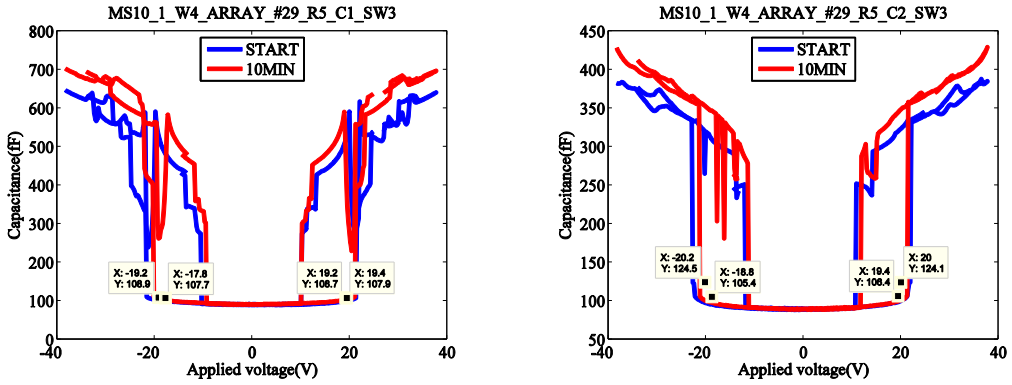

(a) Sample14.1 CV curve (b) Sample14.2 CV curve

Figure 4.19: CV curves for unilevel, unipolar, cycling, 25 V, 100 Hz, 50% duty cycle, positive bias in vacuum

Table 4.10: Results for unilevel, unipolar, cycling, 25 V, 100 Hz, 50% duty cycle, positive bias in vacuum

Switch Label	s_V_{PI-} (V)	s_V_{PI+} (V)	Switch Label	s_V_{PI-} (V)	s_V_{PI+} (V)
Sample14.1	1.4	0	**Sample14.2**	1.4	-0.6
Sample14.3	1.6	-1.2	**Sample14.4**	1.4	-0.2

- Following the unexpected result for unipolar, cycling, positive bias opposite polarity bias is also tried on another switch. Sample is from MS10.1-W4.

  Actuation type: Unipolar, unilevel, cycling, negative bias

  Actuation frequency: 1 kHz (50% duty cycle)

Applied voltage: 30 V

Bias period: From START to 30 MIN

Environment: Vacuum

Sample15.1 CV curve is shown in Figure 4.20 and as expected from the Sample14 group results the asymmetric CV curve shift together with a positive s_V_{PI-} value is observed although s_V_{PI-} is expected to have a negative value for a unipolar, negative bias. The dominancy of CV curve narrowing as also been verified for unipolar, cycling, negative bias in vacuum. As an explanation to this fact following explanation can be done:

Due to the effect of vacuum on dynamic response of an RF MEMS switch such that the lack of a mechanical damping environment, the charge injection and distribution on the dielectric layer might be strongly disturbed by the bridge causing this result.

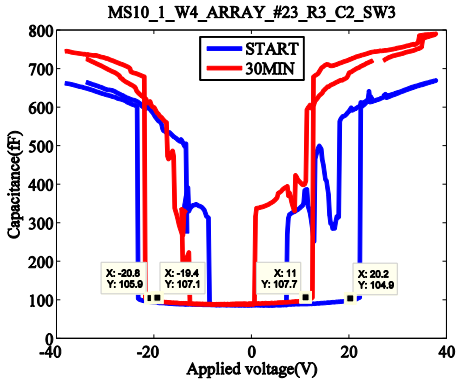

Sample15.1 CV curve

Figure 4.20: CV curves for unilevel, unipolar, cycling, 30 V, 1 kHz, 50% duty cycle, negative bias in vacuum

- Thinking that vacuum has an adverse effect on reliability the frequency of actuation is increased preserving the duty cycle for Sample14 group hence keeping the ON-state time the same but increasing the number of up and down movements. Samples are from MS10.1-W4.

  Actuation type: Unipolar, unilevel, cycling, positive bias

Alternation frequency: 10 kHz (50% duty cycle)

Applied voltage: 25 V

Bias period: From START to 10 MIN

Environment: Vacuum

Two of the measured switches exhibited failure (Sample16.1 and Sample16.4) and other measured two switches (Sample16.2 and Sample16.3) only exhibited CV curve narrowing. Note that CV curve narrowing is obviously asymmetric for this case and the amount of shift is higher than 100 Hz case. Comparing the 100 Hz and 10 kHz actuation frequencies higher number of movements is worse for the switches. This supports the idea in [64] that the same ON-state time causes different results minding the effect of charge injection during the transitions between ON and OFF-states.

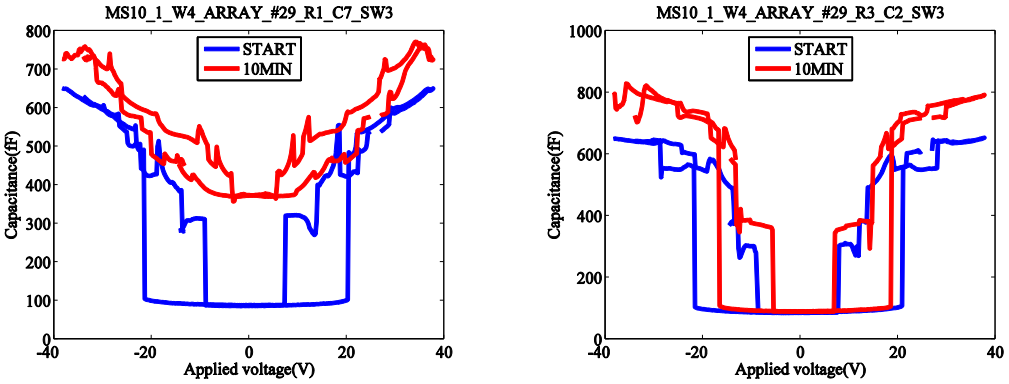

(a) Sample16.1 CV curve (b) Sample16.2 CV curve

Figure 4.21: CV curves for unilevel, unipolar, cycling, 25 V, 10 kHz, 50% duty cycle, positive bias in vacuum

Table 4.11: Results for unilevel, unipolar, cycling, 25 V, 10 kHz, 50% duty cycle, positive bias in vacuum

Switch Label	s_V_{PI-} (V)	s_V_{PI+} (V)	Switch Label	s_V_{PI-} (V)	s_V_{PI+} (V)
Sample16.2	4.8	-2.2	**Sample16.3**	4.4	-1

4.3.4 N_2 Environment Measurements

As a solution to humidity in testing atmosphere, the environment could be filled with pure N_2 gas. This allows both removal of humidity and control over environmental gas pressure. The measured samples are SWAE's. For reliability and lifetime measurements the N_2 pressure is kept close to the pressure of open air which is nearly equal to 900 mbar for the testing lab.

- This first part investigates the effect of bias polarity for continuous bias cases. The samples are from MS10.1-W4.
  Actuation type: Unipolar, unilevel, continuous, positive and negative bias
  Applied voltage: 25 V
  Bias period: From START to 10 MIN
  Environment: N_2 environment
  CV curves for Sample17.1 and Sample18.1 are provided in where the applied bias polarities are positive and negative respectively. Sample17 group are stressed with positive polarity and Sample18 group with negative polarity. Shifting amounts for both Sample17 and Sample18 group samples are provided in Table 4.12.
  Asymmetric CV curve shift is also observed for N_2 environment as can be seen from Table 4.12. It is deduced that in all environments the CV curve shift on samples of MS10.1-W4 occur asymmetrically. Moreover the shift amount, s_V_{PI+}, for Sample18 group hence for negative polarity is more with respect to positive bias shift, s_V_{PI-}. Any observation on this is not given in literature and no obvious reason for this phenomenon comes out. A rough explanation can be made such that the polarity of injected charge into the dielectric from top electrode is reverse of each other for different bias polarities. The number of charge traps in the dielectric for opposite charges might be different causing a difference in amount of injected charges. For our measurements Si_xN_y seems to have more traps for positive charges since the top electrode potential is higher than the bottom electrode for Sample18 group.

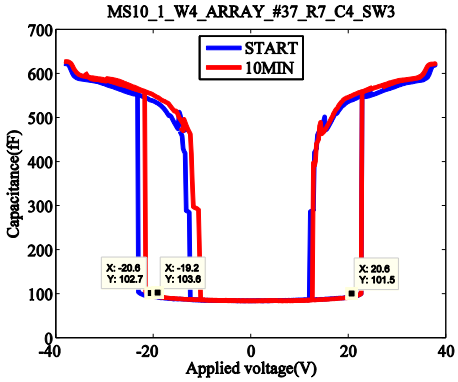

(a) Sample17.1 CV curve

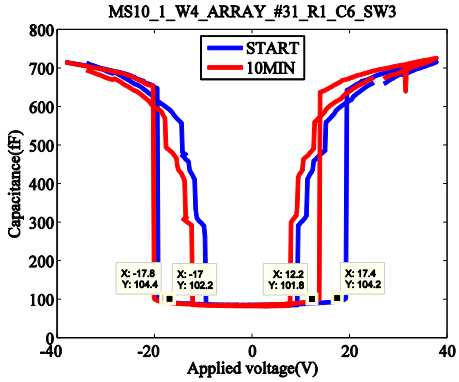

(a) Sample18.1 CV curve

Figure 4.22: CV curves for unilevel, unipolar, continuous, 25 V, positive and negative bias in N_2 environment

Table 4.12: Results for unilevel, unipolar, continuous, 25 V, positive and negative bias in N_2 environment

Switch Label	**s_V_{PI-} (V)**	**s_V_{PI+} (V)**	**Switch Label**	**s_V_{PI-} (V)**	**s_V_{PI+} (V)**
Sample17.1	1.4	0	**Sample17.2**	1.4	0
Sample17.3	1.2	0	**Sample17.4**	3.6	0.8
Sample17.5	1.6	1			
Switch Label	**s_V_{PI-} (V)**	**s_V_{PI+} (V)**	**Switch Label**	**s_V_{PI-} (V)**	**s_V_{PI+} (V)**
Sample18.1	-0.8	-5.2	**Sample18.2**	-0.2	-3.6
Sample18.3	0	-4	**Sample18.4**	-0.4	-3.8
Sample18.5	-0.6	-4.4			

- To verify the results for Sample17 and Sample18 group more switches from a different wafer are measured. The samples of this test are from MS9-W1.

  Actuation type: Unipolar, unilevel, continuous, positive and negative bias

  Applied voltage: 25 V

  Bias period: From START to 10 MIN

Environment: N_2 environment

CV curves for Sample19.1 and Sample20.1 are given in Figure 4.23. Asymmetric CV curve shifts for both polarities are again observed. Results of all measured switches from Sample19 and Sample20 group are given in Table 4.13. The expected results are also obtained for this test. s_V_{PI+} under negative bias is higher than s_V_{PI-} under positive bias. So the result seen from Sample17 and Sample18 measurements is verified on MS9-W1 samples.

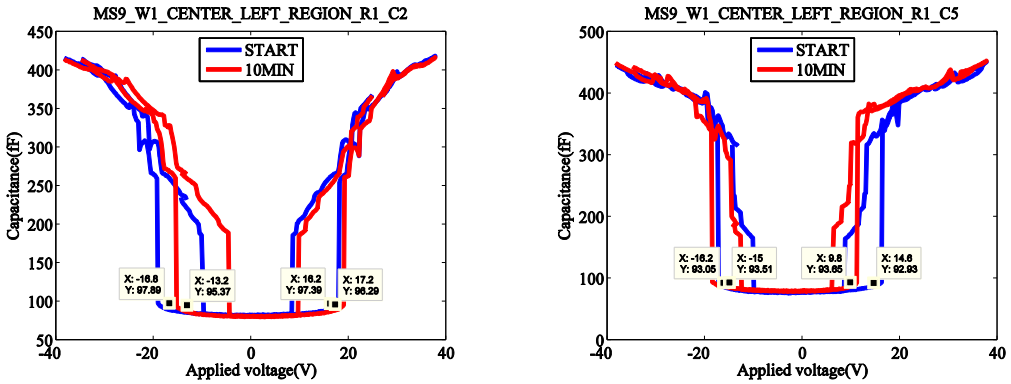

(a) Sample19.1 CV curve (b) Sample20.1 CV curve

Figure 4.23: CV curves for unilevel, unipolar, continuous, 25 V, positive and negative bias in N_2 environment

Table 4.13: Results for unilevel, unipolar, continuous, 25 V, positive and negative bias in N_2 environment

Switch Label	**s_V_{PI-} (V)**	**s_V_{PI+} (V)**	**Switch Label**	**s_V_{PI-} (V)**	**s_V_{PI+} (V)**
Sample19.1	3.6	1	**Sample19.2**	5.4	2.4
Sample19.3	2.8	1			
Switch Label	**s_V_{PI-} (V)**	**s_V_{PI+} (V)**	**Switch Label**	**s_V_{PI-} (V)**	**s_V_{PI+} (V)**
Sample20.1	-1.2	-4.8	**Sample20.2**	-1.2	-5.6
Sample20.3	-2.4	-6.4			

- To test the durability of switches in N_2 environment against unilevel, bipolar, continuous bias with high voltage a waveform with following parameters are applied:

  Actuation type: Bipolar, unilevel, continuous bias

  Alternation frequency: 100 Hz, 50% duty cycle

  Applied voltage: 40 V

  Bias period: From START to 10 MIN

  Environment: N_2 environment

  The switches are from MS10.1-W4 and to make a fair comparison with open air and vacuum environments the voltage amplitude is set to 40 V. Four of the measured five switches exhibited failure like Sample21.1 and only one of them could withstand which is Sample21.4. This result shows that for all three environments applying bipolar bias with voltages far higher than the pull-in voltage causes a switch most likely to fail. In any case the switches should be protected against long time high voltage stresses.

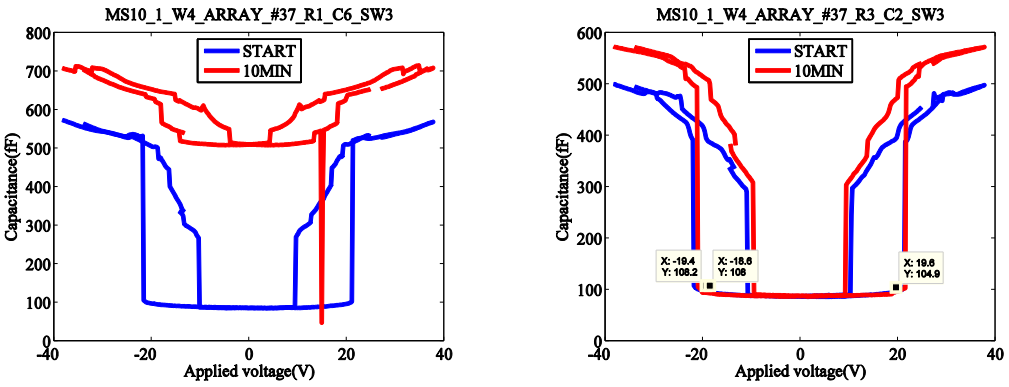

(a) Sample21.1 CV curve (b) Sample21.4 CV curve

Figure 4.24: CV curves for unilevel, bipolar, continuous, 40 V, 100Hz, 50% duty cycle bias in N_2 environment

- For comparing the environments the configuration for Sample21 group is preserved and voltage is lowered to 25 V.

  Actuation type: Bipolar, unilevel, continuous bias

Alternation frequency: 100 Hz, 50% duty cycle

Applied voltage: 25 V

Bias period: From START to 10 MIN

Environment: N_2 environment

The CV curves of Sample22.1 and Sample22.2 are provided in Figure 4.25 and none of the measured switches in Sample22 group failed. Superiority of N_2 environment over open air is clearly seen from this test that there are failed switches in open air with identical bias configuration. Furthermore the amount of shifts, s_V_{PI-} and s_V_{PI+}, are a bit less than the vacuum case as can be seen from Table 4.9 and Table 4.14. This test proves that with other counterpart tests in open air and vacuum even using bipolar actuation for preventing dielectric charging is not enough, in all environments definitely non-uniform charging occurs.

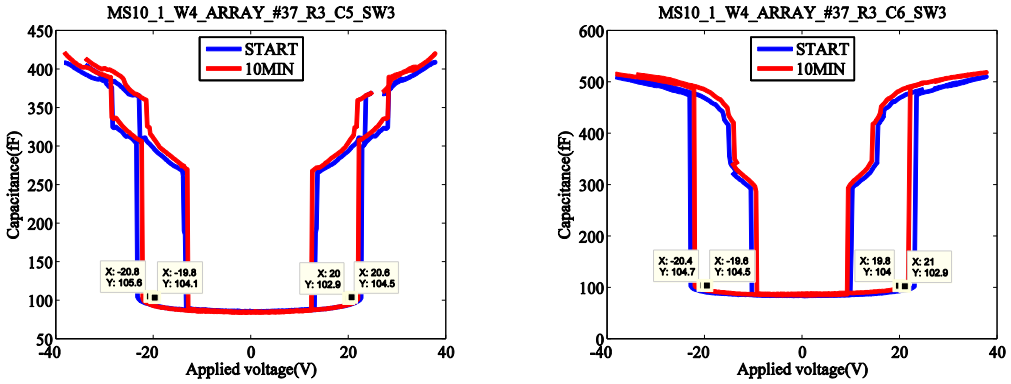

(a) Sample22.1 CV curve (b) Sample22.2 CV curve

Figure 4.25: CV curves for unilevel, bipolar, continuous, 25 V, 100Hz, 50% duty cycle bias in N_2 environment

Table 4.14: Results for unilevel, bipolar, continuous, 25 V, 100 Hz, 50% duty cycle bias in N_2 environment

Switch Label	s_V_{PI-} (V)	s_V_{PI+} (V)	Switch Label	s_V_{PI-} (V)	s_V_{PI+} (V)
Sample22.1	1	-0.6	**Sample22.2**	0.8	-1.2
Sample22.3	0.8	-0.8	**Sample22.4**	1.4	-1.2

- To see the effect of ON-state time on response of the switch bipolar, unilevel cycling bias waveform with high voltage amplitude is used. The test is performed for two different duty cycles. Samples are from MS10.1-W4.

  Actuation type: Bipolar, unilevel, cycling bias

  Actuation frequency: 1 kHz, 50% and 2.5% duty cycles

  Applied voltage: 50 V

  Bias period: From START to 10 MIN

  Environment: N_2 environment

  The DOV are given in Figure 4.26 for Sample23.1 and Sample24.1 group switches. 50% duty cycle bias is applied on Sample23 and 2.5% duty cycle bias is applied on Sample24 group. Among the measured nine switches of Sample23 group only one switch did not fail during 10 minutes, all of the other exhibited failure as shown in Figure 4.26-a. None of the five switches in Sample24 group stuck down during actuation period, all of them had DOV data similar to the given one in Figure 4.26-b. This shows that short contact time prevents the switch from collapsing down during actuation even if the applied voltage is more than twice the pull-in voltage but this high voltage shows the effect in CV curve measurements. All of the switches, except only one switch from Sample24 group, exhibited failure as indicated by CV curve of Sample23.1 in Figure 4.27. Although switches of Sample24 group withstood during actuation four of them failed during CV curve measurements. Being a tricky method the duty cycle might be decreased to increase the lifetime in terms of number of cycles for long-term lifetime measurement tests since duty cycle is directly effective on degradation as shown.

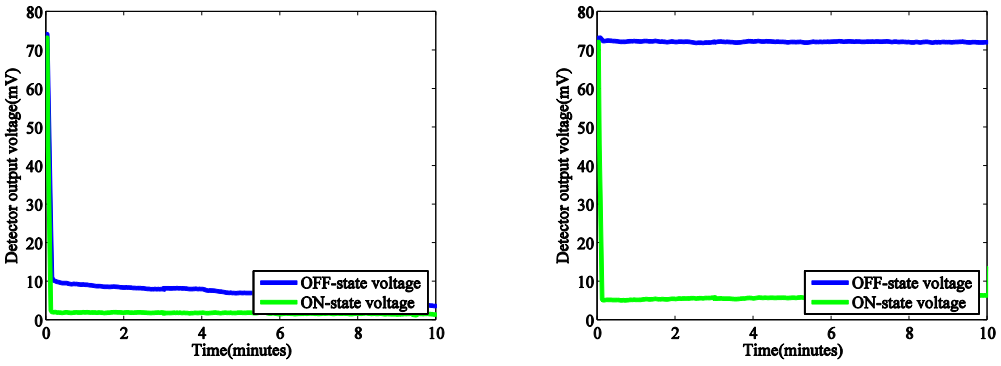

(a) Sample23.1 DOV vs. time (b) Sample24.1 DOV vs. time

Figure 4.26: DOV data for unilevel, bipolar, cycling, 50 V, 1 kHz, 50% and 2.5% duty cycle bias in N_2 environment

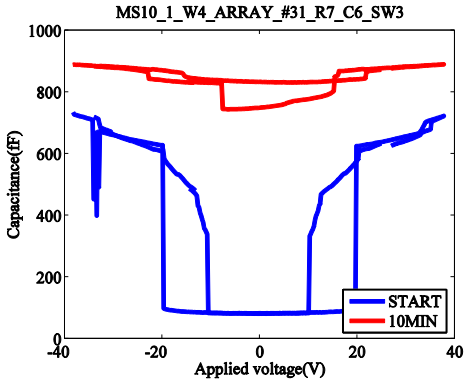

Sample23.1 CV curve

Figure 4.27: CV curve for unilevel, bipolar, cycling, 50 V, 1 kHz, 50% duty cycle bias in N_2 environment

- To increase the adhesion of base metal layer to the substrate the roughness is increased by inserting the wafer into BHF solution for a short time before deposition of base metal. Thinking that there might be an effect of roughness on dielectric charging two wafers are fabricated with the same process and dimension parameters except for the roughness increase step. BHF is *not* applied on MS10.1-W1 and is applied on MS10.1-W3. Sample 25 group is from MS10.1-W1 and

Sample26 group is from MS10.1-W3. Results are given in Table 4.15 and measurement parameters are as follows:

Actuation type: Unipolar, unilevel, continuous bias

Applied voltage: 40 V

Bias period: From START to 10 MIN

Environment: N_2 environment

As Table 4.15 shows that asymmetric CV curve shift also occurs for these samples and the s_V_{PI-} for Sample25 group is less than Sample26 group. This fact may be explained as the increased number of charge traps in a dielectric layer grown on a rougher surface. Although this phenomenon should be studied further, these results give an idea about roughness impact on dielectric charging.

Table 4.15: Results for unilevel, bipolar, continuous, 25 V, 100 Hz, 50% duty cycle bias in N_2 environment

Switch Label	**s_V_{PI-} (V)**	**s_V_{PI+} (V)**	**Switch Label**	**s_V_{PI-} (V)**	**s_V_{PI+} (V)**
Sample25.1	3.2	1.8	**Sample25.2**	4.2	3.8
Sample25.3	5.8	3.6	**Sample25.4**	6.2	3.2
Sample25.5	4.6	2	**Sample25.6**	4.8	2.6
Average	**4.8**	**2.83**			
Switch Label	**s_V_{PI-} (V)**	**s_V_{PI+} (V)**	**Switch Label**	**s_V_{PI-} (V)**	**s_V_{PI+} (V)**
Sample26.1	5.8	2.4	**Sample26.2**	5.4	1
Sample26.3	5	3	**Sample26.4**	8	2.6
Sample26.5	5.4	0.8	**Sample26.6**	6.4	3.2
Sample26.7	6	4	**Sample26.8**	4.6	1.2
Sample26.9	5.4	2.6	**Sample26.10**	4.8	0.4
Sample26.11	5.6	2.8	**Sample26.12**	4.4	0
Sample26.13	5	1	**Sample26.14**	5.6	2
Average	**5.53**	**1.93**			

- Measurements on MS10.1-W4 samples with perforated dielectric are also performed. All of the perforated dielectric type switches have burned due to shortage between signal and ground lines. Reason for this failure can be explained through Figure 4.28. Figure 4.28 gives the profile of structural metal layer at the bridge region. The hills and valleys are easily seen from Figure 4.28-b and measurement results are given in Figure 4.28-a. Measurement along the vertical axis shows that the level difference between hills and valleys is approximately 0.2 um. When the switch is actuated the bridge approaches to the signal line very much at the regions between islands causing the burn up. CMP might be proposed as a solution to this problem since it will make the sacrificial polyimide layer flat eliminating the effects of conformal coating.

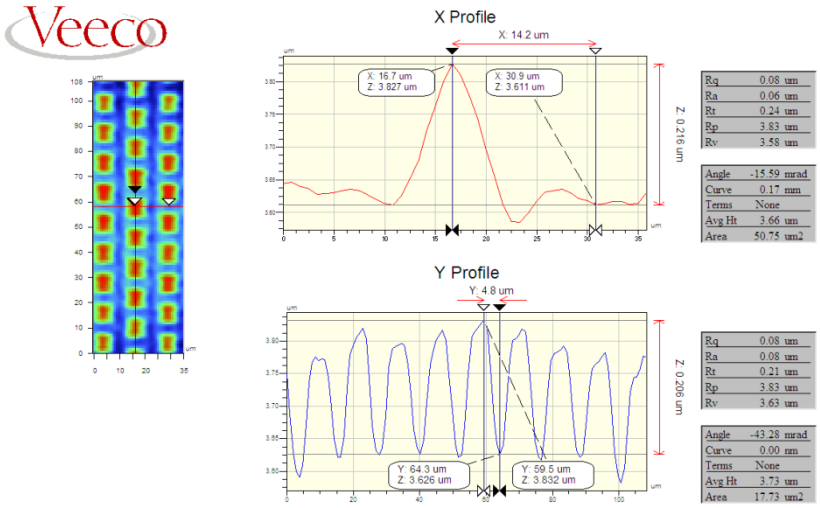

(a) Top view and measurement

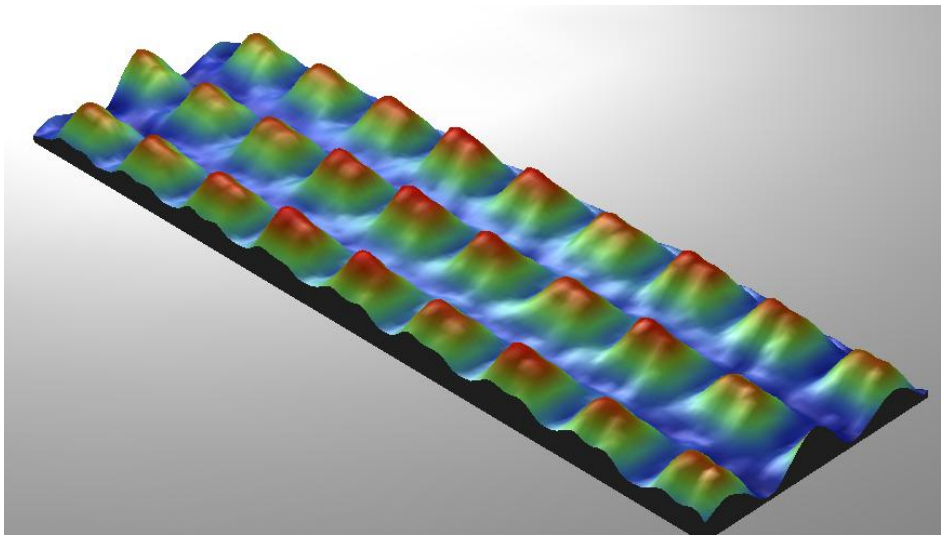

(b) 3-dimensional view

Figure 4.28: Optical profiler measurement of a sample switch with square shape dielectric islands

4.3.5 Long-term Measurements

As the main aim of this study is set to be improvement of the reliability and lifetime of RF MEMS devices long-term measurements are performed to determine the lifetime of RF MEMS switches fabricated in METU MEMS Center facilities by METU RF MEMS Research Group. The environment is chosen to be N_2.

- The first long-term test was performed to see how long a switch could withstand after staying continuously in ON-state. Knowing that unipolar, continuous bias stress shift the CV curve in a direction, polarity change with long intervals is tried i.e. if he test starts with polarity it is biased for a certain time, a CV curve measurement is performed, the test continuous with biasing at opposite polarity and this alternation procedure is repeated. Sample is chosen from M10.1-W4 and is called Sample27.

  Actuation type: Unipolar, unilevel, continuous bias

  Applied voltage: 25 V

  Environment: N_2 environment

  The idea behind this test is very simple. For opposite polarities the CV curve moves in opposite directions. By changing the polarity regularly balancing on the shifting of CV curve could be done. CV curves at different instants are given in Figure 4.29. As can be seen from Figure 4.29-a and Figure 4.29-b the bias starts with positive polarity up to 30 minutes and it is reversed for the following 30 minutes. Right and left shift of CV curve is obviously seen. The previously observed phenomenon, non-uniform dielectric charging occurs again here and it can be seen from Figure 4.29-c as the difference between CV curve at start and at 3 hours 30 minutes after consecutive alternation of the bias polarity with 30 minutes intervals. The degradation mechanism at last causes the failure of RF MEMS switch after 4 hours as indicated by Figure 4.29-d.

  This test clearly shows that alternation of the polarity even with very low frequencies (For this test approximately 0.56 mHz) is not enough for increasing lifetime.

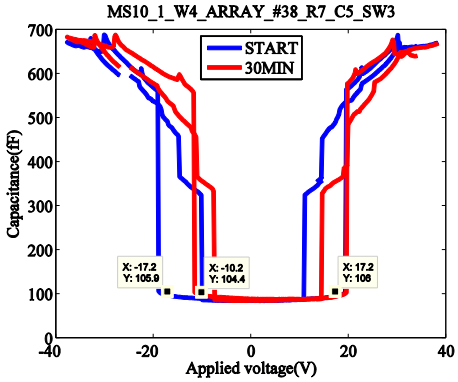

(a) START and 30MIN

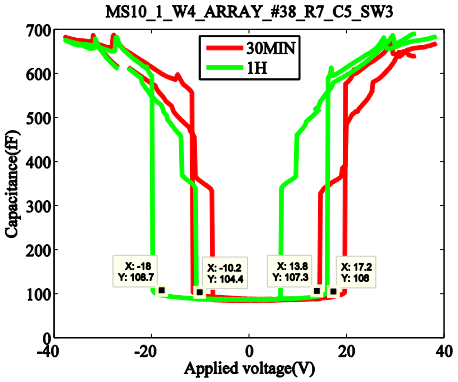

(b) 30MIN and 1HOUR

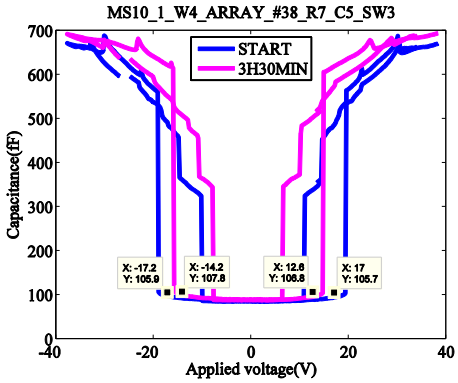

(c) START and 3HOUR30MIN

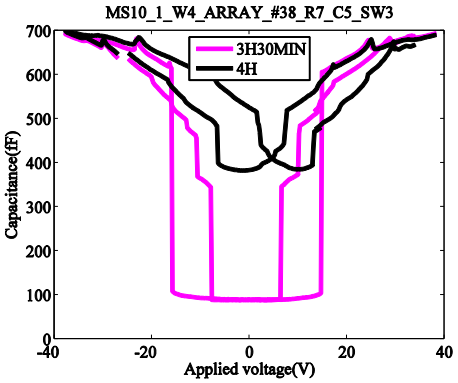

(d) 3HOUR30MIN and 4HOUR

Figure 4.29: Sample27 CV curves at different instants

- Despite the definite knowledge on the degradation mechanism of bipolar bias waveforms long-term lifetime measurements with bipolar waveforms are also performed. Samples are from MS10.1-W4.

  Actuation type: Bipolar, unilevel, continuous bias

  Alternation frequency: 1 Hz, 50% duty cycle

  Applied voltage: 25 V

  Environment: N_2 environment

  The most durable switch, Sample28, for this test has failed between 19 hours 30 minutes and 25 hours 52 minutes. The CV curves of Sample28 for different instants are given in Figure 4.30. The expected CV curve narrowing is observed. This test on the other hand minds a dielectric charging saturation opinion as can be

deduced from Table 4.16.[15] The amount of change in pull-in voltages is less for 17 hours bias period after 2 hours 30 minutes than the initial 2 hours 30 minutes bias period. Deceleration of dielectric charging is obvious as the pull-in voltages indicate but although it slows down as time passes, it does not stop resulting with the failure shown in Figure 4.30-b.

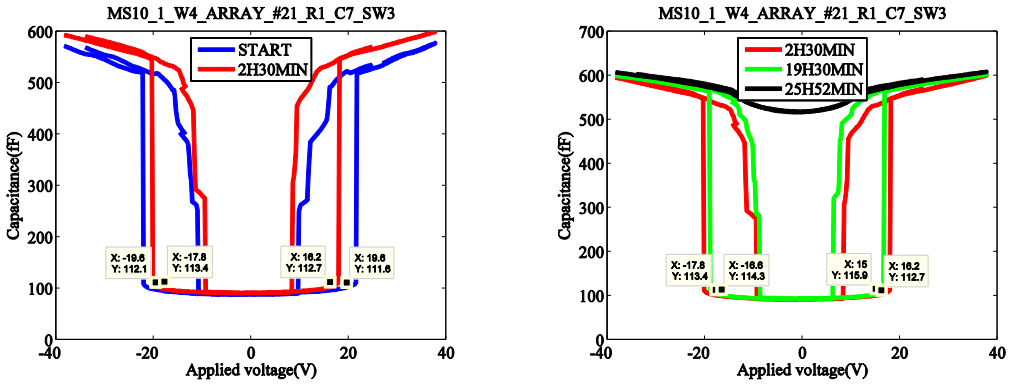

(a) START and 2HOUR30MIN

(b) 2HOUR30MIN, 19HOUR30MIN and 25HOUR52MIN

Figure 4.30: Sample28 CV curves at different instants

Table 4.16: Shifting amount of CV curves for Sample28

Time Interval	s_V_{PI-} (V)	s_V_{PI+} (V)
START to 2 HOURS 30 MINUTES	1.8	-3.4
2 HOURS 30 MINUTES to 19 HOURS 30 MINUTES	1.2	-1.2

[15] Saturation of dielectric charging seems logical since there should be finite number of charge traps giving a finite charge storage capacity to the isolation dielectric.

- Since charge injection could approach to a saturation point for bipolar bias it might also be the case for unipolar bias. For this reason long-term unipolar continuous bias test is performed. Sample29 is from MS10.1-W4.

  Actuation type: Unipolar, unilevel, continuous bias

  Applied voltage: 25 V

  Environment: N_2 environment

  CV curves for Sample29 are given in Figure 4.31. DOV data in binary manner for different instants are given in Table 4.17. *HIGH* accounts for the value of DOV in OFF-state and *LOW* accounts for the value in ON-state.

  As shown several times by different tests the asymmetric CV curve shift is also observed for this test as seen from Figure 4.31-a. The contact enhancement for ON-state can be also noticed from Figure 4.31-a and Figure 4.31-b. Slowing down of dielectric charging is observed from the comparison of CV curves at START, 22HOUR19MIN and 69HOUR52MIN instants. (Figure 4.31-b) s_V_{PI-} value from START to 22HOUR19MIN is obviously greater than the s_V_{PI-} value from 22HOUR19MIN to 69HOUR52MIN although the bias period for the second case is greater. This phenomenon minds that if an optimum spring constant could be found for the RF MEMS switch then the applied voltage could not inject (or inject very slowly) more charges into the dielectric after a point and the injected charges could not stick down the switch i.e. the switch could be moved up and down with the applied voltage without further dielectric charging which could be a subject of investigation.

  One more fact on unipolar, unilevel, continuous bias is that the interval of uninterrupted bias is important in terms of proper operation where the idea developed from the analysis of data in Table 4.17. The switch is continuously biased without any termination for 5 hours starting from 97 hours to 102 hours. When the bias is terminated at 102 hours the switch could come to OFF-state as DOV states that the value is *HIGH*. Biasing from 102 hours to 121 hours 22 minutes has resulted with a DOV value of *LOW* at bias termination instant. The switch has been recovered to OFF-state by CV curve measurement at 121 hours 22 minutes. Then the switch is again biased continuously from 121 hours 22 minutes to 122 hours 3 minutes and the DOV was *HIGH* when the bias was terminated. Here comes the fact that the length of bias is important. Although the switch is biased further after 121 hours 22 minutes since the bias period is 41 minutes which

is shorter than the previous bias period of 19 hours 22 minutes. Another point to notice is that the easy recoverability of RF MEMS bridge. Even if the switch collapses down as seen at the instant of 121 hours 22 minutes it can easily be pulled up by a CV curve measurement where the measured proper CV curve could be seen from Figure 4.31-c. This could be explained as follows:

The dielectric grabs the switch due to dielectric charging holding it down. The applied negative bias during CV curve measurement could discharge the injected charge into the dielectric causing release of the bridge after CV curve measurement. This explanation comes to another point. For this easy recovery during CV curve measurement the injected charge should be located at close regions to the top surface of dielectric or they might be just surface charges so that they can be removed away very quickly.

Considering the mentioned fact a method could be proposed for fast recovery of switches. At certain times for long ON-state times or when the actuation is stopped the polarity might be changed for a short time to discharge the injected charge and returned back for continuing the bias at regular polarity. Instead of changing the polarity a triangular waveform sweeping from negative voltages to positive voltages might also be used for recovery purpose.

Finally Figure 4.31-d indicates that even after totally 164 hours 15 minutes of bias the CV curve is nearly the same with the 22 hours 19 minutes instant. The CV curve at 164 hours 15 minutes is still a proper one with clear pull-in and hold-down voltages and the same OFF-state capacitance with the starting value pointing out that the switch is still operational.

Table 4.17: Sample29 DOV data at different instants

CV Curve Measurement-Bias Termination Instant (From START)	**Bias Start**	**Bias Interval**	**Detector Output Voltage At Bias Termination Instant**
102HOUR	97HOUR	5 hours	HIGH
121HOUR22MIN	102HOUR	19 hours 22 minutes	LOW
122HOUR3MIN	121HOUR22MIN	41 minutes	HIGH

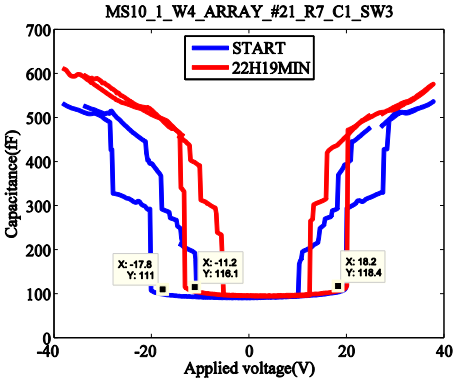

(a) START and 22HOUR19MIN

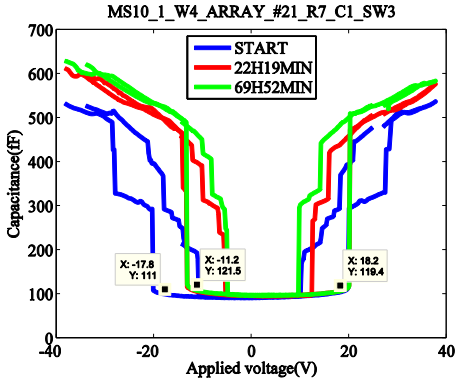

(b) START, 22HOUR19MIN and 69HOUR52MIN

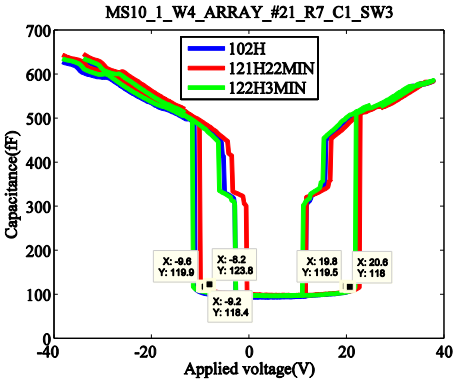

(c) 102HOUR, 121HOUR22MIN and 122HOUR3MIN

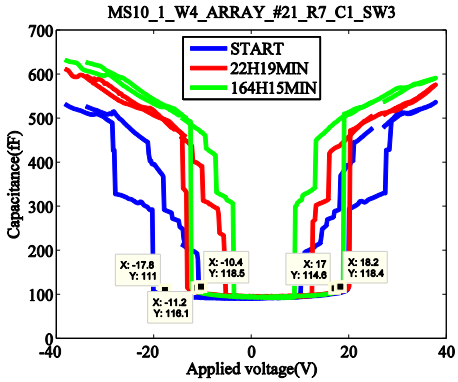

(d) START, 22HOUR19MIN and 164HOUR15MIN

Figure 4.31: Sample29 CV curves at different instants

- Considering the adverse effect of unipolar, unilevel, cycling bias waveforms in open air as very fast dielectric charging and in vacuum as strong disturbance on charge uniformity on the dielectric, the same bias waveform is also used for long-term test in N_2 environment. Sample30 is from MS10.1-W4.

  Actuation type: Unipolar, unilevel, cycling bias

  Actuation frequency: 1 kHz, 50% duty cycle

  Applied voltage: 25 V

  Environment: N_2 environment

The measurement results for Sample30 are given in Figure 4.32. The decreasing trend of OFF-state DOV and increasing trend of ON-state DOV is immediately noticed from Figure 4.32-a. Decrease of OFF-state DOV shows the effect of additional electrostatic force created by the injected charges and increase of ON-state DOV shows the effect of screening.[16] Although the measured CV curve after terminating the bias is an improper one just after the CV curve measurement finished DOV has returned to its pristine value. This test indicates that even for unipolar, cycling bias performance of the switch slowly degrades and easily recoverable. For further lifetime improvement a long-term test with unilevel, bipolar, cycling bias waveform is also performed.

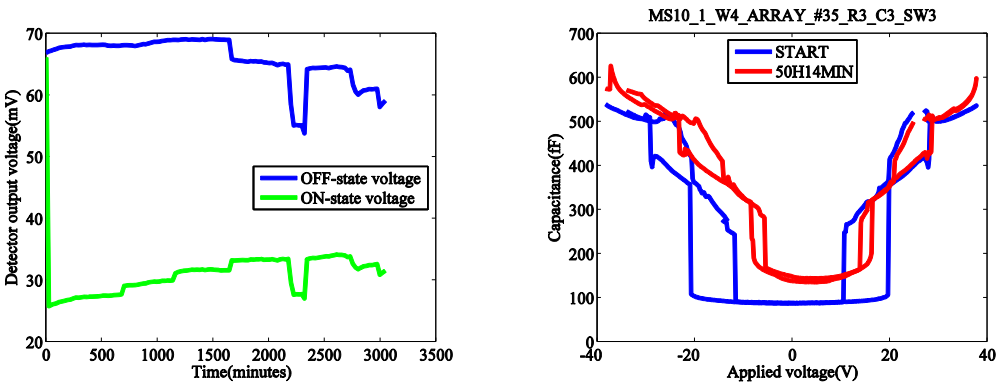

(a) Sample30 DOV data (b) Sample30 CV curve

Figure 4.32: Sample 30 DOV data and CV curve

- As the follower of unipolar, unilevel, cycling bias for long-term test bipolar, unilevel, cycling bias waveform is also used. This test led to the most remarkable result of this study. Sample31 is from MS10.1-W4.

  Actuation type: Bipolar, unilevel, cycling bias

  Actuation frequency: 1 kHz, 50% duty cycle

[16] The sharp decrease and increase in DOV data between 2000 and 2500 minutes is caused by a data acquisition problem due to bad contact of probes on the switch.

Applied voltage: 25 V

Environment: N_2 environment

Figure 4.33 gives the time domain and CV curve measurement data of Sample32. Figure 4.33-a presents the DOV measurement result for Sample31 from beginning to the end. With corruptions due to CV curve measurements and short blackouts during the test the switch has operated successfully for approximately 885 hours 13 minutes which corresponds to approximately 3.2 billion of operation cycles. In terms of operation time for low microwave power testing this result is more than 30 times better than the longest lifetime[17] measured in METU RF MEMS Research Group. [92] At the end of 885 hours 13 minutes DOV value dropped to a level between OFF-state and ON-state value which shows that partial stiction has occurred. Additionally during this test the longest uninterrupted actuation session has lasted in 259 hours 40 minutes which started at 625 hours 33 minutes and finished with failure. In other words the switch was able to operate for 259 hours 40 minutes continuously in a cycling manner. Figure 4.33-b shows the proper operation of switch at START and 625H33MIN. As the OFF-state capacitance increase indicates the switch has failed after 885 hours 13 minutes.

Figure 4.33-c the interesting after failure behavior of the switch. The CV curve is taken twice after failure as indicated by the 886H59MIN and 886H59MIN#2 curves in Figure 4.33-c. The third measurement performed just after 886H59MIN#2 is given as 886H59MIN#3 where a proper CV curve is observed with OFF-state capacitance equal to its pristine value and clear pull-in and hold-down voltages. This reminds the recovering effect of CV curve measurement or in other words sweeping the voltage from one polarity to other comes in to play again as seen in long-term test with unipolar, unilevel, continuous bias.

[17] 90 million cycles

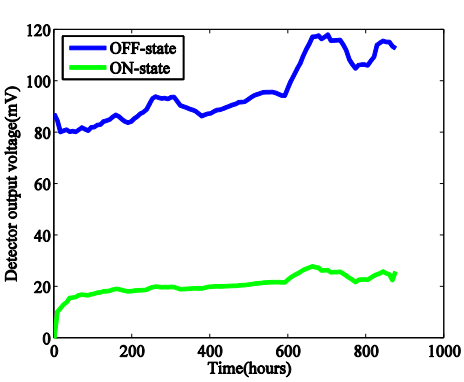

(a) Sample31 DOV data

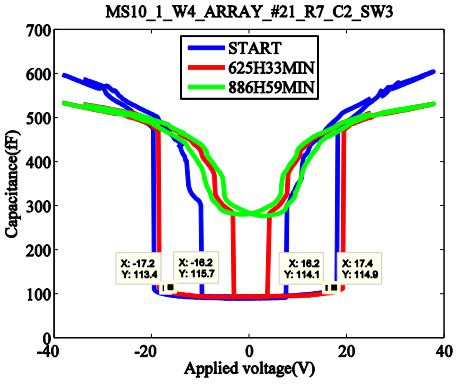

(b) Sample31 CV curves

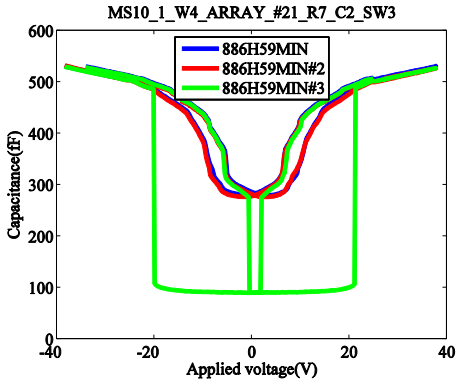

(c) Sample31 CV curves

Figure 4.33: Sample31 DOV data and CV curves

4.3.6 Future Work

Although the test results show that the fabricated switches in MS10.1 have improved performances with respect to the previous measurements further advancements could be achieved.

- All of the bias waveforms used in this study are unilevel. By modifying the bias circuit as to generate bilevel bias waveforms the lifetimes could be increased.
- The mentioned triangular voltage waveform could be embedded into the regular bias waveform by programmable supplies so that better lifetimes for long-term continuous bias cases could be obtained.

- CMP could be used to planarize the top surface of sacrificial layer polyimide so that the switches with perforated dielectrics could be measured without burning. Due to less charging expectation the lifetime could be increased.
- Tests could be repeated at different temperatures and higher microwave power levels to investigate the effect of temperature and incident power.

4.4 Conclusion

In this chapter the main focus of this study, the reliability and lifetime measurements are presented. First the measured samples and measurement methods are introduced. Then the results for partial CV curve measurements, open air measurements, vacuum measurements and N_2 environment measurements are given. After that the results of long-term tests in N_2 environment are given and finally the further improvements as future work are proposed.

CHAPTER 5

CONCLUSION AND FUTURE WORK

This thesis presents mainly a reliability investigation and lifetime improvement for the RF MEMS switches fabricated using METU RF MEMS Process in METU MEMS Center Clean Room facilities. This study consists of mainly three parts. First the designed switches are fabricated. The switches are of shunt, capacitive contact type and designed to have maximum isolation at 35 GHz. To have sufficient number of samples a wafer layout consisting of different types of switches has been prepared and fabrication is completed according to this layout and mm-wave measurements are performed to verify the success of process. Second accomplishment is the establishment of a setup required for reliability and lifetime measurements. Since no specific measurement device for reliability exists, some of the research effort is spent to constructing the setup. Finally the most important topic of the thesis, the reliability investigation and lifetime improvement comes. Highly satisfactory results in terms reliability obtained from the measurements both shows the maturity of METU RF MEMS Process and takes the METU RF MEMS Research Group reliability studies to a far better point with respect to its previous situation.

Considering the research effort throughout this thesis the following conclusions can be written:

- Fabrication of switches designed previously according to the provided mm-wave performance specifications is successfully completed. This fabrication has been an evidence for the maturity of the METU RF MEMS process due to the similar mm-wave measurement results obtained in the context of this thesis.

- Importance of etch holes on RF MEMS bridge is shown in this study. For the switch design of interest the bridges could not be suspended successfully in the lack of etch holes.
- For real-time monitoring of switch performance a time domain setup is established and the RF performance of the switch can be observed during actuation. Also the dynamic behavior of the switch can be deduced by measuring the switching times using this setup where switching times of fabricated switches in METU RF MEMS group which are measured outside the scope of this study are typically ranging from 5 us to 10 us .
- Operation of RF MEMS switches under different bias conditions in different environments is investigated. Accelerating effect of uncontrolled, humid environment on dielectric charging is observed as indicated by the screening phenomenon in open air measurements.
- Insufficient useful contribution of controlling the humidity by taking into vacuum is also observed. Vacuum environment makes the dielectric prone to charging due to high voltage transition under bipolar bias stresses and the observation for different actuation frequencies shows the inconvenience of using vacuum for frequent switching applications.
- Trying the N_2 environment to remove humidity has given better results than open air and vacuum measurements in terms of reliability leading the way to use this environment for lifetime measurements. So the investigation of the effects of environmental parameters on reliability and lifetime is successfully completed by this study and the most suitable conditions are chosen for long-term tests.
- For long-term continuous actuation case the switch was still operational even after totally 160 hours of bias. For long-term cycling bias the switch has been operational for approximately 885 hours of actuation where 35 times improvement has been accomplished with respect to the previously measured best lifetime in METU RF MEMS Research Group.
- In conclusion throughout this study, RF MEMS switches are successfully fabricated, reliability investigations are done and improved lifetimes are measured in the chosen suitable conditions.

In the light of research done in this study the following works can be proposed for further improvement:

- To prevent the buckling down hence the mechanical degradation of bridge either the side regions can be remained as coated with isolation dielectric or CMP might be used to obtain a plain surface of sacrificial layer.
- In the time domain setup DC blocks can be removed to decrease the loss of the system and couplers might be used. These couplers might also be used to measure the input signal power to the coupler to be used as a reference where this information may be used for calibrating the output data against a possible drift in the power levels.
- More robust test beds might be produced to ensure good RF contact on the RF MEMS switch so that the measurement would not be affected by the vibrations of environment.
- Bilevel bias waveforms might be used to decrease the bias stress on the isolation dielectric during actuation.
- During continuous long-term actuations the bias polarity could be reversed with regular intervals for discharging the isolation dielectric.
- CMP could be also useful for proper measurement of perforated dielectric switches by removing the hills and valleys on the bridge due to the conformal coating of sacrificial layer over the gaps between dielectric islands.
- More variables can be introduced in the tests such as the temperature and microwave signal power level.
- Based on the measurements comparing the rough and flat dielectric switches, samples with different roughness levels might be prepared for investigation of roughness effect.
- Different materials for base metal, isolation dielectric, structural layer bridge and different deposition conditions for the materials can be tried for improvement of reliability and lifetime.

It is believed that the measurements which are the heart of this thesis study provide useful information for future works related to RF MEMS reliability. It is author's opinion that enhanced results with respect to the ones presented in this study could be obtained by working more on this subject.

REFERENCES

[1] L. E. Larson, "Microwave MEMS technology for next-generation wireless communications," in *Microwave Symposium Digest, 1999 IEEE MTT-S International*, 1999, pp. 1073-1076 vol.3.

[2] G. M. Rebeiz, *RF MEMS: Theory, Design and Technology*: John Wiley and Sons, 2003.

[3] J. B. Muldavin and G. M. Rebeiz, "High-isolation CPW MEMS shunt switches. 1. Modeling," *Microwave Theory and Techniques, IEEE Transactions on*, vol. 48, pp. 1045-1052, 2000.

[4] J. B. Muldavin and G. M. Rebeiz, "High-isolation CPW MEMS shunt switches. 2. Design," *Microwave Theory and Techniques, IEEE Transactions on*, vol. 48, pp. 1053-1056, 2000.

[5] S. P. Pacheco, *et al.*, "Design of low actuation voltage RF MEMS switch," in *Microwave Symposium Digest., 2000 IEEE MTT-S International*, 2000, pp. 165-168 vol.1.

[6] S. Duffy, *et al.*, "MEMS microswitches for reconfigurable microwave circuitry," *Microwave and Wireless Components Letters, IEEE*, vol. 11, pp. 106-108, 2001.

[7] J. B. Muldavin and G. M. Rebeiz, "All-metal high-isolation series and series/shunt MEMS switches," *Microwave and Wireless Components Letters, IEEE*, vol. 11, pp. 373-375, 2001.

[8] S. Majumder, *et al.*, "A packaged, high-lifetime ohmic MEMS RF switch," in *Microwave Symposium Digest, 2003 IEEE MTT-S International*, 2003, pp. 1935-1938 vol.3.

[9] P. Blondy, *et al.*, "Dielectric less capacitive MEMS switches," in *Microwave Symposium Digest, 2004 IEEE MTT-S International*, 2004, pp. 573-576 Vol.2.

[10] J. McKillop, *et al.*, "Design, Performance and Qualification of a Commercially Available MEMS Switch," in *Microwave Conference, 2006. 36th European*, 2006, pp. 1399-1401.

[11] J. Muldavin, *et al.*, "Wafer-Scale Packaged RF-MEMS Switches," in *Microwave Symposium Digest, 2006. IEEE MTT-S International*, 2006, pp. 267-270.

[12] H. Sedaghat-Pisheh, *et al.*, "A Novel Stress-Gradient-Robust Metal-Contact Switch," in *Micro Electro Mechanical Systems, 2009. MEMS 2009. IEEE 22nd International Conference on*, 2009, pp. 27-30.

[13] Y. Uno, *et al.*, "Development of SPDT-structured RF MEMS switch," in *Solid-State Sensors, Actuators and Microsystems Conference, 2009. TRANSDUCERS 2009. International*, 2009, pp. 541-544.

[14] Z. J. Yao, *et al.*, "Micromachined low-loss microwave switches," *Microelectromechanical Systems, Journal of*, vol. 8, pp. 129-134, 1999.

[15] W. Ye, *et al.*, "Low-voltage lateral-contact microrelays for RF applications," in *Micro Electro Mechanical Systems, 2002. The Fifteenth IEEE International Conference on*, 2002, pp. 645-648.

[16] A. Dec and K. Suyama, "Micromachined electro-mechanically tunable capacitors and their applications to RF IC's," *Microwave Theory and Techniques, IEEE Transactions on*, vol. 46, pp. 2587-2596, 1998.

[17] Z. Jun, *et al.*, "Development of a wide tuning range MEMS tunable capacitor for wireless communication systems," in *Electron Devices Meeting, 2000. IEDM Technical Digest. International*, 2000, pp. 403-406.

[18] L. Dussopt and G. M. Rebeiz, "High-Q millimeter-wave MEMS varactors: extended tuning range and discrete-position designs," in *Microwave Symposium Digest, 2002 IEEE MTT-S International*, 2002, pp. 1205-1208.

[19] R. L. Borwick, III, *et al.*, "A high Q, large tuning range, tunable capacitor for RF applications," in *Micro Electro Mechanical Systems, 2002. The Fifteenth IEEE International Conference on*, 2002, pp. 669-672.

[20] J. B. Rizk and G. M. Rebeiz, "Digital-type RF MEMS switched capacitors," in *Microwave Symposium Digest, 2002 IEEE MTT-S International*, 2002, pp. 1217-1220.

[21] N. Hoivik, *et al.*, "Digitally controllable variable high-Q MEMS capacitor for RF applications," in *Microwave Symposium Digest, 2001 IEEE MTT-S International*, 2001, pp. 2115-2118 vol.3.

[22] J. De Coster, *et al.*, "Variable RF MEMS capacitors with extended tuning range," in *TRANSDUCERS, Solid-State Sensors, Actuators and Microsystems, 12th International Conference on, 2003*, 2003, pp. 1784-1787 vol.2.

[23] B. Lakshminarayanan and G. Rebeiz, "High-Power High-Reliability Sub-Microsecond RF MEMS Switched Capacitors," in *Microwave Symposium, 2007. IEEE/MTT-S International*, 2007, pp. 1801-1804.

[24] B. Lakshminarayanan, *et al.*, "High-Reliability Miniature RF-MEMS Switched Capacitors," *Microwave Theory and Techniques, IEEE Transactions on*, vol. 56, pp. 971-981, 2008.

[25] S. Barker and G. M. Rebeiz, "Distributed MEMS true-time delay phase shifters and wide-band switches," *Microwave Theory and Techniques, IEEE Transactions on,* vol. 46, pp. 1881-1890, 1998.

[26] A. Malczewski, *et al.*, "X-band RF MEMS phase shifters for phased array applications," *Microwave and Guided Wave Letters, IEEE,* vol. 9, pp. 517-519, 1999.

[27] A. S. Nagra and R. A. York, "Distributed analog phase shifters with low insertion loss," *Microwave Theory and Techniques, IEEE Transactions on,* vol. 47, pp. 1705-1711, 1999.

[28] J. S. Hayden and G. M. Rebeiz, "2-bit MEMS distributed X-band phase shifters," *Microwave and Guided Wave Letters, IEEE,* vol. 10, pp. 540-542, 2000.

[29] J. S. Hayden and G. M. Rebeiz, "Very low-loss distributed X-band and Ka-band MEMS phase shifters using metal-air-metal capacitors," *Microwave Theory and Techniques, IEEE Transactions on,* vol. 51, pp. 309-314, 2003.

[30] J. B. Hacker, *et al.*, "A Ka-band 3-bit RF MEMS true-time-delay network," *Microwave Theory and Techniques, IEEE Transactions on,* vol. 51, pp. 305-308, 2003.

[31] K. Topalli, *et al.*, "A Monolithic Phased Array Using 3-bit Distributed RF MEMS Phase Shifters," *Microwave Theory and Techniques, IEEE Transactions on,* vol. 56, pp. 270-277, 2008.

[32] M. Ünlü, "Novel Impedance Tuner, Phase Shifter, and Vector Modulators Using RF MEMS Technology," PhD Thesis, Dept. of Electrical and Electronics Engineering, Middle East Technical University, Ankara, 2009.

[33] M. Ünlü, "An adjustable impedance matching network using RF MEMS technology," M.Sc. Thesis, Dept. of Electrical and Electronics Engineering, Middle East Technical University, Ankara, 2003.

[34] S. Qin and N. S. Barker, "Distributed MEMS tunable matching network using minimal-contact RF-MEMS varactors," *Microwave Theory and Techniques, IEEE Transactions on,* vol. 54, pp. 2646-2658, 2006.

[35] M. Unlu, *et al.*, "A Reconfigurable RF MEMS Triple Stub Impedance Matching Network," in *Microwave Conference, 2006. 36th European*, 2006, pp. 1370-1373.

[36] S. Fouladi, *et al.*, "Distributed MEMS Tunable Impedance-Matching Network Based on Suspended Slow-Wave Structure Fabricated in a Standard CMOS Technology," *Microwave Theory and Techniques, IEEE Transactions on,* vol. 58, pp. 1056-1064, 2010.

[37] K. Entesari, *et al.*, "A 25–75-MHz RF MEMS Tunable Filter," *Microwave Theory and Techniques, IEEE Transactions on,* vol. 55, pp. 2399-2405, 2007.

[38] C. A. Hall, *et al.*, "A 25 watt RF MEM-tuned VHF bandpass filter," in *Microwave Symposium Digest, 2003 IEEE MTT-S International*, 2003, pp. 503-506 vol.1.

[39] R. M. Young, *et al.*, "Low-loss bandpass RF filter using MEMS capacitance switches to achieve a one-octave tuning range and independently variable bandwidth," in *Microwave Symposium Digest, 2003 IEEE MTT-S International*, 2003, pp. 1781-1784 vol.3.

[40] G. M. Kraus, *et al.*, "A widely tunable RF MEMS end-coupled filter," in *Microwave Symposium Digest, 2004 IEEE MTT-S International*, 2004, pp. 429-432 Vol.2.

[41] K. Entesari and G. M. Rebeiz, "A differential 4-bit 6.5-10-GHz RF MEMS tunable filter," *Microwave Theory and Techniques, IEEE Transactions on*, vol. 53, pp. 1103-1110, 2005.

[42] A. Pothier, *et al.*, "Low-loss 2-bit tunable bandpass filters using MEMS DC contact switches," *Microwave Theory and Techniques, IEEE Transactions on*, vol. 53, pp. 354-360, 2005.

[43] K. Entesari and G. M. Rebeiz, "A 12–18-GHz Three-Pole RF MEMS Tunable Filter," *Microwave Theory and Techniques, IEEE Transactions on*, vol. 53, pp. 2566-2571, 2005.

[44] A. Abbaspour-Tamijani, *et al.*, "Miniature and tunable filters using MEMS capacitors," *Microwave Theory and Techniques, IEEE Transactions on*, vol. 51, pp. 1878-1885, 2003.

[45] B. Pillans, *et al.*, "6-15 GHz RF MEMS tunable filters," in *Microwave Symposium Digest, 2005 IEEE MTT-S International*, 2005, p. 4 pp.

[46] I. Reines, *et al.*, "1.6-2.4 GHz RF MEMS tunable 3-pole suspended combline filter," in *Microwave Symposium Digest, 2008 IEEE MTT-S International*, 2008, pp. 133-136.

[47] S. J. Park, *et al.*, "Low-Loss 4–6-GHz Tunable Filter With 3-Bit High-<formula formulatype="inline"> <img src="/images/tex/228.gif" alt="Q"> </formula> Orthogonal Bias RF-MEMS Capacitance Network," *Microwave Theory and Techniques, IEEE Transactions on*, vol. 56, pp. 2348-2355, 2008.

[48] M. A. El-Tanani and G. M. Rebeiz, "High-Performance 1.5–2.5-GHz RF-MEMS Tunable Filters for Wireless Applications," *Microwave Theory and Techniques, IEEE Transactions on*, vol. 58, pp. 1629-1637, 2010.

[49] A. Ocera, *et al.*, "A MEMS-Reconfigurable Power Divider on High Resistivity Silicon Substrate," in *Microwave Symposium, 2007. IEEE/MTT-S International*, 2007, pp. 501-504.

[50] J. H. Schaffner, *et al.*, "Reconfigurable aperture antennas using RF MEMS switches for multi-octave tunability and beam steering," in *Antennas and Propagation Society International Symposium, 2000. IEEE*, 2000, pp. 321-324 vol.1.

[51] P. Panaia, *et al.*, "MEMS-based reconfigurable antennas," in *Industrial Electronics, 2004 IEEE International Symposium on*, 2004, pp. 175-179 vol. 1.

[52] B. A. Cetiner, *et al.*, "Multifunctional reconfigurable MEMS integrated antennas for adaptive MIMO systems," *Communications Magazine, IEEE*, vol. 42, pp. 62-70, 2004.

[53] L. M. Feldner, *et al.*, "RF MEMS reconfigurable triangular patch antenna," in *Antennas and Propagation Society International Symposium, 2005 IEEE*, 2005, pp. 388-391 vol. 2A.

[54] L. Sunan, *et al.*, "A frequency-reconfigurable circularly polarized patch antenna by integrating MEMS switches," in *Antennas and Propagation Society International Symposium, 2005 IEEE*, 2005, pp. 413-416 vol. 2A.

[55] M. Mowler, *et al.*, "A 2-bit reconfigurable meander slot antenna with RF-MEMS switches," in *Antennas and Propagation Society International Symposium, 2005 IEEE*, 2005, pp. 396-399 vol. 2A.

[56] J. Chang won, *et al.*, "Reconfigurable scan-beam single-arm spiral antenna integrated with RF-MEMS switches," *Antennas and Propagation, IEEE Transactions on*, vol. 54, pp. 455-463, 2006.

[57] D. E. Anagnostou, *et al.*, "Design, fabrication, and measurements of an RF-MEMS-based self-similar reconfigurable antenna," *Antennas and Propagation, IEEE Transactions on*, vol. 54, pp. 422-432, 2006.

[58] E. Erdil, *et al.*, "Frequency Tunable Microstrip Patch Antenna Using RF MEMS Technology," *Antennas and Propagation, IEEE Transactions on*, vol. 55, pp. 1193-1196, 2007.

[59] K. Topalli, *et al.*, "Tunable dual-frequency RF MEMS rectangular slot ring antenna," *Sensors and Actuators A: Physical*, vol. 156, pp. 373-380, 2009.

[60] C. Goldsmith, *et al.*, "Lifetime characterization of capacitive RF MEMS switches," in *Microwave Symposium Digest, 2001 IEEE MTT-S International*, 2001, pp. 227-230 vol.1.

[61] W. M. van Spengen, *et al.*, "Experimental characterization of stiction due to charging in RF MEMS," in *Electron Devices Meeting, 2002. IEDM '02. Digest. International*, 2002, pp. 901-904.

[62] R. Chan, *et al.*, "Low-actuation voltage RF MEMS shunt switch with cold switching lifetime of seven billion cycles," *Microelectromechanical Systems, Journal of*, vol. 12, pp. 713-719, 2003.

[63] W. M. van Spengen, *et al.*, "The influence of the package environment on the functioning and reliability of RF-MEMS switches," in *Reliability Physics Symposium, 2005. Proceedings. 43rd Annual. 2005 IEEE International*, 2005, pp. 337-341.

[64] P. Czarnecki, *et al.*, "Effect of Gas Pressure on the Lifetime of Capacitive RF MEMS Switches," in *Micro Electro Mechanical Systems, 2006. MEMS 2006 Istanbul. 19th IEEE International Conference on*, 2006, pp. 890-893.

[65] C. L. Goldsmith, *et al.*, "High-Cycle Life Testing of RF MEMS Switches," in *Microwave Symposium, 2007. IEEE/MTT-S International*, 2007, pp. 1805-1808.

[66] H. S. Newman, *et al.*, "Lifetime Measurements on a High-Reliability RF-MEMS Contact Switch," *Microwave and Wireless Components Letters, IEEE*, vol. 18, pp. 100-102, 2008.

[67] J. Muldavin, *et al.*, "Wafer-Scale Packaged RF Microelectromechanical Switches," *Microwave Theory and Techniques, IEEE Transactions on*, vol. 56, pp. 522-529, 2008.

[68] MEMtronics Corporation. *http://www.memtronics.com/page.aspx?page_id=13* [last visited on 26 August 2010].

[69] Radant MEMS. *http://www.radantmems.com/radantmems/products.html* [last visited on 26 August 2010].

[70] X. Rottenberg, *et al.*, "Distributed dielectric charging and its impact on RF MEMS devices," in *Microwave Conference, 2004. 34th European*, 2004, pp. 77-80.

[71] Y. Xiaobin, *et al.*, "Initial observation and analysis of dielectric-charging effects on RF MEMS capacitive switches," in *Microwave Symposium Digest, 2004 IEEE MTT-S International*, 2004, pp. 1943-1946 Vol.3.

[72] S. Melle, *et al.*, "Reliability modeling of capacitive RF MEMS," *Microwave Theory and Techniques, IEEE Transactions on*, vol. 53, pp. 3482-3488, 2005.

[73] G. Papaioannou, *et al.*, "Temperature study of the dielectric polarization effects of capacitive RF MEMS switches," *Microwave Theory and Techniques, IEEE Transactions on*, vol. 53, pp. 3467-3473, 2005.

[74] Y. Xiaobin, *et al.*, "A transient SPICE model for dielectric-charging effects in RF MEMS capacitive switches," *Electron Devices, IEEE Transactions on*, vol. 53, pp. 2640-2648, 2006.

[75] P. Zhen, *et al.*, "Top vs. bottom charging of the dielectric in RF MEMS capacitive switches," in *Microwave Conference, 2006. APMC 2006. Asia-Pacific*, 2006, pp. 1535-1538.

[76] G. J. Papaioannou and T. Lisec, "Dielectric charging process in AlN RF-MEMS capacitive switches," in *Microwave Conference, 2007. European*, 2007, pp. 1338-1341.

[77] P. Blondy, *et al.*, "Effects of atmosphere on the reliability of RF-MEMS capacitive switches," in *Microwave Conference, 2007. European*, 2007, pp. 1346-1348.

[78] P. Zhen, *et al.*, "Superposition Model for Dielectric Charging of RF MEMS Capacitive Switches Under Bipolar Control-Voltage Waveforms," *Microwave Theory and Techniques, IEEE Transactions on*, vol. 55, pp. 2911-2918, 2007.

[79] R. W. Herfst, *et al.*, "Center-Shift Method for the Characterization of Dielectric Charging in RF MEMS Capacitive Switches," *Semiconductor Manufacturing, IEEE Transactions on*, vol. 21, pp. 148-153, 2008.

[80] R. Daigler, *et al.*, "Effect of dielectric film thickness on dielectric charging of RF MEMS capacitive switches," in *Microwave Symposium Digest, 2008 IEEE MTT-S International*, 2008, pp. 1275-1278.

[81] U. Zaghloul, *et al.*, "A comprehensive study for dielectric charging process in silicon nitride films for RF MEMS switches using Kelvin Probe Microscopy," in *Solid-State Sensors, Actuators and Microsystems Conference, 2009. TRANSDUCERS 2009. International*, 2009, pp. 789-793.

[82] D. Mardivirin, *et al.*, "Charging in Dielectricless Capacitive RF-MEMS Switches," *Microwave Theory and Techniques, IEEE Transactions on*, vol. 57, pp. 231-236, 2009.

[83] P. Zhen, *et al.*, "Impact of Humidity on Dielectric Charging in RF MEMS Capacitive Switches," *Microwave and Wireless Components Letters, IEEE*, vol. 19, pp. 299-301, 2009.

[84] M. Fernandez-Bolanos, *et al.*, "Reliability of RF MEMS Capacitive Switches and Distributed MEMS Phase Shifters using AlN Dielectric," in *Micro Electro Mechanical Systems, 2009. MEMS 2009. IEEE 22nd International Conference on*, 2009, pp. 638-641.

[85] S. M. Sze, *Physics of Semiconductor Devices*, 3rd ed. New York: John Wiley & Sons, 2007.

[86] Y. Xiaobin, *et al.*, "Acceleration of Dielectric Charging in RF MEMS Capacitive Switches," *Device and Materials Reliability, IEEE Transactions on*, vol. 6, pp. 556-563, 2006.

[87] P. Blondy, *et al.*, "Packaged Millimeter Wave Thermal MEMS Switches," in *Microwave Conference, 2001. 31st European*, 2001, pp. 1-4.

[88] R. Meichun, *et al.*, "Latching micromagnetic relays," *Microelectromechanical Systems, Journal of*, vol. 10, pp. 511-517, 2001.

[89] T. D. Hudson, "Development of Piezoelectric RF MEMS Switch and Phase Shifter," in *University/Government/Industry Micro/Nano Symposium, 2008. UGIM 2008. 17th Biennial*, 2008, pp. 112-115.

[90] Ç. Çetintepe, "Development of MEMS Technology Based Microwave and Millimeter-Wave Components," M.Sc. Thesis, Dept. of Electrical and Electronics Engineering, Middle East Technical University, Ankara, 2010.

[91] K. Topallı, "A Monolithic Phased Array Using RF MEMS Technology," PhD Thesis, Dept. of Electrical and Electronics Engineering, Middle East Technical University, Ankara, 2007.

[92] H. İ. Atasoy, "Design and Fabrication of RF MEMS Switches and Instrumentation For Performance Evaluation," M.Sc. Thesis, Dept. of Electrical and Electronics Engineering, Middle East Technical University, Ankara, 2007.

[93] Krytar Company. *http://www.krytar.com/pdf/200zbs.pdf* [last visited on 26 August 2010].